



universität
wien

MASTERARBEIT

Titel der Masterarbeit

„Development and evaluation of enzymes loaded gold
nanoparticles“

verfasst von

Marcella Patricia Eder BSc

angestrebter akademischer Grad

Master of Science (MSc)

Wien, 2013

Studienkennzahl lt.
Studienblatt:

A 066 862

Studienrichtung lt.
Studienblatt:

Masterstudium Chemie

Betreut von:

Dr. Wolfgang Lindner

Acknowledgments

Für die Möglichkeit, diese Masterarbeit zu schreiben, möchte ich mich sehr herzlich bei Prof. Dr. Wolfgang Lindner bedanken.

Weiters danke ich Dr. Helmut Hinterwirth für die gute Betreuung und die Unterstützung während meiner Arbeit.

Ganz besonders möchte ich all meinen Kollegen der Lindner/Lämmerhofer Arbeitsgruppe danken, die aus der Zeit meiner Masterarbeit nicht nur einen lehrreichen, sondern auch geselligen und lustigen Lebensabschnitt gemacht haben.

All meinen Freunden möchte ich für die vielen schönen Stunden während meines Studiums danken. Ich habe während diesen Jahren, sei es im selben Studienfach oder auch durch Bekannte aus anderen Fächern, viele liebe Menschen getroffen die ich auch in Zukunft nicht mehr missen möchte und auf die ich mich stets verlassen kann.

Meinen lieben Freundinnen Claudia und Verena danke ich nicht nur für die viele gemeinsam durchgestanden Stunden, in denen wir für Prüfungen gelernt, auf Ergebnisse gewartet oder Rückschläge verarbeitet haben. Auch für unzählige schöne Erlebnisse, gute Gespräche und aufbauende Worte sowie ihr Verständnis und ihren Rat in allerlei Lebenslagen bin ich ihnen dankbar.

Ihr alle habt meine Studienzeit zu unvergleichlich schönen und wertvollen Jahren gemacht!

Ganz besonders möchte ich meinen Familienmitgliedern danken, die mir nicht nur mein Studium ermöglicht haben, sondern mir auch immer mit Rat und Tat zur Seite gestanden sind. Sie haben, wann immer es ihnen möglich war, keine Gelegenheit ausgelassen mich zu unterstützen und mir kleine und große Lasten abgenommen.

Von meinem Freund Florian durfte ich immer bedingungslose Unterstützung erfahren, ebenso wie er stets meine Schulter zum Anlehnen war und sich mit mir über Erfolge gefreut hat.

Ich schätze mich sehr glücklich, mit dir durch unser gemeinsames Leben gehen zu dürfen!

Table of Contents

Acknowledgments.....	0
Table of Contents	2
1 Abstract (Deutsch).....	5
2 Abstract (English)	7
3 Introduction.....	9
3.1 Aim of the master thesis.....	9
3.2 Chirality.....	9
3.2.1 Enantiomers	11
3.2.2 Importance in biological and pharmaceutical applications	13
3.2.3 Enantioseparation – Direct and indirect approach	15
3.3 HPLC separation – chiral stationary phases	19
3.3.1 Quinidine (QD) and Quinine (QN), Homotau-QD type CSPs	20
3.4 Gold nanoparticles - applications and characteristics.....	22
3.4.1 Preparation of GNPs.....	23
3.4.2 Characterization of GNPs by SPR, DLS and ZP	28
3.4.3 Immobilization chemistry.....	33
3.5 Enzymes – Stereospecificity and enantioselectivity.....	36
3.5.1 Trypsin and α -chymotrypsin.....	39
3.5.2 Immobilized Trypsin	42
3.5.3 Enzym modifications (Acetylation).....	43
3.5.4 Michaelis-Menten (M.M.) kinetics	44
4 Instruments and methods.....	49
4.1 Instruments.....	49

4.1.1	Gold nanoparticle (GNP) characterization	49
4.1.2	Photometry	50
4.1.3	HPLC separation	50
4.2	Methods.....	52
4.2.1	Gold nanoparticle (GNP) preparation	52
4.2.2	Enzyme immobilization onto GNPs (GNP@enzyme)	52
4.2.3	Enzymatic digestion of different substrates with enzyme linked GNPs	53
4.2.4	Long-term study of the storage stability of GNPs.....	57
4.2.5	Reusability of GNP conjugated enzymes.....	57
4.2.6	HPLC assays - Limit of detection (LOD)	58
5	Results and discussion.....	59
5.1	GNP characterization.....	59
5.1.1	SPR, ZP and DLS of GNPs and GNP@enzyme	59
5.1.2	Long-time stability study of GNPs	65
5.1.3	Reuseability of GNP@enzyme.....	71
5.2	Determination of enzyme activity – Stereoselectiv and nonstereoselectiv D,L-BApNA digestion assay	73
5.2.1	Solubility of BApNA	73
5.2.2	Determination of M. M. constants K_m , v_{max} and specific enzyme activity.....	74
5.3	D,L-BApNA hydrolysis – Determination of enantioselectivity of GNP@enzyme	76
5.3.1	Enantioselective cleavage of D,L-BApNA	76
5.3.2	Enantioselectivity – influence of different solvents.....	84
5.4	Acetylation of trypsin and GNP@trypsin to improve enzyme activity.....	87
5.4.1	Comparison of acetylated and not acetylated trypsin in-solution	87
5.4.2	Comparison of acetylated and not acetylated GNP@trypsin	89
5.5	Digestion of mimic peptides – Development of a new enzyme assay.....	91

5.5.1	Optimization of HPLC separation	91
5.5.2	Determination of M.M. constants.....	97
5.5.3	Enantioselectivity of tryptic digestion of enantiomeric peptides with GNP@trypsin	99
5.5.4	Digestion of peptides containing the amino acid arginine	105
5.6	Determination of limit of detection (LOD)	107
6	Conclusion	108
7	Chemicals and Materials	111
7.1	Buffers.....	111
7.2	Source of Supply	111
8	Abbreviations	112
9	List of Tables.....	114
10	List of Figures.....	115
11	References.....	121
12	Curriculum Vitae.....	127

1 Abstract (Deutsch)

Um die Sicherheit und Effizienz in der pharmazeutischen Industrie zu verbessern, gewinnt die Produktion enantiomerenreiner Medikamente immer größere Bedeutung. Eine Möglichkeit der enantioselektiven Synthese ist der Einsatz von Enzymen, die effektive Biokatalysatoren darstellen. Die Vorteile dieser chemo-enzymatischen Synthese sind nicht nur hohe Stereospezifität, Regioselektivität und Chemoselektivität, sondern auch milde Reaktionsbedingungen, welche die Bildung unerwünschter Nebenprodukte verringern können. Allerdings ist diese Art der Produktsynthese teuer und führt zu einem hohen Verbrauch an als Biokatalysator dienenden Enzymen. Darum ist die Immobilisierung der Enzyme auf Trägermaterialien wie etwa Goldnanopartikeln (GNPs), welche einfach durch Zentrifugieren aus den betreffenden Reaktionslösungen entfernt werden können, von großer Bedeutung.

Das Ziel dieser Masterarbeit war die Entwicklung eines Assays um die Enantioselektivität immobilisierter Enzyme näher zu untersuchen. Zu diesem Zweck wurden die Serinproteasen Trypsin und α -Chymotrypsin auf Goldnanopartikeln via Polyethylenglykol (PEG₇) spacerimmobilisiert. Die hergestellten enzymimmobilisierten GNP wurden charakterisiert und die Herstellung auf Reproduzierbarkeit überprüft. Dabei konnte eine zufriedenstellende Übereinstimmung der Ergebnisse erzielt werden.

Zur Bestimmung der Enzymaktivität sowie der Michaelis-Menten Konstanten K_M und V_{max} , wurden Assays mit verschiedenen chiralen Substraten wie etwa D,L-BAPNA, α -N-benzoyl-D,L-Lys-Gly-OH und N-benzoyl-D,L-Arg-Gly-OH getestet. Im Vergleich mit Trypsin in Lösung wurde etwas geringere Werte für die Michaelis-Menten (M.M.) Konstante K_M für immobilisiertes Trypsin erreicht.

Weiters wurde die Enantioselektivität der Assays mittels HPLC unter Verwendung von chiralen Ionenaustauschersäulen, gekoppelt mit einem UV/Vis Detektor, bestimmt. Für D,L-BAPNa zeigte sich eine Abhängigkeit der Enantioselektivität von der Substratkonzentration ebenso wie von der Dauer des Verdaus. Bei den Peptiden α -N-benzoyl-D,L-Lys-Gly-OH und N-benzoyl-D,L-Arg-Gly-OH konnte eine vollständige Enantioselektivität zu Gunsten des L-Enantiomers erkannt werden. Hierbei konnte weder eine Abhängigkeit von der Zeit noch von der Substratkonzentration erkannt werden.

Der Einfluss einer Enzymmodifikation, im Besonderen einer Acetylierung, auf die

Enzymaktivität ebenso wie auf die Enantioselektivität wurde untersucht. Während die Enzymaktivität des Trypsins in Lösung annähernd unverändert blieb, zeigte sich für das immobilisierte Trypsin eine geringe Zunahme für K_M beziehungsweise eine Abnahme für V_{max} .

Zusätzlich wurde der Effekt verschiedener organischer Lösungsmittel auf die Enantioselektivität überprüft. Dabei wurde für keines der getesteten Lösungsmittel ein Einfluss auf die Spaltung von D,L-BApNA erkannt.

Bei der Untersuchung der Wiederverwendungsmöglichkeiten der enzymimmobilisierten GNPs wurde zwar ein geringfügiger Verlust der Aktivität detektiert, eine Wiederverwendung ist aber auf jeden Fall denkbar. Eine Langzeitstudie des Lagerungsverhaltens der Partikel zeigte eine hohe Lagerbeständigkeit sowohl für die enzym- (GNP@trypsin) als auch für die PEG₇-Liganden modifizierten GNPs (GNP-PEG₇-COOH). Eine Lagerung von mehr als 5 Monaten ist somit möglich.

2 Abstract (English)

To enhance safety and efficiency, the production of enantiopure drugs is gaining importance in the pharmaceutical industry. One approach of enantioselective synthesis is the use of enzymes as effective biocatalysts. The advantages of chemo-enzymatically synthesis are high stereospecificity, regioselectivity and chemoselectivity as well as mild reactions conditions to avoid side products. However, this approach can be wasteful and expensive. Therefore the immobilization of enzymes onto support materials such as gold nanoparticles (GNPs), which can easily be removed from solution by centrifugation and eventually reused, is of high interest.

The aim of this master thesis was the development of an assay to investigate the enantioselectivity of immobilized enzymes. For that purpose the serin proteases trypsin and α -chymotrypsin were immobilized onto GNPs via a polyethyleneglycol ligand (PEG₇). The prepared enzyme immobilized GNPs were characterized and tested for reproducibility whereby a sufficient accordance of the results was achieved. Assays with different chiral substrates such as D,L-BApNA, α -N-benzoyl-D,L-Lys-Gly-OH and N-benzoyl-D,L-Arg-Gly-OH were accomplished. The enzyme activity and the Michaelis Menten constants K_M and V_{max} were determined and compared to the enzymes in-solution. A slight decrease of activity was detected for immobilized trypsin.

Moreover, the enantioselectivity for the assays was analyzed by HPLC using chiral ion exchanger columns coupled with UV/Vis detector. For D,L-BApNa, an influence of the substrate concentration and of digestion time on the enantioselectivity was observed. For the peptides α -N-benzoyl-D,L-Lys-Gly-OH and N-benzoyl-D,L-Arg-Gly-OH a complete enantioselectivity towards the L-enantiomer was found.

The influence of enzyme modification, in particular acetylation, on both, the enzyme activity and the enantioselectivity, was determined. Thereby, no influence on the enzyme activity trypsin in-solution was observed, while the acetylation affected an increase of K_M and a decrease V_{max} , respectively, for the immobilized trypsin.

Furthermore, the effect of different organic solvents in combination with aqueous buffer solution on the enantioselectivity was investigated. For none of the tested solvents an influence to the enantioselective cleavage of D,L-BApNA was observed.

The reuseability of the immobilized GNPs was reviewed. Though a certain loss of activity was

detected, a reuse can be considered as possible. A long-term study showed an excellent storage stability of enzyme [GNP@trypsin] and spacer immobilized GNPs (GNP-PEG₇-COOH) up to 5 months.

3 Introduction

3.1 Aim of the master thesis

Due to the great interest in enantioselective synthesis for different purposes, the intention of this thesis was the development of an appropriate assay to review the enantioselectivity of serine proteases, more precisely trypsin and α -chymotrypsin. Therefore the cleavage of several chiral substrates was screened and the influence of diversification of the digestion conditions, and hence modification of an enantioselective digest, was analyzed. The advantage of enzyme conjugated nanoparticles is the straightforward removal of the enzyme due to centrifugation. Furthermore, an optional reuse may arise out of this mode of operation.

3.2 Chirality

Deriving from the ancient Greek word $\chi\epsilon\iota\rho$ ("hand"), chirality refers to the geometric property of a rigid object or a spatial arrangement of points or atoms of being non-superposable on its mirror image [1]. Demonstrative examples are the left and the right hand, why a synonym for chirality is also "handedness". A chiral object has no symmetry elements, such as a mirror plane σ , a centre of inversion i , or a rotation-reflection axis, but they can have rotation C_n -axis. These symmetry elements are second kind. If the object is superposable on its mirror image the object is described as being achiral [1].

The appearance of chirality depends on the existence of at least one of various chiral elements. These may be centers of chirality (stereogenic centers), chiral axes (axial chirality), chiral planes (planar chirality), chiral helices (helical chirality), and topologically chiral elements (topological chirality). Particularly stereogenic centers and axial chirality are highly represent in the pool of chiral molecules. Considering rotameres, stereoisomere which may be converted into each other by rotation of single bonds, axial chirality may induce a special case known as atropisomers. Due to a limited rotation because of bulky substituents of a covalent single bond, and thus, the conformers can be isolated [1].

Stereogenic centers may either be tetra-coordinated, tri-coordinated or higher coordinated. Tetra-coordinated stereogenic centers have a tetrahedral central atom, substituted by four distinct different ligands. These centers of chirality may have different central atoms, a well

known example is the asymmetrically substituted sp^3 -hybridized carbon atom like in lactic acid [2].

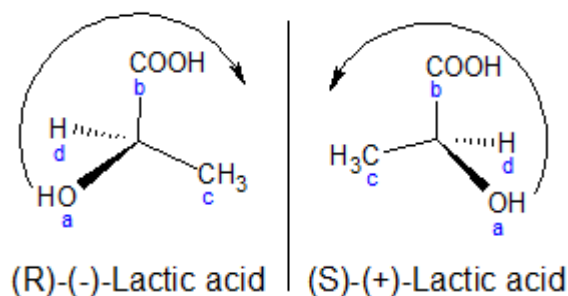
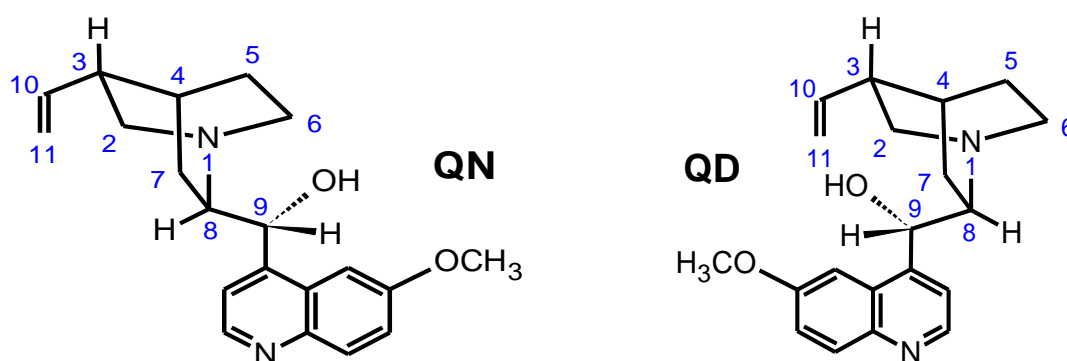


Figure 1: Both possible configurations of the stereogenic center of lactic acid, ligands numbered according to the CIP system from highest priority (a) to lowest priority (d).

Further central atoms may be silicon, germanium, ammonium, phosphonium or arsonium. Yet another possibility for a stereogenic center is a tri-coordinated center of chirality with pyramidal geometry, obtained due to 3 distinct substituents, attached to sulfur (sulfonium, sulfoxides), phosphorus (phosphane) or nitrogen. Concerning the configurational instability, rapid inversions between the enantiomeric forms of particularly tertiary amines are quite common [2]. Tri-coordinated stereogenic center can be stabilized by fixation of the central nitrogen atom in a cyclic ring system, such as in (*R,S*)-(6-methoxyquinolin-4-yl)((*2R,4S,8R*)-8-vinylquinuclidin-2-yl)methanol, (quinine, QN and quinidine, QD) (Figure 2). Quinidine and its pseudo-enantiomer quinine are very prominent chiral natural compounds and used as chiral selectors for enantiomeric separations (see 3.3.1) [2], [3].



Quinine (1*S*, 3*R*, 4*S*, 8*S*, 9*R*)

Quinidine (1*S*, 3*R*, 4*S*, 8*R*, 9*S*)

Figure 2: (*S*)-(6-methoxyquinolin-4-yl)((*2R,4S,8R*)-8-vinylquinuclidin-2-yl)methanol, commonly known as quinidine (QD) and the pseudo-enantiomer (*R*)-(6-methoxyquinolin-4-yl)((*2S,4S,8R*)-8-vinylquinuclidin-2-yl)methanol (quinine, QN).

Due to the existence of a free electron pair besides 3 distinct substituents such tri-coordinated stereogenic centers can be considered as tetra-coordinated. Therefore, the same nomenclature for stereochemical descriptors can be applied for both, tri- and tetra-coordinated stereogenic centers. They are described by the *R/S*-nomenclature according to the Cahn-Ingold-Prelog sequence rule procedure, also known as CIP-convention. For , amino acids and sugars also the *D,L*-nomenclature is common.[4].

The CIP rules were first published by Cahn, Ingold and Prelog in 1966 [5]. The CIP-convention is a system of priority rules, applied for three-dimensional models of the molecule to specify the absolute molecular chirality of a compound. The purpose of this system is to give information of the enantiomeric form of each chiral element in a molecule by assigning an *R* or *S* descriptor to each stereogenic center or an *E* or *Z* descriptor to each double bond. By including these descriptors in the systematic name of a molecule, it can be specified uniquely.

To determine the absolute configuration of a chiral center, the ligands must be arranged in an order of precedence. The ligand with highest order is conveniently named as a, the second highest with b up to d for the ligand with lowest precedence. Therefore, the atomic number of the atoms directly attached to the stereocenter are compared, the highest atomic number receives the highest priority. In the case of equality, the next but one atom must be considered, this can be done as long as to the earliest difference. Rules in detail and special rules can be looked up in the IUPAC recommendations "Rules for the nomenclature of organic chemistry" [4]. Then, by tracing a path from a to b to c, the course is determined. An anticlockwise course is symbolized with *S* for sinister (which means left), a clockwise course with *R* for rectus (which means right). Conversion of one enantiomer into another always changes the configuration of each stereogenic center from *R* to *S* and from *S* to *R*. Helical chirality is nomenclated with *P* (equates plus) for a right-handed helix and *M* (equates minus) for a left-handed helix [6], [7].

3.2.1 Enantiomers

Stereoisomers are isomers with identical constitution, but differences in the spatial arrangement of atoms. These types of isomers are always chiral. On the contrary, constitutional isomers have identical empirical formula, but are different in their atom

connectivity. Due to different line formulas they can be distinguished, such as CH_3OCH_3 (Methoxymethane) and $\text{CH}_3\text{CH}_2\text{OH}$ (Ethanol). [8]

Stereoisomers can be further distinguished between diastereomers and enantiomers (see Figure 3). Diastereoisomers are characterized by different physical properties, distinct energy and even by some differences in chemical behavior towards achiral reagents.

Enantiomers are non-superimposable mirror images while diastereomers are no mirror images. The word enantiomer derives from the ancient Greek words $\acute{\epsilon}\nu\acute{\alpha}\nu\tau\iota\omicron\varsigma$ for opposite, and $\mu\acute{\epsilon}\rho\omicron\varsigma$ for part or portion. An example is the left and the right hand. They have the same energy due to identical atomic distances, angles, torsions and interatomic interactions (see Figure 3). Due to these properties they are not distinguishable in an achiral environment and therefore, they cannot be separated with common chromatographic methods like reversed-phase chromatography (RP) [2], [6], [8].

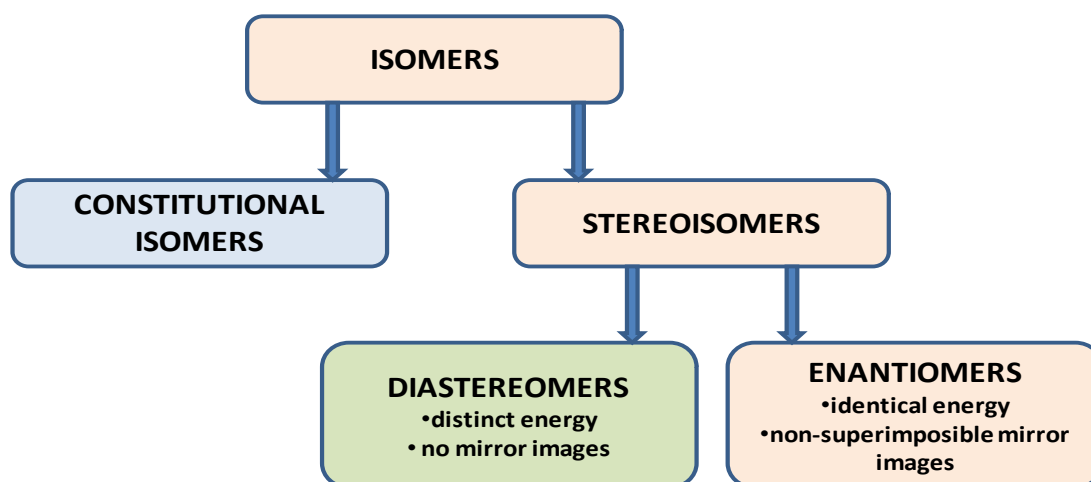


Figure 3: Classification of diastereomers and enantiomers and their characteristic properties.

If an analyzed sample only contains molecules with the same chirality sense, the compound is enantiomerically pure, while a racemate is an equimolar mixture of a pair of enantiomers, described with the symbols RS or SR . In mixtures with unequally distributed ratio, the percentage of one enantiomer to the other is given by the enantiomeric ratio (er %), e.g. 70%(S): 30%(R). The enantiomeric excess (ee%) of a mixture can be calculated using the formula of eq.1

$$\text{(eq.1)} \quad ee = \frac{|m_R - m_S|}{m_R + m_S} \times 100\%$$

where m_R and m_S are the mole fractions of the enantiomers and the sum is always equal 1. The term enantiomeric excess was introduced in the early 1970s by Morrison and Mosher [9]. They described the equality of optical purity (op) and ee % in samples without impurities [10].

The optical purity is defined as the ratio of the observed optical rotation of a sample consisting of a mixture of enantiomers to the optical rotation of one pure enantiomer. Although enantiomers have identical chemical and physical properties, they rotate plane-polarized light in equal amounts but in opposite directions. This ability is labeled with + and -, respectively. In equimolar mixtures the positive rotation is exactly counteracted by the negative rotation, therefore a racemate with equimolar mixture of a pair of enantiomers does not exhibit optical activity [8].

Despite to their identical condition in matters of chemical and physical properties, one enantiomer may show different behavior in chemical reactions compared to the other when being present in a chiral environment or involved in a stereochemically driven reaction pathway [7].

3.2.2 Importance in biological and pharmaceutical applications

In living biological systems there is a high appearance of chiral molecules. Chiral centers can be found in the amino acids, carbohydrates and DNA/RNA building blocks, which are building up proteins and carbohydrates. These biomolecules are built of units with the same configuration. The 21 essential amino acids are all L-enantiomers, while most carbohydrates are D-enantiomers. Therefore, many essential physiological processes are highly sensitive to stereochemistry [11], [12]. Chiral compounds show different activity and kinetic profiles in binding chemistry to chiral targets like receptors, enzymes, ion channels or drug transporters [13]. Due to the fact that stereoselectivity is one of the characteristic features of enzymatic reactions, messenger-receptor interactions and metabolic processes, stereochemistry is an important point which has to be well-considered in studying xenobiotics, such as drugs, agrochemicals, food additives, flavours, and fragrances. In particular, there was paid much attention on the differences of therapeutic effects of natural products, alkaloids, toxics and many more other chiral enantiomeric drugs on the human body during the last decades [13]. In drugs, the enantiomer which effects the desired physiologic effects is called eutomer,

while the other one is named diastomer. The diastomer can be less active, inactive (isomeric ballast) or even be responsible for unwanted side-effects. Furthermore, one enantiomer can act as a competitive antagonist of the other and thus minimize the effectiveness of the drug [11]. Due to the pharmacokinetic and pharmacodynamic differences, the single enantiomers of a chiral drug can differ in bioavailability, distribution, metabolic, and excretion behavior. Examples of different efficiency by oral or intravenous administration as racemates are the β -blocker propranolol and the cardiotoxic agent verapamil. By reason of the stereoselective first-pass metabolism, the more active enantiomer of verapamil and the less active one of propranolol is absorbed with a higher rate [14]. Furthermore, enantiomers may have a totally different pharmaceutical effect and therefore different application areas. Levopropoxyphene is administered as antitussive agent, while dextropropoxyphene is used as analgesic [2], for instance.

In the late 1950's and the early 1960's, a worldshaking pharmaceutical affair took place. In these days, the observation of the enantioselective action of chiral drugs was not considered as an important point in drug activity profiles. This attitude changed after the "Thalidomide tragedy". From 1957 till 1961 a pharmaceutical with the active agent Thalidomide, in the German-speaking market sold under the name "Contergan", was commonly used as sedative and barbiturate-like drug due to the low adverse effects and the positive side effects on the morning sickness, in particular from pregnant women. Though, Contergan was classified as nonhazardous after rodent test series before bringing into the market, teratogenic effects on humans were observed thereafter. The administration of racemic thalidomide went hand in hand with an unusual high rate of miscarriages and extreme malformation of surviving newborns. It was recognized that only the (*R*)-enantiomer possessed the desirable effects, while the (*S*)-enantiomer caused the teratogenicity [13], [15]. However, more recent studies found out that (*R*)-thalidomide undergoes a fast-rate racemization in the human body and therefore the tragedy may also have happened with enantiomerically pure (*R*)-thalidomide [16], [17]. Overall, more than 10,000 babies in 46 countries were born with serious physical deformities [16]. Due to this tragic episode in pharmaceutical research, the potential risk of chiral drug compounds became a much-discussed topic. Drug stereochemistry advanced to a key issue in the development of new pharmaceutically active ingredients [13], [18-20].

We encounter enantiomers with different sensory properties in daily life, as well. A well-known example is the sweetener aspartame, where the (*R*)-enantiomer has a sweet taste,

while the (*S*)-enantiomer tastes bitterly [2]. Also the flavor and taste of chiral flavoring agents depends often on the configuration of the chiral center. With its orange odor, (*R*)-limonene is used as a flavor, whereas (*S*)-limonene has an unsavory turpentine smell [2].

3.2.3 Enantioseparation – Direct and indirect approach

As a result of increasing knowledge of the importance of enantioselectivity in drug research, in 1992 a workshop of the Drug Information Association (DIA) was held, concerning with the regulatory requirements on chiral drugs [21]. Regulatory issues were discussed and shortly afterwards regulatory guidance documents were published in the U.S., Canada, EU and Japan [22]. In 2000, the International Conference of Harmonization (ICH) summarized and adapted these guidelines to a consistent regulatory guidance [23]. Nowadays, single-enantiomeric drug sales constitute a significant percentage of top-selling drugs. In 2009, the worldwide sales amounted to over 150 billions USD [24]. But also in other fields of research, like in food production, enantioseparation of racemic compounds is of great interest [2].

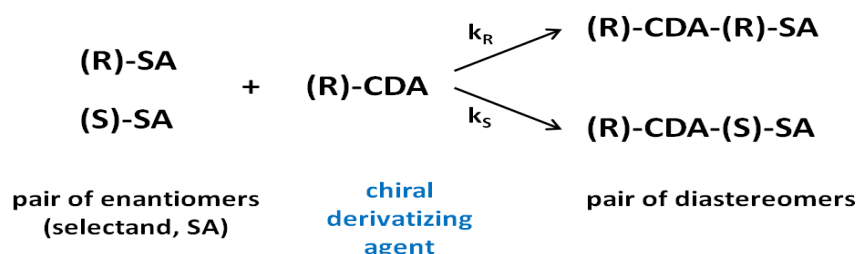
The most important requirements on enantioseparation are high sensitivity and good reproducibility. Besides separation of racemic mixtures with crystallization [25], capillary electrophoresis [26] and simulated moving bed technology [27], the enantioselective liquid chromatography LC is used for this approach quite commonly and effectively [13]. In this application area, LC is mainly used analytically for determination of enantiomeric purity [11], [12], but of course also preparative LC is most common.

As outlined above (q.v. 3.2.1), enantiomers have identical physicochemical properties. They migrate with same velocity through the column and capillary, respectively, and thus, no separation is obtained in an achiral environment such as e.g. in conventional reversed-phase liquid chromatography (RP-LC) or in gas chromatography (GC) with achiral stationary phases. To be distinguishable, the common approach for enantiomer separation technologies is the conversion of enantiomers to diastereomers or diastereomeric associates which can be separated due to their different physicochemical properties. Generally two different modes can be used, the indirect and the direct approach [2], [13].

The main principle of the indirect approach is the formation of diastereomers (Figure 4). This is realized with a covalent linkage between the selectand (SA), which is the pair of

enantiomers that should be separated, and an enantiomerically pure chiral auxiliary. The derivatization of the enantiomeric mixture with an enantiomerically pure chiral derivatizing agent (CDA) (*e.g.* Mosher's reagent, ortho-phthalaldehyde (OPA) plus a chiral thiol) yields a pair of diastereomers to each other. By reason of the formed covalent bond the reaction is irreversible and the products chemically stable. For separation purposes achiral systems like RP-LC can then be applied. Disadvantages of the indirect approach are besides the irreversibility also the necessity of a high enantiomeric purity of the CDA. In case of impurities of the CDA, undesirable side-products can be formed. Furthermore, the obviation of a kinetic racemate resolution has to be considered. This problem occurs when the reaction rate constants for the derivatization reaction of both enantiomers, k_R and k_S , are different and the reaction is stopped before completion. As consequence of different reaction rates, the origin enantiomeric ratio deviates from the half-and-half racemic ratio. Possibilities to avoid this phenomenon are the complete conversion of the reaction by addition of CDA in excess [2], [13].

Indirect approach



Direct approach

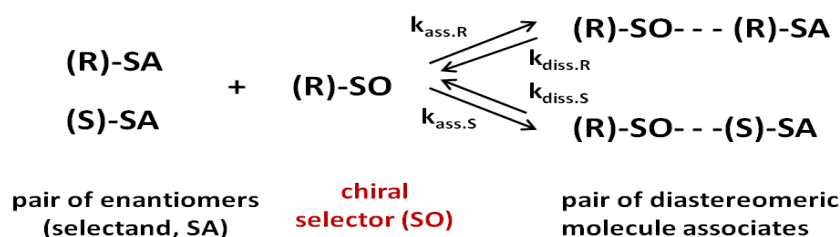


Figure 4: Main principle of indirect and direct approach in enantiomeric separation, adapted from [2].

Contrariwise, the direct approach is based upon the reversible formation of diastereomeric molecule associates (Figure 4). By interaction of a chiral selector (SO) with both enantiomers, diastereomeric associates with different binding strength are formed. There

are two experimental modes of the direct approach: the chiral stationary phase (CSP) mode and the chiral mobile phase (CMP) mode.

The CSP mode is nowadays the most commonly used method for enantioseparation with HPLC and GC. Thereby, the chiral SO is covalently linked or physically adsorbed onto a chromatographic support material, while the mobile phase does not contain any chiral compounds. By reaction of the enantiomers of the selectand (SA) with the chiral SO, diastereomeric complexes are formed on the surface of the stationary phase. According to their stereochemistry, the enantiomers interact differently with the CSP. The enantiomer which forms the more stable diastereomeric complex or adsorbate is more retarded compared to the less stable and will therefore elute later. Hence, a separation is obtained due to different retention times. Thus, the enantiomers are detected separately according to their elution order, whereupon the detector response factor is the same for both enantiomers. The advantages of this method are the absence of selector waste and the possibility to separate underivatizable compounds. Furthermore, a variation of the CSP according to the compound to be separated makes this method accessible for a broad range of applications (q.v. 3.3).

Less common in HPLC, CMP mode is accomplished with an achiral stationary phase and an eluent containing a chiral selector as additive. Thus, CMP method is possible in HPLC, but also in capillary electrophoresis (CE) and cation-exchange capacity (CEC). After the formation of diastereomeric SO-SA complexes, they are adsorbed to the stationary phase. Both diastereomeric complexes are adsorbed with different strength and therefore, they can be eluted separately with different elution times and the enantiomers can be detected as diastereomeric associates. Because of the residual selector, the response may be different of the one from the pure enantiomers. These distinct response factors have to be corrected after measurement *via* peak area ratio, which is a major drawback of the CMP mode. Due to the high selector waste, precious selectors are not applicable. Furthermore, the adaption for different selectands depends on the solubility of the designated additive in the eluent [2], [13].

As indicated above, both methods are based on the different interaction of enantiomers with the chiral selector. The basic principle of the chiral recognition of compounds with different stereochemistry is the same as for chiral recognition in biological systems. In 1952 K. Dalgliesh created an illustrative model to describe this phenomenon, the so-called "3-

point-interaction model" [28] (Figure 5). It considers a chiral stationary phase which is immobilized onto a preferably inert suitable support. By linkage with an, as possible, inert achiral spacer a chiral selector is bond on the CSP. This selector incorporates 3 different interaction sites A, B and C on its surface, which are accessible for interactions with the SA. The SA exhibits three complementary interaction sites. If they are in a suitable 3-dimensional orientation and spatial arrangement, an interaction between SO and SA can take place. A perfect match of the interaction groups of one enantiomer of the SA and SO is called "ideal fit", the opposite enantiomer depicts the "non-ideal fit". Due to the better fit and thus due to a larger binding constant for the SO-SA equilibrium reaction, the "ideal fit" enantiomer is bond stronger and hence, it will be eluted later from the column than the spatial mismatching one [2].

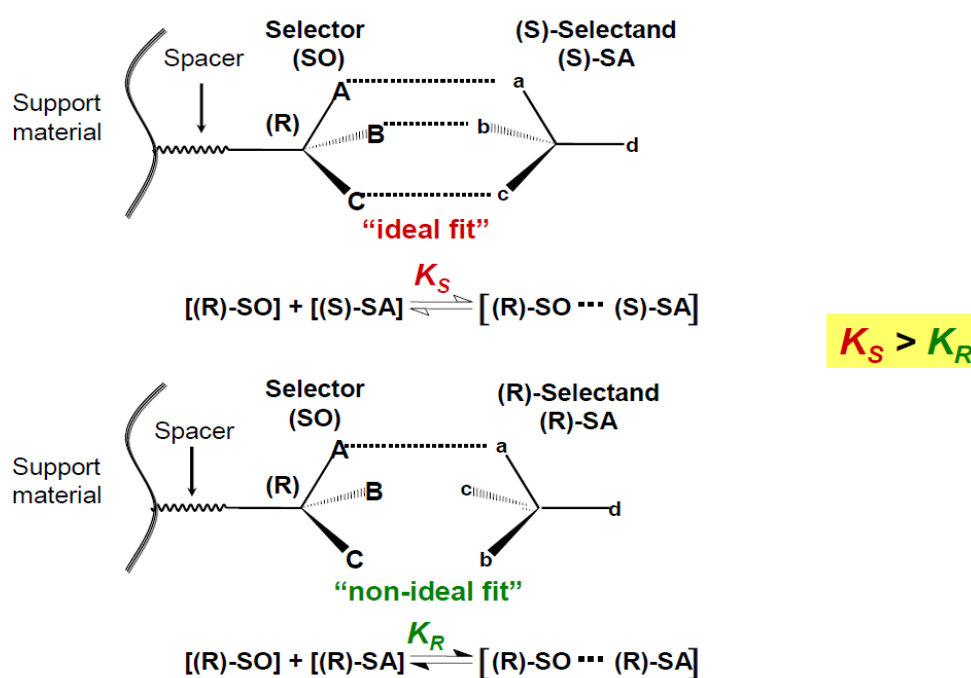


Figure 5: 3-point interaction model according to Dalgliesh, illustrating the "ideal fit" and the "non-ideal fit" [2]. Within this example, the (S)-SA is preferred due to a perfect spatial match of the interaction sites of SA and SO.

The forces in chiral recognition between SO and SA are non-covalent bonds. These can either be repulsive or attractive forces. The major group of these forces are electrostatic interactions. Additionally, there are ionic interactions between positively and negatively charged groups, hydrogen bondings, dipole-dipole- and π - π -interactions. Furthermore, hydrophobic interactions between lipophilic moieties of SO and SA are conducive to the

chiral recognition, but depend strongly on the type of mobile phase.

A main point to be considered is the influence of the eluent. The electrostatic interactions can be decreased by the increase of the polarity of the eluent. Hydrophobic interactions may play only an important role in aqueous and hydroorganic eluents, respectively. Furthermore, chiral recognition is also influenced by steric factors and barriers, *e.g.* bulky residues [2].

3.3 HPLC separation – chiral stationary phases

One important point to consider in direct enantioselective HPLC separation is the selection of a convenient column material for the respective separation problem. Therefore, not only the different characteristics of available CSP should be considered, but also the principal application spectra and the operation conditions. Generally, three types of chiral stationary phases can be distinguished: support modified with chiral moieties (brush type), chiral organic polymer (polymer type), and molecular imprinted polymers (MIP type) CSPs [29]. The most commonly employed chiral SO for HPLC enantiomer separation are subclassified according to their molecular mass into macromolecular, macrocyclic, and low-molecular mass SOs. Figure 6 represents an overview of the most important commercially available CSPs. Depending on the characteristics of the compound (*e.g.* acidic, basic, bulky, hydrophobic) to be separated, the SOs has to be adapted. Several suppliers offer in total more than 100 CSPs for different kind of analytes and separation needs [30].

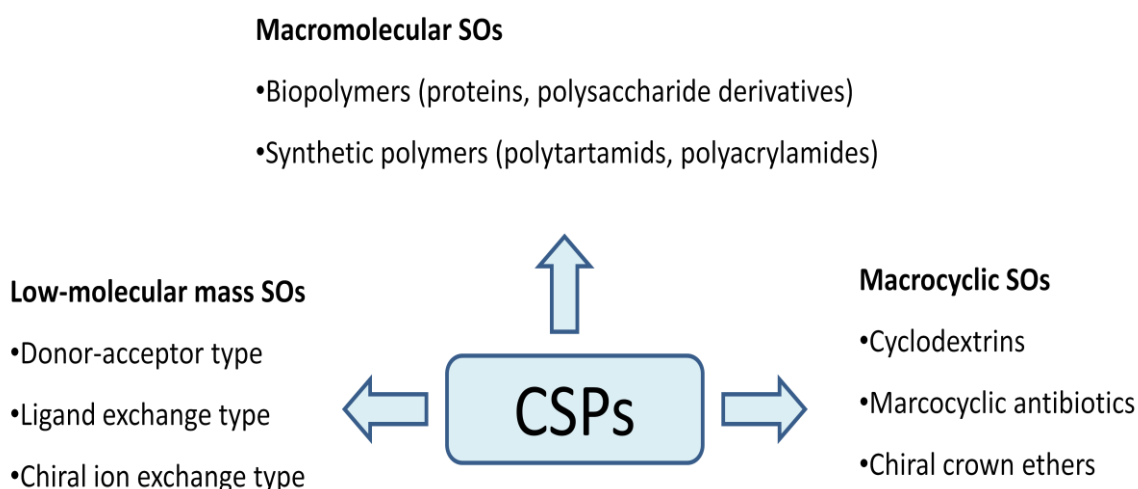


Figure 6: Overview of common commercially available CSPs and their classification, modified after [2] .

Besides crown ether and glycopeptides CSPs, the chiral ion exchange type CSPs are counted among the ionizable CSPs. Chiral ion exchangers utilize ionizable SOs and take advantage of long-range ionic interaction between oppositely charged SO and SA for ion-pairing. This is the driving force for solute adsorption and retention. Chiral ion exchange type CSPs based on miscellaneous materials were developed for different applications. For separation of chiral acids, weak chiral anion-exchange (WAX) phases e.g. based on cinchona alkaloids may be employed [3], while strong chiral cation-exchanger (SCX) based on chiral amino sulfonic acids or carboxylic acids can be used for separation of basic compounds [31]. Meanwhile, zwitterionic ion-exchangers (ZWIX) were developed, obtained by merging structural elements of anion and cation exchangers. Their purpose is the separation of chiral acids, bases and chiral zwitterionic compounds, by way of example of amino acids and peptides [32], [33].

3.3.1 Quinidine (QD) and Quinine (QN), Homotau-QD type CSPs

The commercially available chiral anion-exchangers Chiralpak QN-AX and Chiralpak QD-AX with cinchona carbamate SO were developed by Lämmerhofer and Lindner[3]. AX derives from the weak anion exchanger (WAX) characteristics, while QN and QD specify the type of cinchona alkaloid which is used as backbone of the selectors. These columns exhibit a broad applicability for enantiomer separation of chiral acids, especially in polar organic and reversed-phase modes. As cation exchange groups carboxylic-, sulfonic-, sulfonic-, phosphoric-, phosphonic- and phosphinic acids, respectively, may be employed [30]. The structure of QN and QD is built up by a planar quinoline and a rigid quinuclidine ring, both connected by a secondary methyl alcohol bridge (Figure 2). Because of this semirigid framework these molecules may be seen as promising SO molecules. By radical reaction attack of the thiogroup to the vinyl doublebound of the alkaloid, the alkaloid residue can be anchored to the γ -mercaptopropyl silica gel. It refers to the so called thiol-ene reaction type [3].

As mentioned in chapter 3.2, QN and QD are pseudo-enantiomers (diastereomers which act quasi like enantiomeres) with 5 stereogenic centers, whereat they exhibit opposite absolute configuration at C8 and C9 (Figure 2). Out of this stereoantimeric difference the same enantioselectivity, but inversed elution orders arise. N-protected (D)-amino acids elute first

on QN-based WAX-CSP, while (L)-amino acid derivatives elute first when using QD-based WAX-CSP.

Intermolecular interactions may take place at several sites of the molecules. The basic aliphatic nitrogen group of the quinuclidine ring permits electrostatic interactions, while the hydrogen-donor-acceptor site of the carbamate group allows hydrogen bonding and dipole-dipole interactions. At the π -basic quinoline ring intermolecular π - π -interactions may happen. Furthermore, the bulky quinuclidine group and the planar quinoline ring cause steric interactions [3].

In slightly acidic mobile phases, the quinuclidine nitrogen acts, after protonation, as the fix-charge of the chiral AX. Accordingly, acidic analytes get primarily retained by an ion-pairing process, while the buffer anions (counterions) act as competitors for the solute at the charge center of the ion-exchanger. Hence, one should bear in mind that type and concentration of the buffer anions in the eluent play a major role in variation of the solute retention [30].

Beside type and concentration of buffer and counterions, the retention and enantioselectivity may be controlled by the sort of organic modifier and the temperature. Moreover, the derivatization of the functional groups of the cinchona alkaloid SO backbone offers the possibility to optimize the stereoselectivity [34]. Preferentially, cinchona alkaloid-based ion exchange CSPs are used in polar organic or RP-mode. Especially for the separation of N-derivatized α -, β - and γ -amino acids in hydro-organic mobile phase these CSPs exhibit great achievements [35].

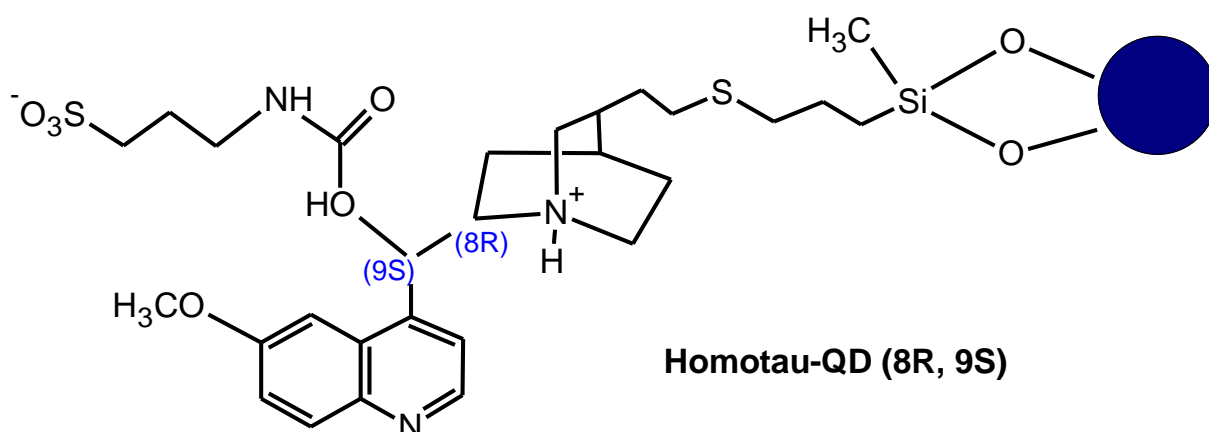


Figure 7: Homotau-QD (8R, 9S), an aminosulfonic acid-cinchona-based SCX-WAX/ZWIX-type CSP.

The Homotau-QD is a zwitterionic (ZWIX)-type CSP which combines the SCX-type structure of the homotaurine (aminopropanesulfonic acid) and the WAX-type structure of quinidine. In 2008, Hoffmann *et al.* first published the fusion of a cinchona-alkaloid WAX modified with sulfonic acid-based SCX structures *via* a carbamate bond to obtain a ZWIX-type chiral selector [32]. These CSPs may achieve a sufficient retention and enantioseparation of amphoteric analytes, for instance amino acids and peptides, by means of simultaneous double ion pairing of their charged functional groups. However, this cannot be achieved by using the corresponding SCX or WAX-type CSPs because of the electrostatic repulsion applied on the second charge of the zwitterionic analyte. This leads to affected retention and a deficiency of enantioselectivity. As mentioned above for WAX-type CSPs, also Homotau-QD and Homotau-QN show the same enantioselectivity, but reversed elution order, which may be quite convenient for preparative but also analytical purposes. These CSPs, run in non-aqueous, polarorganic mobile phase mode, turned out as particularly favorable for the separation of small peptides [36].

3.4 Gold nanoparticles - applications and characteristics

During the last decades intensive research, aiming the development of materials at nanometric scale and to investigate their intrinsic properties, has been done. Two phenomena may occur by reducing materials to nanometer dimensions: First the so-called quantum size effect, which occurs when a material shows a drastic change in its physical-chemical properties due to the reduction of size. The second feature is the increased surface area to volume ratio compared with bulky particles [37]. In particular, gold nanoparticles (GNPs) are quite advantageous due to the well-investigated procedures to control the size, monodispersity, morphology, and surface chemistry [37]. Another benefit is the straightforward modification of GNP surface is its straightforward reaction with thiol containing molecules. Thereby, the strong dative gold-sulfur bond is utilized for the formation of self-assembled monolayer. This strategy enables their use in many different biological assemblies [38, 39]. Application areas are, for instance, the use as biosensors [37], they are utilized for DNA detection, peptide/protein analysis and enrichment [40-42], for enzymatic activity assays [43] and cellular analysis [39]. Moreover, they may also be used in separation sciences [44, 45] and sample preparation [46].

Another interesting feature concerning GNPs is their characteristic surface plasmon resonance (SPR) band. Due to collective oscillations of the electrons at the conduction band of the nanoparticle surface, a broad adsorption band within the visible region around 520 nm arises [38]. These properties are often used in chemical sensing and imaging, but also utilized for determination of size and concentration of the GNPs (q.v. 3.4.2).

3.4.1 Preparation of GNPs

The preparation of GNPs in a range of 15 – 60 nm can be done easily and economically by reduction of gold(III)chloride. One of the most common synthesis procedures is the method according to Frens [47] and Turkevich [48], in which gold(III)chloride is not only reduced, but also simultaneously stabilized with sodium citrate whereby citrate introduces an electrostatic stabilization (see below). Hence, contrary to other reducing agents, no further stabilizing agent is required.

The size of the nanoparticles can be regulated by variation of the molar ratio of gold(III)/sodium citrate (reducing agent), (q.v. 4.2.1). Thereby, spherically shaped GNPs are obtained. A key issue in nanoparticle preparation is the stability of the colloidal particles. Due to forces such as Brownian motion, convection and so forth, the particles converge and may collide. When the distance between two particles is small enough, they get attracted by the “Van-der-Waals” force. In the case of absence of counteracting forces, the particles agglomerate. To increase the stability, a balance of the attractive and repulsive forces is necessary. There are two possibilities of particle stabilization, the electrostatic stabilization and the polymeric stabilization, respectively [49, 50].

The main principle of the electrostatic stabilization of colloids is the balancing of the attractive "Van-der-Waals" forces with the repulsive Coulomb forces between the negatively charged colloidal particles. One important phenomenon in the mechanism of the electrostatic stabilization is the electric double layer. For example, adsorbing negatively charged ions of the dispersion medium on the particle surface, the colloidal particles receive a negative electric charge generated by the sodium ions on the liquid bulk phase. These negatively charged particles attract positive counterions. The double layer is the layer, which surround the particle, the adsorbed ions on the particle and the film of the countercharged dispersion medium. This layer is electrically neutral and consists of three parts (Figure 8).

The surface charge is determined by the charged ions, adsorbed on the particle surface. The stern layer consists of oppositely charged counterions which are attracted and closely attached to the particle surface due to the electrostatic forces. The film of dispersion medium surrounding the particle is the so-called diffuse layer. Because of the electrostatic forces of the charged particle, free ions with a higher concentration of the counterions are affected in this layer. The electrical potential inside the electric double layer has the maximum value on the particle surface. By increasing the distance from the surface, the potential decreases till it reaches 0 at borderline of the electric double layer [49-51].

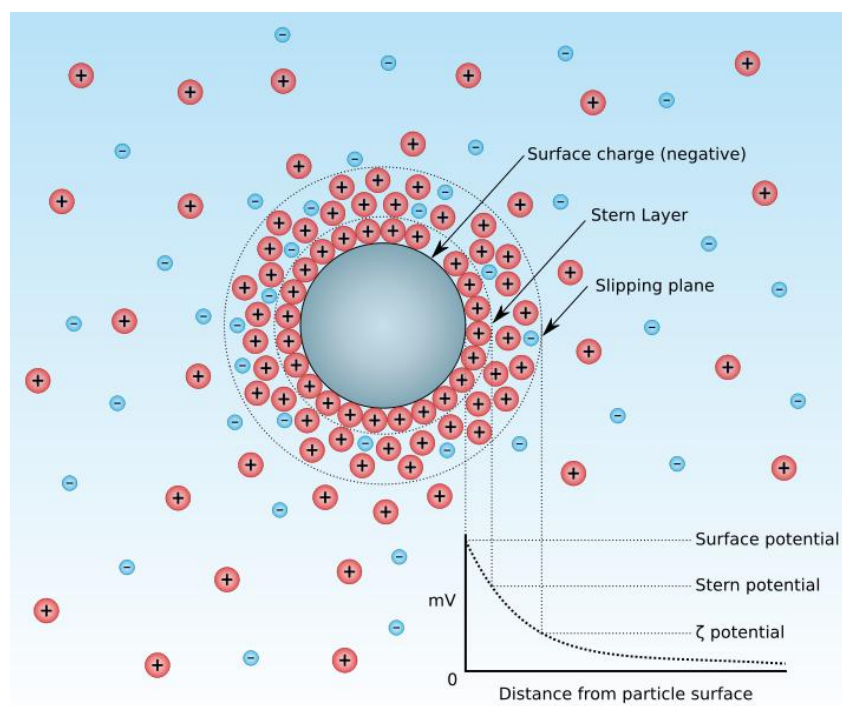


Figure 8: Electric double layer, consisting of three parts: The surface charge, the stern layer and the diffuse layer [49].

When moving through the dispersion medium, the colloidal particle is surrounded by a layer of liquid, which remains attached to the particle. The so-called slipping plane or shearplane is the boundary of this layer and the value of its electric potential is the zeta potential (ZP), with the unit mV. The ZP is the potential difference between dispersion medium and the stationary layer, which is attached to the dispersed particle [52]. This parameter plays an important role in the theory of interaction between colloidal particles as described in the DLVO theory.

Developed in the 1940s, the DLVO theory explains the stability of colloidal systems and

describes the forces between charged surfaces. Figure 9 describes the potential energy of two particles interacting with each other. The distance between two particles corresponding to their stable equilibrium is determined by the minimum of the potential energy. At this distance, the particles form a loose agglomeration, which is redispersible. With further decrease of the distance between the particles and pass of the potential barrier aggregates are formed.

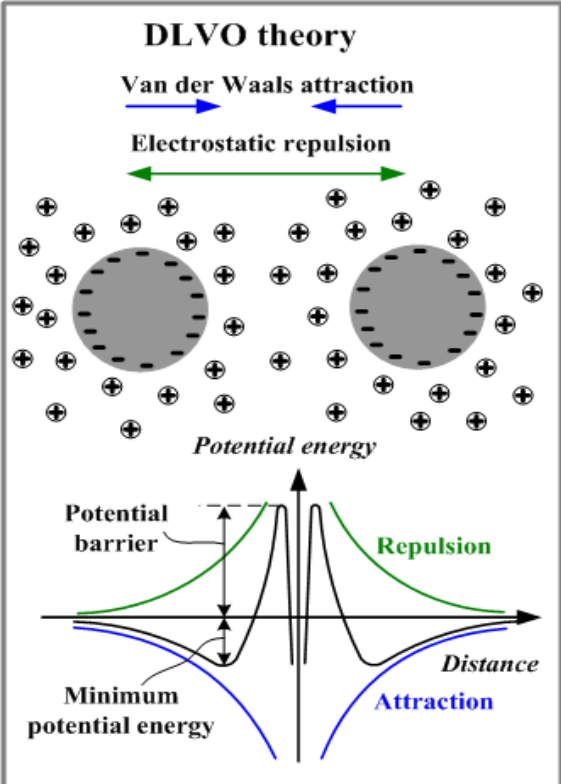


Figure 9: Illustration of the operating forces on two particles interacting with each other in the DLVO theory [49].

The name DLVO derives from the 4 scientists Deryagin, Landau, Vewey, and Overbeek [53, 54]. It is concerned with the combination of the "Van-der-Waals" attraction and the electrostatic repulsion of the double layer in aqueous dispersions. By supposing a uniformly distributed electric charge over the solid surface and a distribution of the ions depending on the electrostatic force, the Brownian motion and the entropic dispersion, the DVLO theory gives a good explanation of the interaction between two approaching particles.

According to theory, the stability of colloids is determined by the potential energy of the particles (V_T) as the sum of the potential energy of the attractive interaction, deriving from the "Van-der-Waals" force (V_A), of the repulsive electrostatic interaction (V_R) and of the potential energy of the solvent (V_S) (eq.2).

$$(eq.2) \quad V_T = V_A + V_R + V_S$$

For spherical particles the "Van-der-Waals" attractive potential energy V_A may be described as (eq. 3):

$$(eq.3) \quad V_A = -\frac{Ar}{(12x)}$$

A.....Hamaker constant

r.....particle radius

x.....distance between the particles' surfaces

The electric repulsive potential energy V_R may be described as (eq.4):

$$(eq.4) \quad V_R = 2\pi\epsilon\epsilon_0r\zeta^2e^{-\kappa x}$$

ϵdielectric constant of the solvent

ϵ_0vacuum permittivity

ζzeta potential

κfunction of the ionic concentration, where κ^{-1} is the characteristic length of the electric double layer

Considering all three terms V_R , V_A , and V_S , the stability of a spherical particle in solution can be calculated [49, 51].

The second possibility of stabilization is the addition of polymeric molecules to the dispersion medium to prevent aggregation of the particles (Figure 10) [49]. By addition of the polymeric molecules, attractive forces between particles are sterically hindered. Two types of polymeric stabilization may be distinguished. First, the steric stabilization, where polymeric molecules are attached to the particle surface, has to be mentioned. Due to a formed coat, a steric obstruction is generated and separates the particles from each other. The second one is the depletion stabilization of colloids, where free polymeric molecules are added to the dispersion medium. Thereby, they create a repulsive force between the approaching particles. A possible polymeric additive would be the nonionic tenside Polysorbate20 (Tween20) (q.v. 4.2.5) [49, 50, 55].

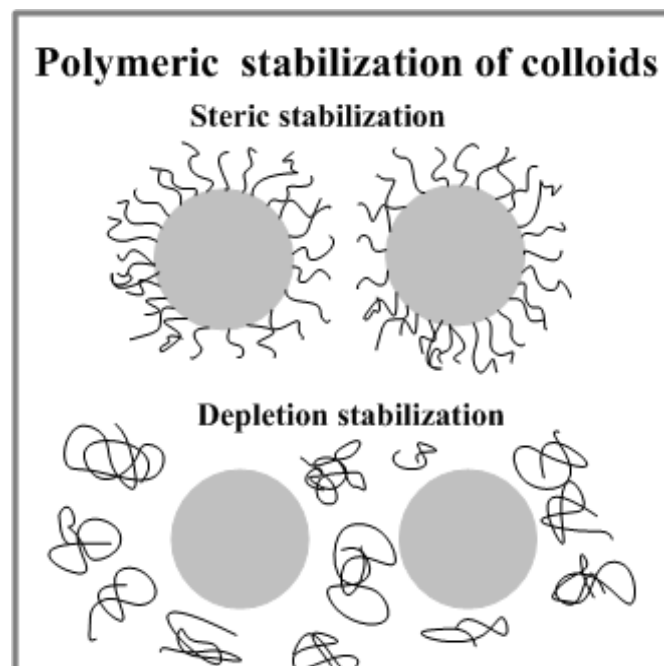


Figure 10: Two approaches of polymeric stabilization of colloids, either by steric or by depletion stabilization [49].

3.4.2 Characterization of GNPs by SPR, DLS and ZP

Surface Plasmon resonance (SPR)

The characteristic surface plasmon resonance (SPR) band at a wavelength of about 520 nm is one favorable advantage of the metallic GNPs compared to other nanoparticle materials. This phenomenon occurs by coupling of the electrons of the conduction band of GNPs with the electric field of the incident light at a certain resonant frequency. Thereby, a plasmonic oscillation on the surface of the nanoparticle is generated, known as the SPR [56]. Measuring the SPR spectra, informations about the size, aggregation properties, and the concentration of GNP solutions can be obtained according to the Mie theory [57], [58]. Contrary to other methods such as transmission electron microscopy (TEM), scanning electron microscope (SEM), atomic force microscope (AFM), and further microscopic techniques, photometric assays are a low cost and fast alternative for GNP characterization in the range of 5 – 100 nm [56]. Furthermore, rapid monitoring during all preparative stages, for example immobilization processes, is possible [57]. Figure 11 shows the characteristic SPR band of sodium citrate stabilized GNPs in a size range of about 30 nm in diameter. A decrease of the absorbance maximum is observed from citrate stabilized GNPs to carboxy-pegylated GNPs (GNP-PEG₇-COOH) and to enzyme immobilized GNP (GNP@enzyme) (q.v. 5.1.1).

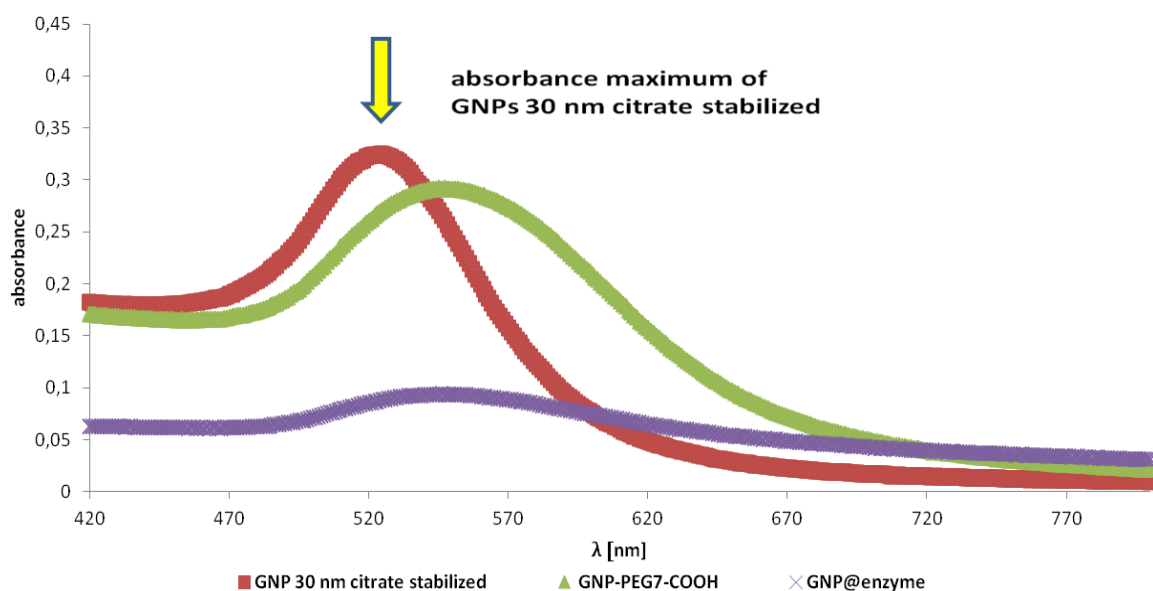


Figure 11: SPR spectra of GNPs with different immobilization states. The characteristic absorbance maximum (SPR band) at 520 nm is most distinct for the citrate stabilized 30 nm GNPs and decreases for ligand modified GNPs (GNP-PEG₇-COOH) and enzyme immobilized GNPs (GNP@enzyme).

Dynamic light scattering (DLS)

The size characterization is an important tool for characterization of colloidal GNPs. Different methods are available for size and size distribution determination to control that the particles are homogenous in diameter and no aggregates were formed. Electron microscopy techniques are used for accurate size characterization. The result is a number-based particle size, as the number of different sized particles are counted.

Dynamic light scattering (DLS) is a fast, low-cost and non-invasive technique for size distribution measurements. The time-dependent fluctuations and the intensity of scattered light from a particle suspension, which are undergoing the Brownian motion, are measured. The Brownian motion is the random movement of the particles, caused by strafing of the solvent molecules in the suspension. Because the Brownian motion is decreasing with the increasing size of the particle, smaller particles move faster. An important point to be considered is a stable, accurately known temperature for correct value of the viscosity and to avoid non-random movement due to convection currents. Analyzing the intensity fluctuations, a determination of the translational diffusion coefficients (which specify the velocity of the Brownian motion) is possible. The particle size may be calculated through the Stokes-Einstein equation [59-61]. (eq.5)

$$(eq.5) \quad d(H) = \frac{kT}{3\pi\eta D}$$

d(H)..... hydrodynamic diameter

D.....translational diffusion coefficient

k.....Boltzman's constant

T.....absolute temperature

ηviscosity of the solvent

One has to keep in mind, that the measured value indicates the diffusion of a particle within a fluid, therefore, it is referred as the hydrodynamic diameter and thus, the particle size is always overestimated. The diffusion coefficient D of the particle depends on several parameters, such as size of the particle core, surface structure, concentration and ion type (ion strength) in the medium.

By changing the thickness of the electric double layer, the ion concentration in the medium

is able to affect the particle diffusion speed. Thus, a medium with low conductivity will lead to an extended double layer and a reduction of the diffusion speed and therefore result in a larger apparent hydrodynamic diameter, while a higher conductivity media will suppress the layer thickness and the hydrodynamic diameter. Also a surface modification may affect the diffusion speed and thus the apparent size of the particle. When the adsorbed polymer layer is standing out into the medium, the diffusion speed will be reduced more than a layer which is lying flat on the surface. Unambiguous and correct size distribution measurement may only be given for spherical particles. For non-spherical particles, the diameter of a sphere with the same translational diffusion speed as the particle is obtained [61].

A typical DLS system is composed of six main components. The sample in a cell is illuminated by a light source from a laser. The scattered light is then measured by a detector, which is, depending on the particular model, either placed at 173° or 90° to the cell. To avoid detector saturation the intensity of scattered light can be reduced by varying the laser intensity by an attenuator. Highly scattering samples need lower input intensity, while for samples which scatter light less the intensity has to be increased. This is regulated by the attenuator. The signal from the detector passes to the correlator, a digital processing board. Its function is the comparison of the scattering intensity at successive time intervals. Hence, the rate at which the intensity is varying may be derived. The obtained information from the correlator is passed to a computer and the size information is analyzed with an appropriate software [61].

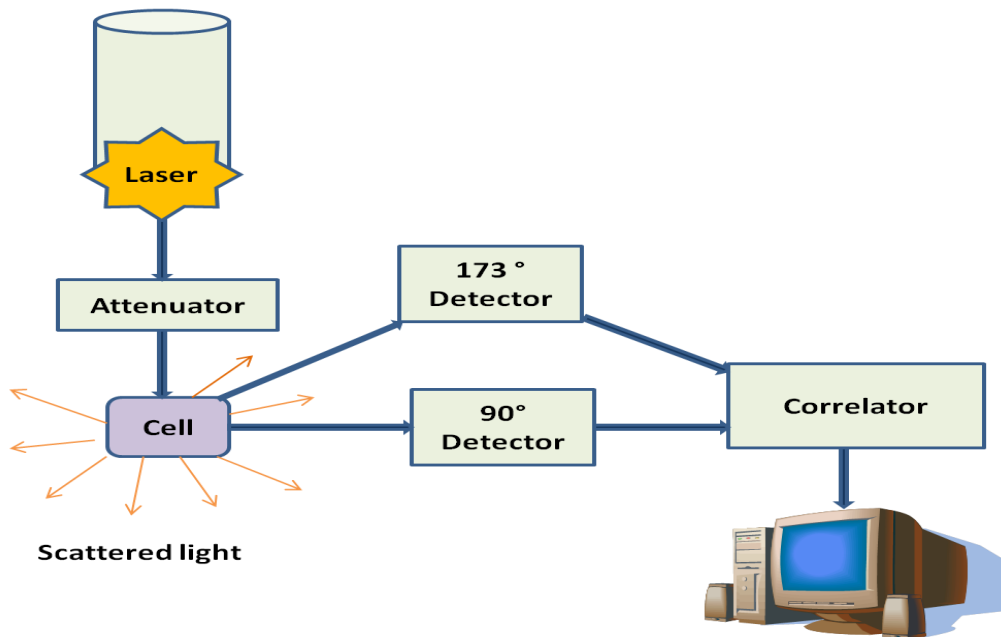


Figure 12: Constituent parts of a typical DLS system: Laser, attenuator, cell, detector, correlator and computer, modified after [61].

Zeta potential (ZP)

The ZP (definition see 3.4.1) is a physical property which may predict the long-term stability of a colloidal system. If the particles in a suspension have high ZPs, either negative or positive, they will repel each other and thus, the tendency to form aggregates decreases. Otherwise, if the particles have low ZPs, there is no prevention for aggregation. Generally, the boundary between stable or unstable colloidal systems is given at 30 mV, either positive or negative. Above this value, suspensions can be regarded as stable. However, for particles with different density than the dispersant, sedimentation is still possible which can cause a close packed agglomeration.

There are several factors affecting the ZP which have to be considered. First of all, the pH is an important influencing parameter [62]. For instance, we observe a particle in a suspension with a negative ZP. After addition of alkali the negative potential of the particles will increase, while an addition of acid will first lead to a neutral potential and, after further addition, to a positive potential. Therefore, a zeta potential curve plotted against a pH curve is positive at low pH values and is decreasing up to negative values with increasing pH. The least stable point of a colloidal system is the isoelectric point, the point where the pH curve passes through the zero ZP. Second, the conductivity is an important point which has to

be considered in ZP measurements, because the thickness of the double layer (κ^{-1}) depends upon the concentration of ions in solution. The higher the ionic strength, the more compressed and therefore thinner the double layer becomes. Furthermore, the effect of the concentration of a formulation component may influence the ZP value. This can be used to achieve the maximum stability by variation of this formulation component [62].

Resulting from the existence of electrical charges on the surface of particles, an interaction with an applied electric field takes place. These effects can be summarized as electrokinetic effects utilized e.g. in electrophoresis. After applying an electric field to an electrolyte, the charged particles are attracted towards the electrode of opposite charge. This movement is opposed by viscous forces, acting on the particles. When the equilibrium between these opposing forces is reached, the movement of the particles undergoes a constant velocity. This velocity, which is referred to as electrophoretic mobility, is contingent upon the strength of the electric field, the dielectric constant and viscosity of the medium and the ZP. The relation for the ZP and the electrophoretic mobility U_E is the Henry equation (eq.6).

$$(eq.6) \quad U_E = \frac{2\varepsilon\zeta f(\kappa a)}{3\eta}$$

U_Eelectrophoretic mobility

ζzeta potential

εdielectric constant

ηviscosity

$f(\kappa a)$Henry's function

For electrophoretic determinations of ZP in aqueous media with low electrolytic concentrations, the term $f(\kappa a)$ is considered as 1.5, which is referred to as the Smoluchowski approximation. For particles larger than 0.2 microns, which fit the Smoluchowski model, an easy and straightforward calculation of the ZP from the electrophoretic mobility is possible. For small particles in non-aqueous media, $f(\kappa a)$ becomes 1.0 the so-called Huckel approximation [52, 62].

For measurements of the electrophoretic mobility, a capillary cell with electrodes at each end is necessary to apply a potential. When the particles move towards this electrode, the velocity is measured as their mobility. ZP measurement systems consist of the same six main

components like a DLS measurement system (Figure 12: Constituent parts of a typical DLS system: Laser, attenuator, cell, detector, correlator and computer, modified after [61]). Thereby, the light source from the laser is divided in an incident and a reference beam. The incident light passes the cell, and the scattered light is detected at an angle of 13° . After the application of an electric field to the cell, the particles which are moving through the cell cause a fluctuation of the incident light. Thereby, the frequency of the scattered light is proportional to the particle speed. This information is passed from a digital signal processor to a computer. The software produces a frequency spectrum and calculates the electrophoretic mobility and hence, the ZP. To regulate the laser intensity, an attenuator is required, which works equally to the DLS measurement system. Additional compensation optics may be installed. Thus, differences in the cell wall thickness and dispersant refraction are balanced [62].

3.4.3 Immobilization chemistry

One advantage of GNPs is the simple possibility of surface modification for functionalization and/or stabilization [63]. By dative binding and self-assembling of bifunctional ligands, which contain thiol groups, functional groups can be introduced. Another possibility is a ligand exchange with thiol containing molecules. The selected biomolecules, for instance a protein or enzymes, can be either attached directly to the GNPs by ionic and hydrophobic interactions, or immobilized *via* linkers [64].

By means of dative bonds, also known as coordinate covalent bonds, thiol-containing molecules can interact with metal ions and metal surfaces. This type of bond is formed, when the pair of electrons derives from one ligand, in contrast to covalent linkages, where each of the two atoms in a bond contribute one electron [65]. In metal-thiol dative bonds, the unshared pair of electrons deriving from the sulfur atom forms a dative bond with a metal atom. The same is also possible for disulfides without prior reduction. In general, also other atoms containing a lone pair of electrons may be used to form coordinate bonds. For instance, oxygen- and nitrogen-containing organic molecules are used, as well as bidentate ligands such as DOPA. However, thiol organic compounds are nowadays commonly used to coat metallic surfaces and particles to form biocompatible layers or to immobilize functional groups for further conjugation of biomolecules [65]. Already in 1991 Primes and Whitesides

published their application of thiol-containing aliphatic/PEG linkers, which were used to form self-assembled monolayers (SAMs) on gold particles [66].

SAMs are ordered assemblies of molecules, formed by adsorption of active surfactants on a solid surface. The order in these systems arises out of spontaneous chemical synthesis at the interface after the achievement of equilibrium. The most frequently used SAMs consist of functionalized long-chain hydrocarbons. In the field of science and technology SAMs are highly relevant, not only due to their highly ordered constitution in contrast to ultrathin films, but also due to their ability to incorporate a wide range of groups both in the alkyl chain and at the chain terminus. Therefore, they show a high flexibility in production of surfaces with specific interactions. Because of their stable and dense structure, SAMs may have an application field in corrosion prevention, wear protection etc. Furthermore, they are employed for chemical and biochemical sensing [67].

For further immobilization of biomolecules onto functionalized GNPs, zero-length crosslinkers may be used. These are the smallest available reagent systems for bioconjugation. Forming a bond between two molecules without any additional atoms, these compounds are able to mediate the conjugation. One category of these zero-length crosslinkers is carbodiimide, which are used to mediate the formation of amide linkages between carboxylates and amines or phosphoramidate linkages between phosphates and amines. Their high efficiency in forming conjugates and their broad application field makes them probably the most popular type of zero-length crosslinker. Carbodiimides may be used for conjugation between two proteins, between a peptide and a protein, between an oligonucleotide and a protein, between a biomolecule and a surface or particle (e.g. GNPs), or any combination of these with small molecules. Carbodiimides may be distinguished into water-soluble and water-insoluble. Because biological macromolecules are soluble in aqueous buffer solutions, the water-soluble ones are the most common choice. Besides the carbodiimide itself is soluble, but also the isourea, a coproduct of the reaction. This enables simple purification. In peptide synthesis and conjugation involving water-insoluble molecules, water-insoluble carbodiimides are used [65].

1-ethyl-3-(3-dimethylaminopropyl)carbodiimide hydrochloride (EDC) is one of the most frequently used crosslinking agent for conjugation of biological molecules with carboxylates and amine groups. EDC reacts with a carboxylate group and forms an active ester leaving group. A main issue of this reactive complex is the slow reaction with amines and the fast

hydrolyzation in aqueous solutions. If the target amine and the active carboxylate cannot react before the active complex is hydrolyzed, no successful coupling can be obtained. In particular, this problem occurs when the target molecule is in low concentration compared to water, as in the case of protein molecules. By addition of N-hydroxy-succinimide (NHS) or of water-soluble sulfo-NHS to the EDC reactions, an increase of solubility and stability of the intermediate may be achieved. Furthermore, the yield of amide bond formation may be increased by addition of NHS [65].

When the water-soluble EDC is used together with the water-soluble sulfo-NHS, active ester functionalities with carboxylate groups are formed. Due to the hydrophilic reactive sulfo-NHS ester group a fast conjugation with amines on target molecules takes place. Because of their poor solubility in water, non-sulfonated NHS has to be dissolved in organic solvent before their addition to aqueous solutions. By presence of amine nucleophiles, they will attack at the carbonyl group of the ester. Thereby, the NHS-group leaves and a stable amide linkage with the amine will be created. The final reaction product of the two-step reaction is identical to the one obtained by using EDC without NHS [65].

Figure 13 shows the size controlled synthesis of citrate stabilized GNPs. Carboxylic acid functionalized GNP are prepared *via* dative binding and self-assembling of the thiol containing bifunctional linker SH-PEG₇-COOH. Finally, the enzyme trypsin is immobilized using EDC/NHS as coupling agents by linkage the carboxylic acid and the amino group of the protein (q.v. 4.2.1 and 4.2.2).

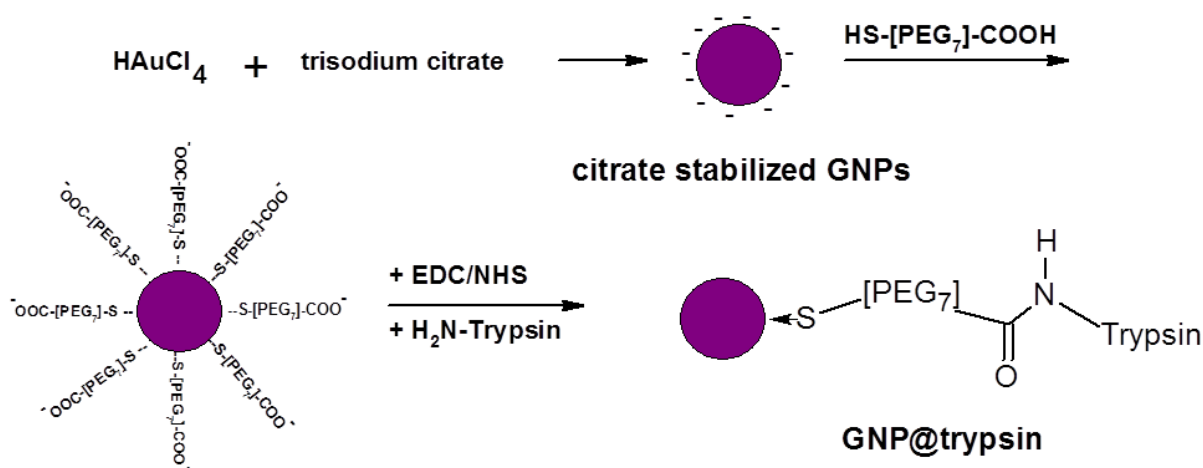


Figure 13: Synthesis of citrate stabilized GNPs with subsequent dative binding and self-assembling of the thiol containing bifunctional linker SH-PEG₇-COOH to yield carboxylic acid functionalized GNPs. In a final step, trypsin is immobilized using EDC/NHS as coupling agents for linkage of carboxylic acid and amino group, adapted from [68].

3.5 Enzymes – Stereospecificity and enantioselectivity

Enzymes are biocatalysts which accelerate biochemical reactions by reducing the activation energy of a chemical reaction. The different mechanisms of this process depend on the constitution of the active site of the respective enzyme. There are several advantages of enzymes over chemical catalysts [69]. Beside higher reaction rates, regulation possibilities and mild reactions conditions related to required temperature and pH value the high reaction specificity is a main benefit. Hence, extreme conditions which can cause side reactions can be avoided [69]. Enzymes are classified after their catalyzed reaction type. Table 1 gives an overview of the 6 main categories of enzymes [69].

Table 1: Classification of enzymes by their catalyzed reaction type, adapted from [69].

Classification	Type of catalyzed reaction
Oxidoreductase	Oxidation/Reduction reactions
Transferase	Transfer of functional groups
Hydrolase	Hydrolysis reactions
Lyase	Elimination of groups by formation of double bonds
Isomerase	Isomerization reactions
Ligase	Linkage of molecule coupled with ATP-hydrolysis

Like as chemical catalysts, enzymes are not able to alter the chemical equilibrium of the reaction. Rather, the reactions occur faster, but still in the same direction as it would without the respective enzyme. Here, the forward and backward reactions are catalyzed equally. Although the activation energy (E_A) is decreasing, the enzyme has no influence on the energies of the reactants or the products. The effect on the progress of a reaction due to the influence on the activation energy of enzymes is shown in the reaction coordinate diagram in Figure 14. In these diagrams, the reaction coordinate (progress of reaction) is plotted against the free energy G [69].

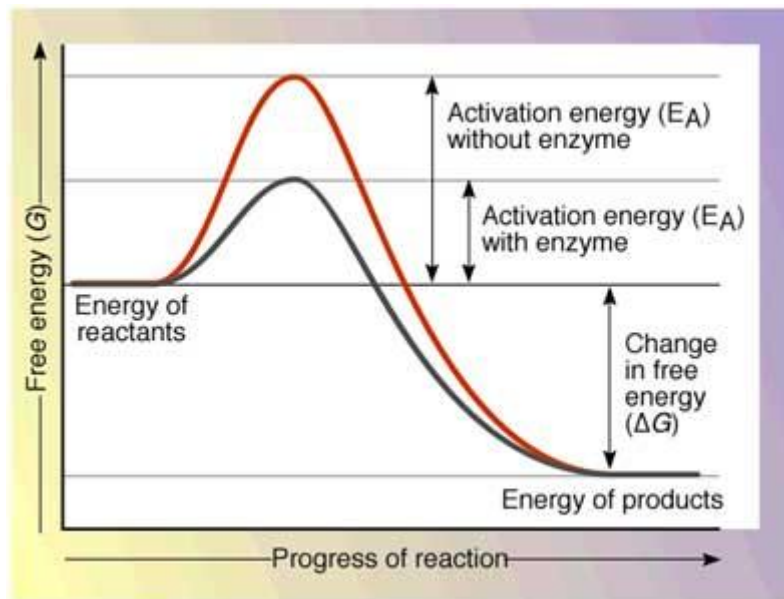


Figure 14: Influence of enzymes on the activation energy and therefore on the progress of a reaction [70].

The substrate binds to the active site of the enzyme by non covalent forces to induce the activity of an enzyme. The active site is the region where the catalytic residues are located. In general, it is built up of a cavity complementary to the substrate (geometric complementarity) [69]. Moreover, due to the arrangement of the amino acid residues at the binding site, specific interactions (electronic complementarity) with the substrate arise. Thus, catalysis of molecules with different arrangement of functional groups cannot take place. Due to X-ray structure analysis it is known, that the substrate binding sites of enzymes are already preformed and during the substrate binding a further conformational adaption occurs [69]. This phenomenon is described as "induced fit". In 1894, Emil Fischer published a model for the complementarity of enzymes and their substrates, the "lock-key model" [69]. This model was modified by David Koshland in the 1950s and is still in use to explain the mode of action in enzyme catalysis [71]. Since enzymes are rather flexible structures, the active site may get reshaped by enzyme-substrate interactions. Due to that fact, the substrate does not bind to a rigid, indeformable active site, but rather the amino acid side-chains of the active site form a precise fitting binding site for the substrate. After a successful catalysis, the products leave the active site of the enzyme, and the binding site turns back to the originally preformed shape (Figure 15). Enzymes also differ in their geometric specificity. Only a few enzymes are specific for one single substrate, most of them catalyze the reactions of a group of related compounds. Thereby, the effectiveness of the

catalysis can diversify for each substrate. For instance, the enzyme alcohol dehydrogenase (ADH) catalyzes the oxidation of ethanol to acetaldehyde substantially faster than the oxidation of methanol to formaldehyde.

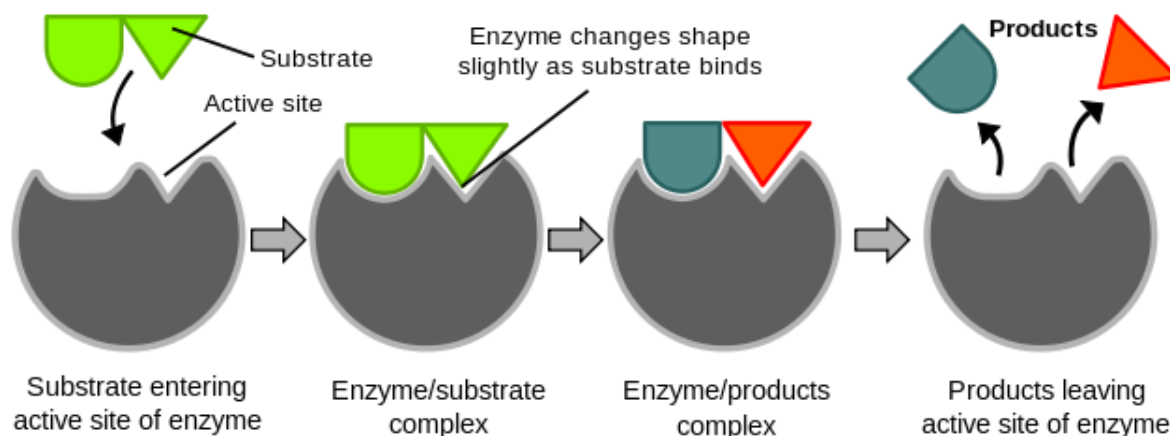


Figure 15: Lock-key model for enzymes and their substrates: The active site of the enzyme is preformed for the corresponding substrates, after substrate binding further adaptation of the binding site takes place for ideal fit. After enzyme catalysis, the active site of the enzyme turns back to the originally preformed shape [72].

Moreover, enzymes which are involved in chiral reactions show a high enantiospecificity pertaining to the chiral substrates and a high enantioselectivity pertaining to the subsequent catalysis [69]. This enantiospecificity and enantioselectivity derives from the chiral composition of the enzymes. As proteins consist of L- amino acids, enzymes form asymmetric active sites. Thus, only substrates with complementary configuration may bind at the site and the reaction can be catalyzed by the enzyme. Due to this, also the products of the catalysis have a predetermined configuration. Figure 16 shows the main principle of enantiospecificity of enzymes. The preset alignment of binding pockets in the enzyme leads to a favoritism of the better fitting substrate and therefore, to a preferred catalysis. To give an example for this enantiodifferentiation, D- and L-Glucose can be mentioned. While D-glucose can be cleaved in the human body, there is no enzyme to catalyze the cleavage of the corresponding enantiomer [69].

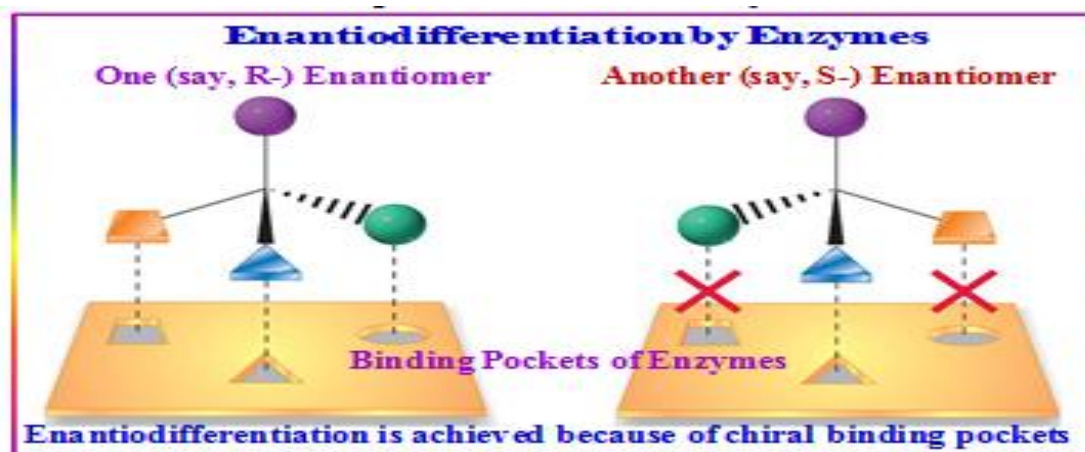


Figure 16: Enantiospecificity of enzymes pertaining to chiral substrates [73].

The benefit that enzyme catalysis is enantioselective nowadays utilized in numerous application areas, such as in organic synthesis and pharmaceutical industry, where enantioselective enzyme catalysis is utilized to obtain single enantiomers [74]. On the one hand, synthesis can be done easier by predicting the resulting products due to enantioselectivity. On the other hand, the avoidance of unwanted side-products may lower the purification effort and therefore the costs. Common limitations of enzyme catalysis are the quite expensive enzymes. Hence, methods for an easy inserting, extracting and, furthermore, reuse of the enzyme are of high interest [74].

3.5.1 Trypsin and α -chymotrypsin

Both, trypsin and α -chymotrypsin belong to the proteases (also peptidase or proteinase), a subcategory of the enzyme category hydrolases, which catalyze the hydrolysis of peptide bonds. These ubiquitous proteases are involved in the digestion of long protein chains into short fragments by splitting specific peptide bonds. Several further subclassification on the basis of ideal pH, occurrence or enzyme commission (EC) numbers may be done. The classification by means of the pH distinguishes in acidic, neutral and basic proteases. According to the occurrence, these enzymes are classified in intra- and extracellular proteases. The intracellular proteases are responsible for the regulation of the protein

concentration in the cell, *e.g.* they are involved in apoptosis pathways, signal cascades *etc.* In mammalian organisms extracellular proteases can be mainly found in the intestinal tract, where they are involved in the hydrolytic digest of proteins ingested by food intake. Furthermore, they may be found in extracellular matrix, where they take part in high specific processes like the blood-clotting cascade [75].

The subclassification on the basis of the EC-numbers is done according to the type of catalyzed reaction and the type of active site. First, a distinction between exo- and endoprotease can be done. While exoproteases cleave at the ends of polypeptide chains, endoproteases split at specific positions within the chain. The subclassification of endoproteases is done after their functional amino acid (AA) and their active site, respectively. For instance cysteine proteases contain cysteine as functional amino acid in their active site. In Table 2 the different proteases, classified according to their functional AA and their active site, respectively, are listed with examples [76].

Table 2: Overview of the subclassification of endopeptidases according to their active sites and functional amino acids, respectively, modified after [76].

Functional amino acid/active site	Protease	Example
Aspartate	Aspartate proteases	Pepsin, chymosin
Cysteine	Cysteine proteases	Papain, calpain
Glutamine	Glutamic proteases	Scytalidoglutamic peptidase
Metallo	Metalloproteases	Thermolysin
Serine	Serine proteases	Trypsin, chymotrypsin
Threonine	Threonine proteases	Proteasome

Trypsin as well as α -chymotrypsin appertain to the subcategory of serine proteases. Both are, together with the enzyme elastase, digestion enzymes which are produced in the pancreas and then secreted to the duodenum. According to the present pH value in their sphere of action, the ideal pH range of these enzymes range from 7.0 up to 8.5 [77].

Although all of them catalyze the hydrolysis of peptide bonds, they show different specificity pertaining to the site chains around the peptide bond, which has to be cleaved. While trypsin shows a high specificity for positive charged residues and cleaves in particular after the amino acids lysine and arginine (except these AA are followed by proline), α -

chymotrypsin cleaves after bulky hydrophobic residues, especially after the amino acids phenylalanine, tyrosine, tryptophan and methionine [69]. The difference in the cleavage characteristics originates from diversity in the active site. The active site in both enzymes is composed by the AAs aspartic acid 102, histidin 57 and serine 195, which form the catalytic triad [69] (Figure 17).

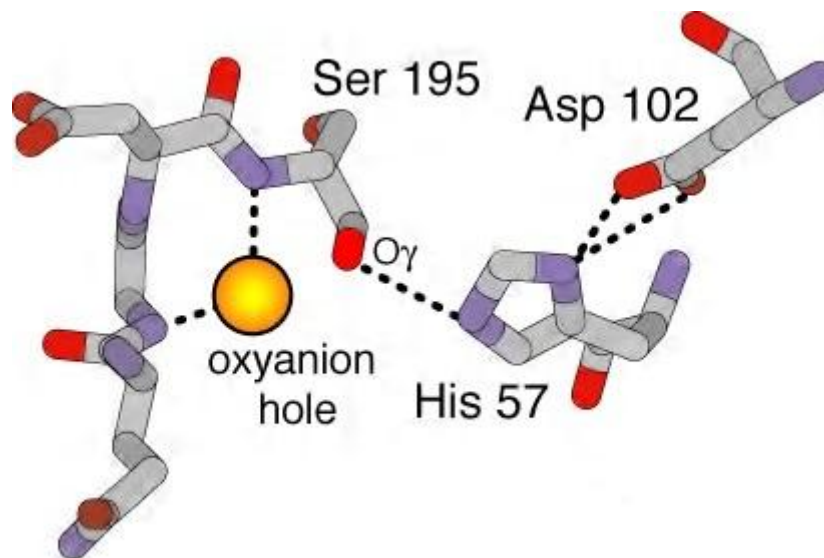


Figure 17: Active site of trypsin [78].

This composition of the active site is similar in all serine proteases and was discovered due to chemical labeling experiments (*e.g.* with diisopropylphosphofluoridate for serine 195) [69]. Next to the active site a non-polar pocket is located. In the case of trypsin an aspartate residue resides in the center of the pocket. Between the negatively charged oxygen atom of the carboxyl group and the positively charged nitrogen atoms electrostatic attractive forces appear. Therefore, the hydrolysis occurs at the peptid bond with lysine or arginine on the N-Terminus (the amino side) of the protein which is cleaved. However, α -chymotrypsin has an uncharged serine molecule in this pocket. Thus, the bulky non-polar side chains of phenylalanine, tyrosine, tryptophan, and methionine match into the side pocket. This fact enables the cleavage of peptide bonds after those amino acids. Nevertheless, an exchange of the aspartate residue in trypsin to serin does not change its specificity to the one of α -chymotrypsin. Equal behavior may be observed by substitution of serin to an aspartate residue in α -chymotrypsin. The result is merely an unspecific, slightly effective protease [69]. One approach to influence the enantioselectivity of serin proteases as trypsin and α -

chymotrypsin is the modification of enzymes. Lv et al. [79] investigated the enantioselective differences of the chemically modified enzymes decanoyl-*R*-chymotrypsin and decanoyl-trypsin to unmodified enzymes. Changes in enantiomeric discrimination to complete enantioselective catalysis in favor of the *L*-enantiomer of decanoyl-chymotrypsin for some of the tested long-chain amino acid esters were obtained, however, with a decrease of enzyme activity. For modified trypsin there was no effect on enantioselectivity compared to unmodified trypsin. It was suggested that hydrophobic groups introduced into *R*-chymotrypsin due to chemical modification enhanced the enantioselectivity for the hydrolysis of hydrophobic ester [79].

Another approach to affect enantioselective reactions of enzymes is the transition of the reaction medium. For instance, for the serine protease subtilisin Carlsberg the enantioselectivity dramatically decreased when the reaction medium was transitioned from water to organic solvents [80].

Bross et al. found out that the enantioselectivity of serine proteases (e.g. α -chymotrypsin) in the transesterification of *N*-acetyl-(*D,L*)-phenylalanine esters is highly influenced by the addition of small amounts of organic additives. For instance, small molecules like ethanol and acetonitril increase the rate of *L*-enantiomer, while bulky alkyl groups enhanced the enantioselectivity towards the *D*-enantiomer [81].

Hence, terms such as the reaction medium and the enzyme modification can influence the enantioselectivity considerably.

3.5.2 Immobilized Trypsin

For trypsin in solution, several drawbacks such as long digestion times up to 24 h, poor enzyme-to-substrate ratio or auto-digestion sub-products occur. Enzyme immobilization is one approach to enhance enzyme-to-substrate ratios, as well as to reduce digestion times [82]. Due to a decreased auto-digestion, also the long-term stability can be improved. Some of these approaches are binding e.g. trypsin onto microbeads [83], silica-based substrates [84, 85] or synthetic polymers [86]. Moreover, nanobeads are commonly used for enzyme attachment and immobilization, particularly silica coated magnetic [87], chitosan nanoparticles and nanofibers [88] and goldnanoparticles [39].

The enzyme properties such as stability and activity are often strongly dependent on the size

of the particles. For instance, Li et al. showed an enhancement of trypsin stabilities even in strongly denaturing environments for small SiO₂ nanoparticles to a great extent than larger ones. As well, the loss of activity under the same conditions was increasing correlated with the increase of nanoparticle size.

When Lv et al. [79] immobilized trypsin onto GNPs they obtained similar enzyme activities for immobilized trypsin and trypsin in solution, but with a higher stability of immobilized trypsin. Hence, longer storage times were possible without a loss of activity. Their interpretation was the big GNPs can block protease or other molecules from approaching trypsin, thus resulting in slower degradation of the enzyme.

3.5.3 Enzym modifications (Acetylation)

Due to its well-defined substrate specificity, trypsin is commonly used in proteomics experiments to digest proteins, yielding a unique peptide mass for mass spectrometry analysis [83]. The digestion for protein identification by database search methods like peptide mass fingerprint is generally performed in solution, which leads to several drawbacks. To avoid the appearance of interfering autolysis peptides, the trypsin-to-substrate ratio is kept as low as possible. From this actuality, long digestion times (typically more than 5 h) result, which confines high throughputs of protein identification on the one hand. Furthermore, a long incubation time results in increased digestion artifacts like traspeptidation, nonspecific cleavage, deamidation, oxidation and trypsin autolysis products. One possible approach to facilitate a higher digestion rate, yield and robustness of the proteolytic digest is the chemical modification of the used enzymes [83]. Chemical modification of trypsin in solution has already been successfully used to enhance the thermal stability and the stability towards autolytic inactivation without a loss of activity [89]. Besides modification with tyrosines [90], PEG (Pegylation) [91], beta-cyclodextrin derivatives [92] and intramolecular crosslinking [93], the acetylation of trypsin is of high interest. Due to the low size, changes in steric interaction of substrate and enzyme may be kept minor in contrast to bulky modification agents like cyclodextrins.

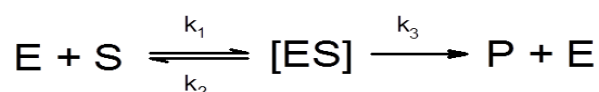
Freije *et al.* first published the acetylation of immobilized trypsin and showed preserved or even improved digestion efficiencies while reducing trypsin autolysis [94]. Therefore, they immobilized trypsin in a one-step reaction to NHS-activated Sepharose. To modify the

primary amino groups of lysine and the N-terminus of trypsin, a mild single step acetylation with acetic acid N-hydroxysuccinimide-ester (AANHS) was accomplished. Thereby, they found no negative effect on the trypsin activity and explained the conversion of positively charged amines into neutral amides. However, an enhancement of the digestion rate of cytochrome C, a slow digestible glycopeptides, was observed. Interestingly, the increase of digestion efficiency was independent of the used type of solid support. Coinciding digestion results for acetylated trypsin immobilized on poroszyme and sepharose were obtained. To confirm that the increased trypsin activity is not related to the immobilization but to the acetylation, the digestion experiments were done also with acetylated trypsin in solution. Acetylated immobilized trypsin and in solution showed an increased digestion rate of cytochrome C likewise.

To investigate the impact of acetylation on the digestion efficiency on other proteins, further digestion experiments with myoglobin were done. Though, no acetylation-dependent enhancement of the myoglobin digestion rate was observed [83]. Similar results were observed for the substrate benzoyl arginine p-nitroanilide D,L-BAPNA) by Murphy *et al.* [95]. This leads to the perception that the digestion efficiency depends on the used protein substrate and a positive effect for a particular one may not be predictive of the digestion efficiency for other proteins.

3.5.4 Michaelis-Menten (M.M.) kinetics

Named after Leonor Michaelis and Maud Menten, the Michaelis-Menten (M.M.) theory describes the rate of an enzymatic reaction by the relation of reaction rate and substrate concentration. Thereby, the total enzymatic reaction consists of two elementary reactions.



First the involved enzyme (E) and the substrate (S) form an enzyme-substrate-complex (ES), which is then converted to the product (P) and the released enzyme. Each elementary reaction is characterized by a rate constant. While k_1 and k_2 denotes the rate constants for the association and dissociation of the reversible formation of the enzyme-substrate-complex, k_3 specifies the conversion rate to the product. Hence, this particular case shows

a first-order reaction and the reaction rate can be given by (eq.7):

$$(eq.7) \quad v = \frac{dt[P]}{dt} = k_3 [ES]$$

Thereby, the conversion rate of the formation of [ES] is the difference of the rate constant of the formation (k_1) and of the dissociation (k_2, k_3) of the enzyme-substrate-complex (eq.8).

$$(eq.8) \quad \frac{d[ES]}{dt} = k_1[E][S] - k_2[ES] - k_3 [ES]$$

In 1925, Briggs and Haldane first suggested the steady-state-assumption as approach to simplify and solve the M.M. equation. For substrate concentration much higher than the enzyme concentration ($[S] \gg [E]$), the concentration of [ES] stays constant till the total consumption of [E] (with exception of few milliseconds in the initial phase of the reaction). Consequently, the formation rate of [ES] has to be equal to the consumption rate in a large part of the reaction and can therefore be considered as constant. In other words, the concentration of [ES] is considered as a steady-state (eq.9):

$$(eq.9) \quad \frac{d[ES]}{dt} = 0$$

Given that [ES] and [E] are in contrast to the total enzyme concentration (E_T) not directly measurable, the free enzyme concentration is replaced by (eq.10):

$$(eq.10) \quad [E] = [E_T] - [ES]$$

By combining eq. 8 with the steady-state-assumption in eq. 9, replacement of [E] by $[E_T] - [ES]$ and transformation the following equation is obtained (eq.11):

$$(eq.11) \quad \frac{([E_T] - [ES])[S]}{[ES]} = \frac{k_2 + k_3}{k_1}$$

The Michaelis constant K_M is defined as (eq.12):

$$(eq.12) \quad K_M = \frac{k_2 + k_3}{k_1}$$

Hence, by transformation of eq. 10 and solvation of this equation for [ES] we obtain (eq.13):

$$(eq.13) \quad [ES] = \frac{[E_T][S]}{K_M + [S]}$$

Thus, the term for the initial reaction rate v_0 at time $t = 0$ is given by (eq.14):

$$(eq.14) \quad v_0 = \left(\frac{d[P]}{dt} \right)_{t=0} = k_3[ES] = \frac{k_3[E_T][S]}{K_M + [S]}$$

At maximum (and hence saturation) substrate concentrations, the maximum reaction rate is given by V_{max} (eq.15):

$$(eq.15) \quad V_{max} = k_3[E_T]$$

By combining eq. 14 and eq. 15 the Michelis-Menten equation is obtained (eq.16):

$$(eq.16) \quad v_0 = \frac{V_{max}[S]}{K_M + [S]}$$

The M.M. equation is the basic equation of enzyme kinetics and delineates a hyperbolic function involving the substrate concentration and the reaction rate (see Figure 18 a). The Michaelis constant K_M gives information about the substrate concentration at which the reaction rate of the enzymatic reaction is the half of its maximal velocity. The lower the K_M value, the higher the affinity between substrate and enzyme. In the case of low values, the maximal catalytic efficiency will be reached at low substrate concentrations. The K_M value is specific for each enzym-substrate-pair and is dependend on reaction conditions such as temperature and pH value. V_{max} describes the maximal achievable velocity of the system at saturable substrate concentrations. The catalytic efficiency is characterized by the ratio of K_M and V_{max} .

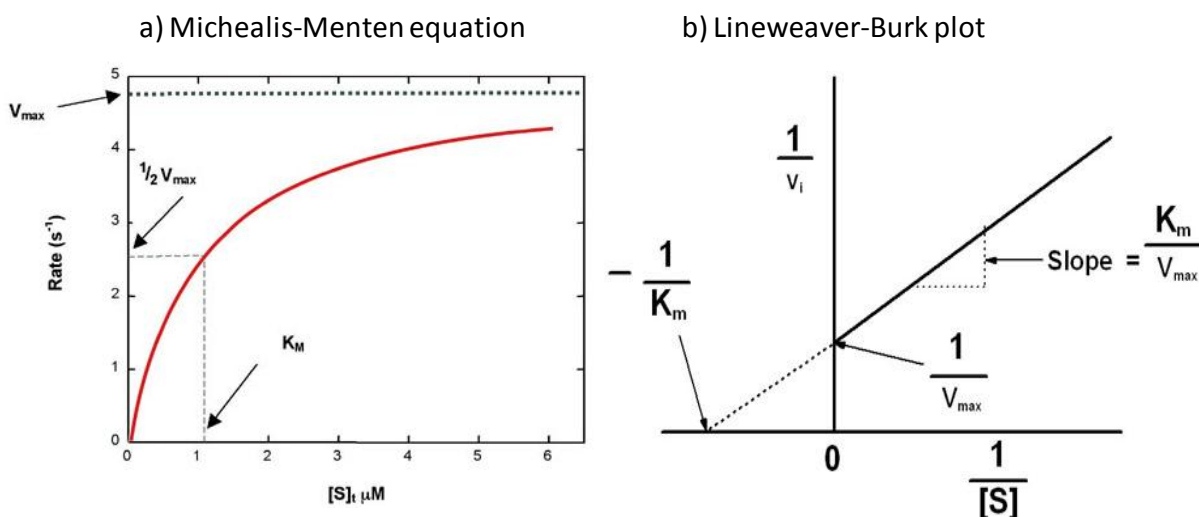


Figure 18: a) Hyperbolic function given by the Michaelis-Menten equation (eq. 15) [96] and b) double reciprocal Lineweaver-Burk plot [97] with the plotted parameters K_M , V_{max} and K_M/V_{max} .

The Michaelis constant K_M may be read off from the plotted M.M.equation (Figure 18a). For an exact determination of the parameters, in particular the maximum reaction rate V_{max} , the Lineweaver-Burk plot, a double reciprocal plot, is more favorable (Figure 18b). By plotting the reciprocal values of the substrate concentration against the reciprocal values of the initial reaction rate ($1/[S]$ against $1/v_o$), a linear slope is obtained to determinate K_M , V_{max} and the catalytic efficiency K_M/V_{max} accurately. Thereby, the extrapolated intersection with the axis of abscissae shows the negative reciprocal K_M value ($-1/K_M$), the intersection with the axis of ordinates shows the reciprocal V_{max} value ($1/V_{max}$) and the slope determinates the catalytic efficiency.

Although the analysis *via* Lineweaver-Burk plot poses some drawbacks *e.g* the data accumulation in the graph at low $1/[S]$ values or the high error rate according to measurement error of v_o , it is a commonly used and reliable method for the graphic presentation of kinetic data [69].

3.5.5 BApNA - a substrate for enzyme assays

To determine the activity of enzymes, M.M. kinetic studies with appropriate substrates may be accomplished. In the case of trypsin assays, the chromogenic substrate N-benzoyl-D,L-Arg-p-nitroanilide (BApNA) is commonly used. By C-terminal cleavage of the arginin the substrate is split into the products N-benzoyl-Arg (Bz-Arg) and p-nitroanilide (pNA). At a wavelength of 410 nm, the absorbance of the released pNA with an extinction coefficient of $8800 \text{ M}^{-1} \text{ cm}^{-1}$ can be measured (see Figure 19). For enzyme activity measurement, BApNA assay with different concentrations of the substrate has to be done and the results are plotted in a Lineweaver-Burk diagram. Hence, the M.M parameter K_M and V_{\max} can be calculated to indicate the enzyme activity [68].

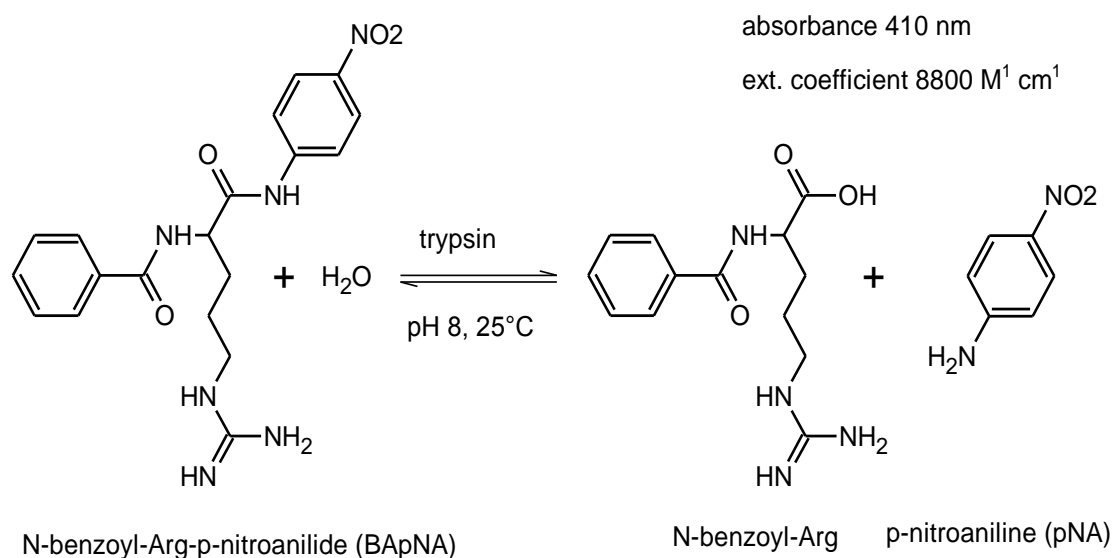


Figure 19: Cleavage of the substrate benzoyl-Arg-p-nitronanilide by trypsin. The enzyme activity can be determined by the release of p-nitroanilide with an extinction coefficient of $8800 \text{ M}^{-1} \text{ cm}^{-1}$ at the absorbance wavelength of 410 nm.

4 Instruments and methods

4.1 Instruments

4.1.1 Gold nanoparticle (GNP) characterization

GNPs with a size of approximately 30 nm were prepared with trisodium citrate as a reducing agent. Thereby the size was controlled by citrate to HAuCl_4 ratio and simultaneously a stabilization of the GNPs by the trisodium citrate was achieved (according to the method of Turkevich and Frens, [48], [47], q.v. 4.2.1). To control the reproducibility of size and size distribution and the sufficient stability of the prepared nanoparticles, GNPs were characterized by surface plasmon resonance (SPR), zeta potential (ZP) and dynamic light scattering (DLS) measurements. Furthermore, the different steps of coupling and immobilization chemistry with the chosen spacer and enzyme can be examined with these methods.

4.1.1.1 Surface plasmon resonance (SPR)

Photometric assays of the synthesized citrate stabilized GNPs, just as the HS-PEG₇-COOH and enzyme immobilized GNPs, were done with 1 mL prepared solution (q.v 4.2.1, 4.2.2). For SPR disposable polystyrene semi-micro cuvettes ISO 9001/14001 certified (12.5 x 12.5 x 45 mm, 1.5 mL) were used. The spectra were taken by SPECORD50 photometer (Analytik Jena, Germany) in a wavelength range from 200 – 800 nm.

4.1.1.2 Dynamic light scattering (DLS) and Zeta potential (ZP)

DLS and ZP of the GNPs were done with MALVERN ZETASIZER INSTRUMENTS Nano series (Prager Instruments). 1 mL prepared solution (q.v 4.2.1, 4.2.2) of citrate stabilized, SH-PEG₇-COOH and enzyme immobilized GNPs were measured.

For DLS disposable polystyrene semi-micro cuvettes ISO 9001/14001 certified (12.5 x 12.5 x 45 mm, 1.5 mL) were used. For ZP a folded polystyrene zeta capillary cell 1 mL with a cell stopper in each of the two ports was used. All measurements were done in triplicate in distilled water as dispersant and at a constant temperature of 25°C. The size distribution was stated in nm, the zeta potential in mV.

4.1.2 Photometry

All samples from Michaelis Menten kinetic series (q.v. 4.2.3.1), BApNA assays (q.v. 4.2.3.2) and acetylation assays (q.v. 4.2.3.14.2.3.3) were centrifuged (12 min, 13400 rpm) and the UV-absorbance of the supernatant was measured at a wavelength of 410 nm (q.v.3.5.5)). The UV/vis spectra were taken with by SPECORD50 (Analytik Jena, Germany) and disposable polystyrene semi-micro cuvettes ISO 9001/14001 certified (12.5 x 12.5 x 45 mm, 1.5 mL) were used. Dilutions, when necessary, were done with distilled water.

4.1.3 HPLC separation

HPLC experiments were performed on an Agilent 1100 and 1200 HPLC system (Agilent Technologies, Waldbronn, Germany), equipped with a binary gradient pump, a vacuum degasser, an autosampler, a column oven and a DAD (diode array detector).

UV-detection was done at wavelengths from 210 to 360 nm. GNP conjugates were removed before injection by centrifugation and the supernatant was measured. The peak identification was done by injection of standard solutions. Void volumes of the columns were determined by injection of 10 μL of a 1:9 solution of acetone in MeOH. The used columns are mentioned in the corresponding chapters below (see 4.1.3.1, 4.1.3.2, 4.1.3.3, 4.1.3.4). Data acquisition was achieved with Agilent ChemStation Software and Evaluation of the data was carried out with Microsoft Excel.

4.1.3.1 D,L-BApNA

For all samples from BApNA assays (q.v. 4.2.3.1, 4.2.3.2, 4.2.3.3, 4.2.3.4, 4.2.4, 4.2.5, 4.2.6) methanol (MeOH) containing 50 mM formic acid (FA) and 25 mM diethylamine (DEA) was used as the standard mobile phase. The mobile phase flow rate was 1.0 mL min⁻¹ and the column temperature was set to 25°C. All samples were injected with an injection volume of 10 μL , injection was done with needle wash.

For enantiomer separation a Homotau-quinidine (Htau-QD) 150 x 4 mm, 5 μm material, SO

coverage 188 $\mu\text{mol/g}$ silica column was used [98].

For standard injection a 1 mg mL^{-1} N-benzoyl-D,L-Arg-p-nitroanilide (D,L-BApNA), L-BApNA and para-nitroaniline (pNA) solution, respectively, in 50 mM ammonium bicarbonate (AmBic) buffer, pH 8.5, was prepared. The pNA standard was diluted 1:10 with distilled water. 0.1 mg D,L-benzoyl-arginine (D,L-Bz-Arg) were dissolved in 135 μL DMSO, 15 μL FA and 850 μL 50 mM AmBic buffer, pH 8.5.

4.1.3.2 Acetylation of D-phenylalanine (D-Phe)

For HPLC detection of the acetylation of D-Phe with in-house made acetic acid N-hydroxysuccinimide (AANHS) MeOH containing 25 mM FA, 12.5 mM NH_4FA was used as standard mobile phase. The mobile flow rate was 0.55 mL min^{-1} , injection volume and column temperature were analogue to 4.1.3.1.

For separation and isolation of the target product a tert-butylcarbamoyl-quinine (QN-AX) type with 390 μmol immobilized selector per g of 3-SHproyl modified Daisogel 5 μm 120 \AA poresize (SH covered 840 $\mu\text{g/g}$ silica) was used.

For standard injection a 1 mg mL^{-1} solution of not acetylated D-Phe and acetylated D-Phe in 50 % (v/v) KHPO_4 buffer, pH 8.0 and 50 % (v/v) Tris/HCl buffer, pH 8.5, was prepared.

4.1.3.3 α -N-benzoyl-D,L-lysine-glycine (α -N-Bz-D,L-Lys-Gly) and N-benzoyl-D,L-arginine-glycine (N-Bz-D,L-Arg-Gly)

For all samples from peptide assays (q.v. 4.2.3.2, 4.2.6) a mobile Phase with 75 % (v/v) acetonitrile (ACN) 90% (v/v)/MeOH 10% (v/v) containing 25 mM FA and 12.5 mM ammoniumformiat (NH_4FA) and 25% (v/v) MeOH containing 25 mM FA, 12.5 mM NH_4FA was used as standard mobile phase. Flow rate, injection volume and column were analogue to 4.1.3.1.

For standard injection a 1 mg mL^{-1} solution of α -N-Bz-D-Lys-Gly, α -N-Bz-L-Lys-Gly, N-Bz-D-Arg-Gly and N-Bz-L-Arg-Gly in 50 mM AmBic buffer, pH 8.5, was prepared. For D,L-Bz-Arg the same standard was used as in 4.1.3.1.

4.1.3.4 Arginine (Arg) containing peptides

For assays with Bz-D,L-Arg-OH (q.v. 4.2.3.2) the same column, mobile phase, flow rate, injection volume and temperature as for BApNA assays were used (q.v. 4.1.3.1) L-Phe-L-Arg and L-Arg-L-Phe samples were separated with a Chiralpak ZWIX+ 150x4mm, 3 μM column. As

standard mobile phase MeOH containing 50 mM FA, 12.5 NH₄FA was used.

For standard injection a 1mg ml⁻¹ L-Phe-L-Arg, L-Arg-L-PHe, L-Arg, L-Phe, and D,L-Arg in 50 mM AmBic buffer, pH 8.5, was prepared. For Bz-D,L-Arg-OH the same standard solution as prepared for BApNA detection was used (q.v. 4.1.3.1).

4.2 Methods

4.2.1 Gold nanoparticle (GNP) preparation

Gold nanoparticles can be fast and low-cost size-controlled prepared by variation of the ratio of reducing agent trisodium citrate to HAuCl₄ according to the method of Turkevich and Frens ([48], [47]). 45 mL GNPs with a size of approximately 30 nm were prepared using the following conditions:

All glasswares and the stirrers were cleaned before use with aqua regia (HCl/HNO₃ 3:1) and then rinsed several times with distilled H₂O. A 50 mL Erlenmeyer flask, containing 20.2 mg HAuCl₄ in 40 mL distilled H₂O (final concentration 1.14 mM) was covered with aluminum foil and the solution was heated up under stirring till boiling. 32.4 mg trisodium citrate were dissolved in 5 mL distilled H₂O (final concentration 2.45 mM) and added rapidly with a pipette through the aluminum foil. After addition the Erlenmeyer flask was covered with another layer of aluminum foil. The solution was stirred for further 10 minutes, whereat the color changes from yellow to dark red-violet. Under further stirring the GNP suspension was cooled down to room temperature. For SPR, ZP and DLS measurements (q.v. 4.1.1) a 1:20 dilution with distilled water was prepared.

4.2.2 Enzyme immobilization onto GNPs (GNP@enzyme)

The immobilization onto GNPs was done according to the optimized protocol published recently in our working group [68]. The enzymes trypsin and α -chymotrypsin, respectively, were used for immobilization onto GNPs.

1 μ L (equals ca. 1 mg or 2.18 mmol) O-(2-carboxyethyl)-O'-(2-mercaptoethyl)heptaethylene glycol (HS-PEG₇-COOH) was added to 1 mL GNP solution (equals ca. 0.44 mg GNPs) (q. v.

4.2.1) in an 1.5 mL reaction tube and shaken overnight (Thermoshaker) forming a self-assembling monolayer (SAM) ([67]). The excess of unbound ligands was removed by several washing steps. Therefore, the solution was centrifuged (12 min, 13400 rpm) and the pellet was washed with distilled H₂O by resuspension. This step was repeated three times and the pellet was finally resuspended in 1 mL distilled H₂O. A 1:20 dilution with distilled water for GNP characterization (q.v. 4.1.1) was prepared. Thereafter, 100 µL of 12 mM *N*-(3-Dimethylaminopropyl)-*N'*-ethylcarbodiimide hydrochloride (EDC) solution and 60 mM *N*-hydroxy-succinimide (1-Hydroxy-2,5-pyrrolidinedione, NHS) solution, both dissolved in methanol, were added. After 2h reaction time (Thermoshaker) the washing step was repeated three times and the pellet resuspended in 1 mL distilled H₂O. 100 µL of enzyme solution (1 mg mL⁻¹ 50 mM PBS buffer, pH 7) were added and the immobilization was accomplished overnight (Thermoshaker). The washing step was repeated three times and the pellet was resuspended in 1 mL 50mM AmBic buffer, pH 8.5. To verify the successful immobilization a 1:20 dilution with distilled water was prepared, the nanoparticles were characterized (q.v. 4.1.1) and the undiluted samples were stored at 4°C until use.

4.2.3 Enzymatic digestion of different substrates with enzyme linked GNPs

4.2.3.1 Determination of Michaelis Menten (M.M.) constants

To determine the Michaelis Menten constants K_m , v_{max} and specific enzyme activity, experimental series with different substrate concentrations were accomplished.

A concentration range from 0.5 to 5.0 mM (0.2175 mg mL⁻¹ to 2.175 mg mL⁻¹) was prepared with the substrate *N*-benzoyl-D,L-Arg-p-nitroanilide (D,L-BApNA). The exactly used concentrations for each series are written in the legends corresponding to the figures and tables. The different substrate concentrations were dissolved in 10 % (v/v) DMSO and 90 % (v/v) 50 mM AmBic buffer, pH 8.5. To 500 µL substrate solution 50 µL GNP@enzyme and enzyme in-solution, respectively, were added. After a digestion time of 15 minutes the reaction was stopped by addition of 1 % (v/v) formic acid (FA) final concentration. The samples were centrifuged to remove GNP@enzyme particles (12 min, 13400 rpm) and the UV-absorbance of the supernatant was measured at a wavelength of 410 nm (q.v. 4.1.2). The

results were applied in a Lineweaver-Burk-Diagram and K_m , v_{max} and the enzyme activity were determined (q.v. 3.5.4).

With the mimic-peptides α -N-benzoyl-D,L-Lys-Gly and N-benzoyl-D,L-Arg-Gly a concentration range of 0.1 to 1 mg mL⁻¹ was used. The different substrate concentrations were dissolved in 50 mM Ambic buffer, pH 8.5. To 200 μ L substrate solution 50 μ L GNP@trypsin were added. After a digestion time of 3.5 hours the digestion was stopped by addition of 1 % (v/v) FA (final concentration). The samples were centrifuged (12 min, 13400 rpm) and the supernatant was analysed by HPLC-UV (4.1.3.3). The results were applied in a Lineweaver-Burk-Diagram and K_m and V_{max} and were determined (q.v. 3.5.4).

4.2.3.2 Enzyme assays

D,L-BApNA assay

For this assays a concentration of 0.1 mM and 0.5 mM D,L-BApNA, respectively, was used. The digestion time was ranged from 30 minutes to 29 hours. The exactly used concentration and digestion times for each experimental series are written in the legends corresponding to the figures and tables.

The different substrate concentrations were dissolved in 50 mM Ambic buffer, pH 8.5 and stirred for 60 minutes at 30°C (Thermoshaker). To 200 μ L substrate solution 50 μ L GNP@enzyme solution were added. After the designated digestion time the reaction was stopped by addition of 1 % (v/v) FA. The samples were centrifuged (12 min, 13400 rpm) and the UV-absorbance of the supernatant was measured at a wavelength of 410 nm (q.v 4.1.2). Subsequently the samples were analyzed with HPLC-UV measurements in order to quantify the enantiomer of N-benzoyl-arginine (q.v. 4.1.3.1).

Determination of the influence of different organic solvents on the enantioselectivity of the BApNA assays

The substrate D,L-BApNA was dissolved in 50 mM AmBic buffer, pH 8.5, and 5 or 10 % (v/v) of the solvents DMSO, EtOH and MeOH, respectively, were added. The final substrate concentration was 0.05 mM. The digestion time range was from 1 to 7 hours.

To determine the effect of DMSO in samples with higher substrate concentration, substrate solutions with a final concentration range from 0.05 to 5.0 mM BApNA were prepared analogue to 4.2.3.1. Before digestion DMSO was added to a final concentration of 10 % (v/v)

in each sample. The digestion time range was from 0 to 24 hours and was done analogue to the BApNA assay mentioned above.

Precipitation of D,L-BApNA

As observed in foregoing experiments, the substrate D,L-BApNA starts precipitating with higher concentration. D,L-BApNA solutions with concentrations from 0.5 to 5 mM were prepared (analogue to 4.2.3.1) to determine the solubility and to figure out the influence of temperature (storage at 25°C and 4°C) The solutions were measured immediately after preparation (q.v. 4.1.2 and 4.1.3.1) and 1 day posterior.

Digestion of peptides

With the substrates α -N-benzoyl-D,L-lysine-glycine (α -N-Bz-D,L-Lys-Gly) and N-benzoyl-D,L-arginine-glycine (N-Bz-D,L-Arg-Gly) a concentration of 1 and 2.5 mg mL⁻¹, respectively, was used. The digestion time ranged from 0, to 24 hours. Furthermore an undigested sample was analyzed as negative control. The exactly used concentration and digestion times for each experimental series are written in the legends corresponding to the figures and tables.

The different substrate concentrations were dissolved in 50 mM Ambic buffer, pH 8.5 as single component standards. To 200 μ L substrate solution 50 μ L GNP@trypsin solution were added. After the designated digestion time the reaction was stopped by addition of 1 % (v/v) FA. The samples were centrifuged (12 min, 13400 rpm) and the supernatant was analyzed with HPLC-UV measurements (q.v. 4.1.3.3).

Digestion of different arginine containing peptides

The peptides L-Phe-L-Arg and L-Arg-L-Phe were prepared as a 1mg mL⁻¹ solution dissolved in 50 mM AmBic buffer, pH 8.5. For HPLC analysis 1 mg mL⁻¹ standard solutions of L-Phe and L-Arg in 50 mM AmBic buffer, pH 8.5, were prepared. Furthermore, 0.5 mg Bz-D,L-Arg-OH were dissolved in 100 μ L DMSO and 900 μ L 50 mM AmBic buffer, pH 8.5. The solution was stirred for 30 minutes at 30 °C and ultrasonicated. Due to the low solubility of Bz-D,L-Arg-OH under basic conditions, which are necessary for a tryptic digest (q.v. 3.5.1) not dissolved solid matter may block the HPLC-column. Therefore the solution was centrifuged (20 min, 13400 rpm) to remove undissolved particles.

To 200 μ L substrate solution 50 μ L GNP@trypsin were added. The digestion time ranged

from 0 to 48 hours for L-Phe-L-Arg, L-Arg-L-Phe and Bz-D,L-Arg-OH, respectively. Digestion was done analogue to peptide digestion and analysis was done with HPLC to detect occurring cleavage products (q.v. 4.1.3.4).

4.2.3.3 Acetylation of enzyme in-solution and immobilized onto GNPs

The acetylation of trypsin was done according to the method of Freije [83]. 1 mg trypsin was dissolved in 1 mL 20 mM K_2HPO_4 buffer, pH 8.0, and GNP@trypsin was prepared according to 4.2.2, washed and resolved finally with 20 mM K_2HPO_4 buffer, pH 8.5. For acetylation 1 M acetic acid N-hydroxysuccinimide (AANHS) solution in acetonitrile was stepwise added to 500 μ L GNP@trypsin and trypsin in-solution, respectively, under shaking (900 rpm, 25°C) at 0, 7, 14 and 21 minutes resulting in final concentrations of 5, 15, 30 and 50 mM. The acetylation was stopped by 1:1 dilution of the samples with 1 M Tris/HCl buffer, pH 8.5. The acetylated GNP@trypsin samples were centrifuged (15 min, 13400 rpm) and the pellet was dissolved in 500 μ L of 50 mM Tris/HCl buffer, pH 8.5. The acetylated trypsin in-solution samples were diluted 1:10 with distilled H_2O . The samples were stored at 4°C till use. To test the enantioselectivity and activity, with aliquots from GNP@trypsin, trypsin in-solution and, as a reference, not-acetylated trypsin and GNP@trypsin, BApNA assays (q.v. 4.2.3.2) with a substrate concentration of 0.05 mM and 30 minutes digestion time were done. Furthermore, the influence of acetylation and immobilization chemistry was studied by acetylation of trypsin before and after immobilization onto GNP-PEG₇-COOH, respectively.

Acetylation of the amino acid D-Phe

To proof the quality of in-house made AANHS, the amino acid D-Phe (1 mg mL⁻¹ 20 mM K_2HPO_4 buffer, pH 8.5) was acetylated stepwise (as outlined above) and stopped after 21 minutes by 1:2 dilution with 50 mM Tris/HCl buffer, pH 8.5. Furthermore a 1 mg mL⁻¹ AA-D-Phe and not-acetylated D-Phe solution was prepared, dissolved in 50 (v/v) % 20 mM K_2HPO_4 and 50 (v/v) % 50 mM Tris buffer. The analysis of the different D-Phe samples was done by HPLC-UV measurements (q.v. 4.1.3)

4.2.3.4 Determination of M.M.constants

D,L-BApNA solutions with concentrations from 0.1 to 6.0 mM (analogue to 4.2.3.1) were prepared. To 200 μL substrate solution 50 μL GNP@trypsin, acetylated and not acetylated, and trypsin in solution, acetylated and not acetylated, respectively, were added. M. M. assays with a digestion time of 30 minutes were done analogue to 4.2.3.1.

To concentrate acetylated and not acetylated GNP@trypsin 1 mL of each sample was centrifuged (12 min, 13400 rpm) and the pellet was again dissolved in 100 μL 50 mM AmBic buffer, pH 8.5. The digestion with the 10times concentrated samples was done analogue to the not concentrated samples.

4.2.4 Long-term study of the storage stability of GNPs

Solutions of citrate stabilized GNPs (size ~ 30 nm in diameter), PEG functionalized GNPs and GNP@trypsin were prepared analogue to 4.2.1 and 4.2.2. Furthermore a 100 μL mercaptohexadecanoic acid (MHA) solution (1 mg mL^{-1} MeOH) was prepared were added to 1 mL citrate stabilized GNP and washed several times to obtain GNPs MHA stabilized.

The samples were stored at 4°C and -25°C , respectively. In intervals from one to 4 weeks the surface plasmon resonance (SPR) spectra, zeta potential and size was measured (q.v. 4.1.1) to investigate the GNP-materials' storage stability.

Aliquots of GNP@trypsin stored at -25°C and 4°C for 6 months, respectively, were used for a BApNA assay. The assay was done with 1.0 mM BApNA (with 10 (v/v) % DMSO) and a digestion time of 1 hours analogue to 4.2.3.2.

4.2.5 Reusability of GNP conjugated enzymes

The reusability of GNP@Trypsin was studied by BApNA assays (q.v. 4.2.3.2). The chosen BApNA concentration was 1.5 mM (with 10 (v/v) % DMSO) with a digestion time of 1 hour. Between each enzyme activity assay a washing step was done in triplicate. The washing solution was prepared either without or with 0.1 % (v/v) Tween20, respectively, in 50 mM AmBic buffer, pH 8.5. The particles were washed with 1 mL washing solution, the solution was centrifuged. After the third washing step the GNPS were resuspended in the same

volume of 50 mM AmBic buffer as before the assay. Thereupon the washed GNP@trypsin particles were used for the next assay.

Next to the activity also the GNP@trypsin solution was characterized by its SPR spectra before every BApNA assay. Comparison with a calibration curve of GNP-PEG₇-trypsin, the remaining GNP concentration after every reuse was calculated.

4.2.6 HPLC assays - Limit of detection (LOD)

All determinations of LOD were done in triplicate and measured by HPLC-UV and UV/Vis spectroscopy, respectively, and according to the ICH Guideline Q2(R1) [99].

LOD of D,L-BApNA

From a 8 mM D,L-BApNA stock solution with 10 % (v/v) DMSO and 90 % (v/v) 50 mM AmBic buffer, pH 8.5, (4.2.3.1) was prepared and a dilution series from 0.005 to 5 mM was prepared.

LOD of Peptides

Of each of the peptides α -N-Bz-D,L-Lys-Gly and N-Bzl-D,L-Arg-Gly a stock solution of 1 mg mL⁻¹ 50 mM AmBic buffer, pH 8.5 was prepared and a dilution series with 9 concentrations from 0.05 to 1 mg mL⁻¹ was made.

LOD of p-nitroaniline

Out of a 0.1 mM stock solution in 50 mM AmBic buffer, pH 8.5, a dilution series with concentrations from 0.5 μ M to 0.1 mM was prepared.

Determination of LOD

This method is based on the measurement of the magnitude of the analytical background response, also called signal-to-noise method. By analyzing an appropriate number of blank samples, commonly 5 measurements, and calculating the average of the blanks and standard deviation (eq.17), the LOD can be determined (eq.18). The standard deviation δ was calculated by eq. (eq.17):

$$(eq.17) \quad \delta = \sqrt{\frac{1}{n} \sum_{i=1}^n (x_i - \bar{x})^2}$$

Limit of detection was determined by (eq.18):

$$(eq.18) \quad LOD = \bar{x} + 3 \times \delta_{Bl}$$

n.....number of measurement

x_iindicated value

\bar{x}average value

σ_{Bl}standard deviation of blank

Another method for determination of LOD is given in (eq.19):

$$(eq.19) \quad LOD = \frac{\delta_{Bl} \times 3.3}{S}$$

By estimating the slope S from the calibration function of the analyte and calculating the standard deviation of the blanks the LOD can be determined (eq.19)

σ_{Bl}standard deviation of blank

S.....slope of the calibration function

5 Results and discussion

5.1 GNP characterization

5.1.1 SPR, ZP and DLS of GNPs and GNP@enzyme

Figure 20 shows the averaged results of the SPR of all prepared GNP batches (manufacturing batch 1-8) and the different immobilization states. The SPR spectrum of the citrate stabilized GNPs with a size of about 30 nm in diameter shows the characteristic absorbance maximum at 527 nm, which is according to the about 520 nm in the literature (q.v. 3.4.2). This SPR band is less distinct after the immobilization of the spacer and the enzyme, respectively. Both, a broadening and a decrease of the peak maxima can be observed for each immobilization step. Furthermore a shift of the absorbance maximum to higher wavelengths for GNP-PEG₇-COOH (572 nm) and GNP@trypsin (540 nm) can be observed.

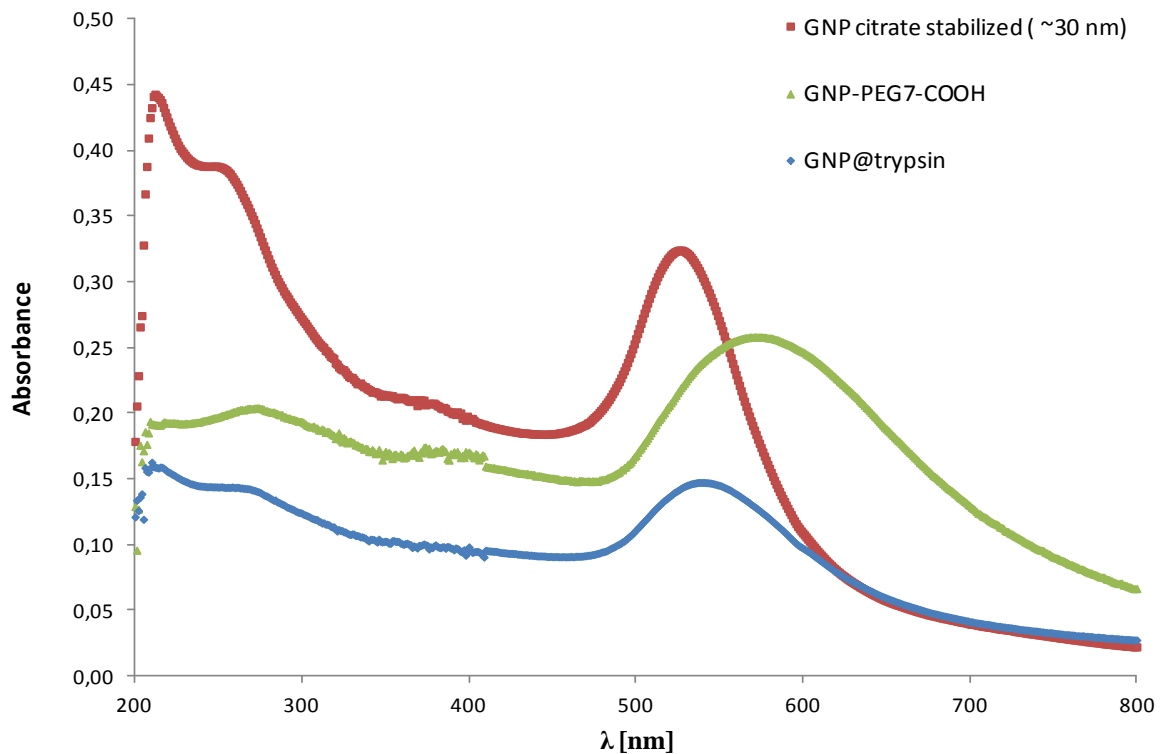


Figure 20: SPR spectra in a range from 200 – 800 nm of GNP citrate stabilized (size ~ 30 nm), GNP-PEG₇-COOH and GNP@trypsin, each 1:20 diluted with distilled water. The average data of all SPR measurements (batch 1-8) was plotted.

In Table 3 the ZP values of the different immobilization states are listed. The ZP of all 8 manufacturing batches were determined for each, GNP citrate stabilized (30 nm), GNP-PEG₇-COOH and GNP@trypsin. By comparison of the averaged ZP values of the different immobilization states, a decrease from -28.4 ± 4.7 mV (GNP citrate stabilized (30nm)) to -31.8 ± 4.1 mV (GNP-PEG₇-COOH) and $-34.3 \text{ mV} \pm 3.4$ (GNP@trypsin), respectively, was observed. Since the ZP is an indicator to predict the stability of GNPs (q.v. 3.4.2), this actuality leads to the assumption that the immobilization of the spacer and the enzyme have positive effects on the long-term stability and therefore the particles are better superposable. At these low ZP (< -30 mV) the repulsion of the particles may prevent the tendency to form aggregates and provides a stable colloidal system, consequently.

Table 3: Zeta potential of GNP citrate stabilized (30 nm), GNP-PEG₇-COOH and GNP@trypsin of manufacturing batch 1 – 8 and the respective averaged ZP values.

ZP [mV] GNP citrate stabilized (30 nm)	ZP [mV] GNP-PEG ₇ -COOH	ZP [mV] GNP@trypsin	Batch
-22.1	-24.0	-27.5	1
-31.6	-31.0	-32.6	2
-30.5	-34.1	-34.4	3
-24.2	-28.3	-37.2	4
-35.4	-36.1	-37.0	5
-34.4	-36.1	-37.0	6
-25.7	-31.6	-33.8	7
-26.9	-33.3	-37.4	8
-28.7 ± 4.7	-31.8 ± 4.1	-34.6 ± 3.4	Average

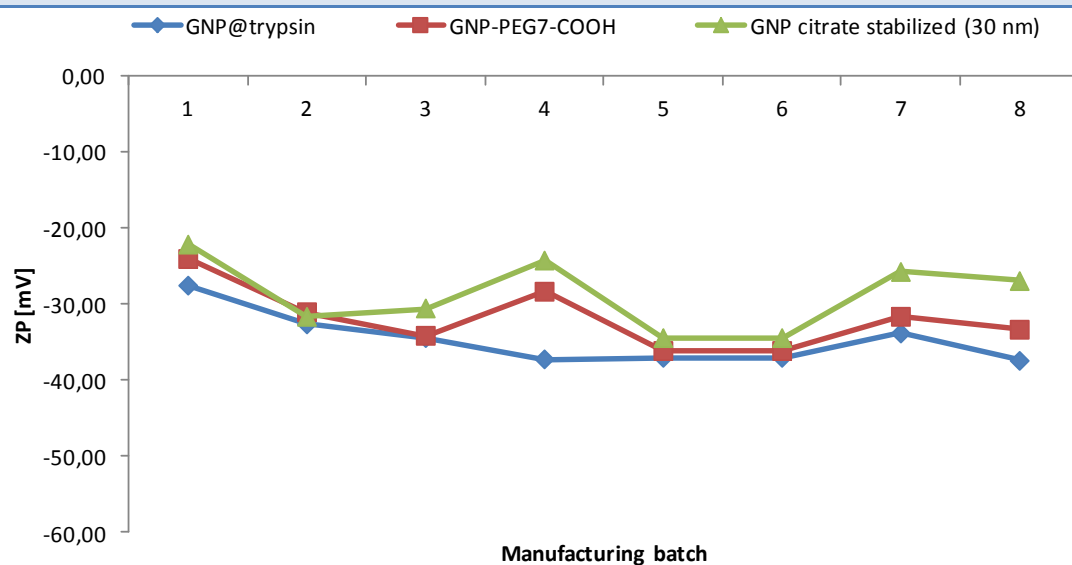


Figure 21 shows the consistency of the ZP in the course of the manufacturing batches. The ZP values of the different immobilization states are in the same range for all independently manufactured batches. Furthermore, one can see the decrease of the ZP value with the immobilization of the spacer and the enzyme, which supports the assumption of additional stabilization due to immobilization and introduction of constantly charged particles.

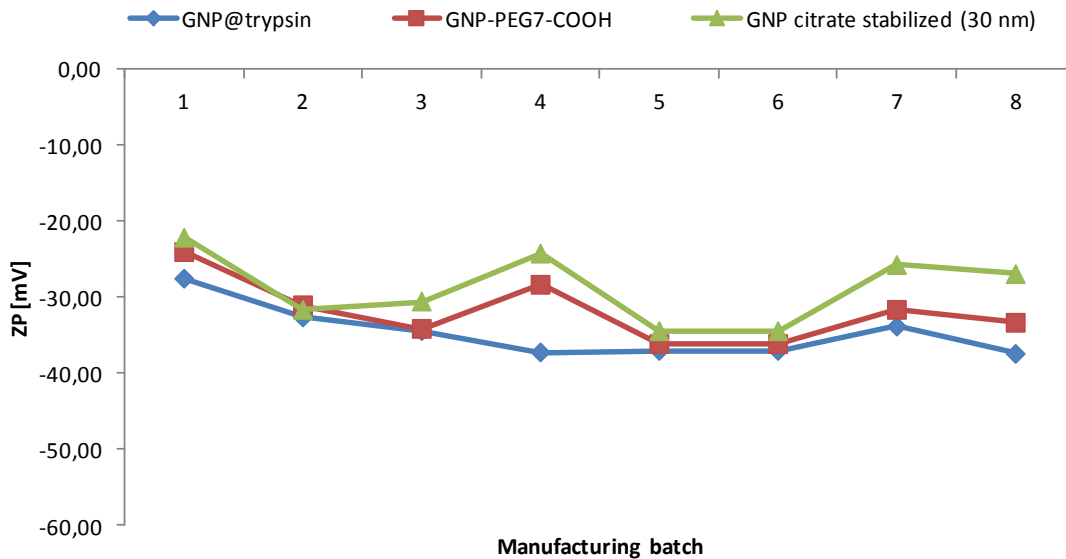


Figure 21: Zeta potential of GNP citrate stabilized (30 nm), GNP-PEG₇-COOH and GNP@trypsin of manufacturing batch 1 – 8 and the corresponding ZP values.

As not the actual size, but rather the hydrodynamic diameter is measured, the resulting size is larger than the actual one [100]. Consequently, for the GNPs prepared in a size range of about 30 nm a size distribution of 38.0 ± 6.7 nm was obtained (see Table 4). The DLS measurements indicated for GNP-PEG₇-COOH an average size of 118.9 ± 16.3 nm and for GNP@trypsin an average size of 157.4 ± 16.9 nm.

Table 4: Size distribution of GNP citrate stabilized (30 nm), GNP-PEG₇-COOH and GNP@trypsin of manufacturing batch 1 – 8 and the corresponding ZP values.

Size distribution [nm] GNP citrate stabilized (30 nm)	Size distribution [nm] GNP-PEG ₇ -COOH	Size distribution [nm] GNP@trypsin	Batch
35.4	105.7	140.1	1
37.3	101.3	164.2	2
37.8	122.4	142.4	3
32.7	124.2	180.1	4
32.7	141.8	180.1	5
32.7	141.8	164.2	6
43.8	108.9	145.7	7
51.8	105.0	142.4	8
38.0 ± 6.7	118.9 ± 16.3	157.4 ± 16.9	Average

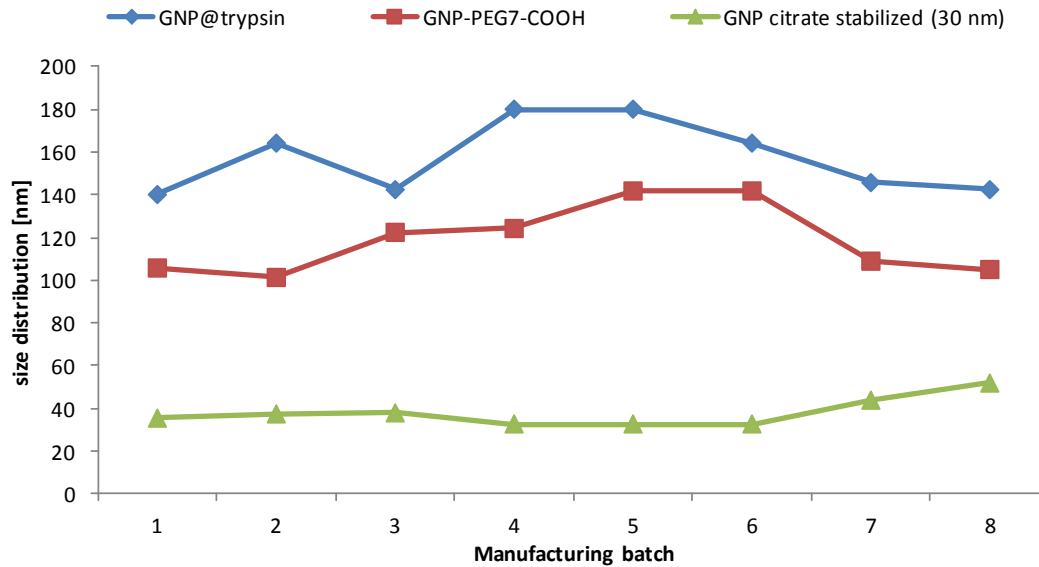


Figure 22: Size distribution of GNP citrate stabilized (30 nm), GNP-PEG₇-COOH and GNP@trypsin of manufacturing batch 1 – 8 and the respective averaged ZP values.

Figure 22 depicts the size distribution for the different immobilization states of all manufactured batches. Here, one may see the increase of size with each immobilization step. The GNPs of the 8 manufacturing batches show similar size distributions in the particular immobilization states and therefore consistent increases in size due to the immobilization steps.

Figure 23 a) gives an example of a typical zeta potential measurement of trypsin immobilized GNPs. Based on a measurement in triplicate the ZP was determined with a value of -37 mV for GNP@trypsin (manufacturing batch 5).

In Figure 23 b) the size distribution of 32.7 nm sized citrate stabilized GNPs (manufacturing batch 5) is shown. As exhibited in the figure, in the range of 1-5 nm the appearance of additional peaks may be observed frequently in size distribution measurement of GNPs in a range of 30-40 nm. This phenomenon was already reported by Khlebtsov et al. [100] and reviewed by comparative measurement with TEM. Hence, they were able to determine these additional peaks as false and not related to individual particles.

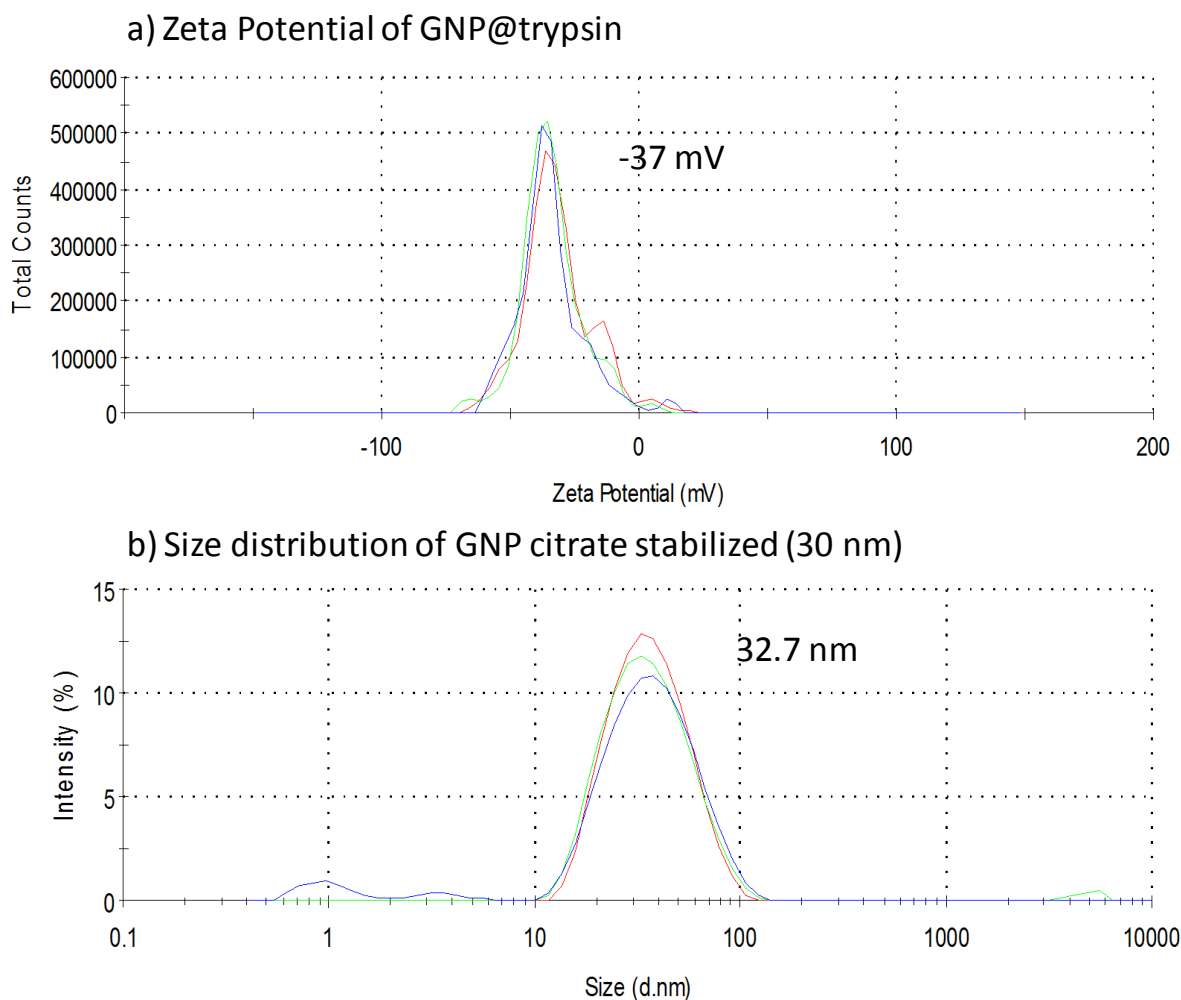


Figure 23: a) Typical ZP measurement of GNP@trypsin (manufacturing batch 5) with a ZP of -37 mV. b) Size distribution of 32.7 nm citrate stabilized GNPs with frequently occurring false additional peaks in the range of 1-5 nm.

To determine the reproducibility of the immobilization chemistry (q.v. 3.4.3) three batches of GNP@trypsin and GNP@chymotrypsin, respectively, were prepared simultaneously under the same conditions.

All three batches show similar absorbance characteristics respective both, absorbance maxima and intensity. The determination of the ZP indicates values in a range of -30 mV and -37.5 mV (

Table 5). Furthermore, the averaged value of -33.8 ± 3.8 mV is comparable with the values listed in Table 3 and the averaged value -34.6 ± 3.4 mV. The size distribution ranges from 164.2 to 202.2 nm and yields an average size of 188.1 ± 20.7 nm, which is at the upper limit compared to the size distributions in Table 4.

Table 5: Size distribution and ZP of GNP@trypsin (batch1-3).

	ZP [mV]	Size distribution [nm]
GNP@trypsin (1)	-34.0	202.2
GNP@trypsin (2)	-30.0	200.0
GNP@trypsin (3)	-37.5	164.2
Average	-33.8 ± 3.7	188.1 ± 20.7

Furthermore, three batches of GNP@chymotrypsin were prepared. All three batches show similar absorbance characteristics respective both, absorbance maxima and intensity. The determination of the ZP yields values in a range of -35.4 mV and -37.6 mV with an averaged ZP of -36.7 ± 1.2 mV. The size distribution ranges from 122.4 to 141.8 nm and yields an average size of 135.3 ± 11.2 nm.

Table 6: Size distribution and ZP of GNP@trypsin 1-3.

	ZP [mV]	Size distribution [nm]
GNP@chymotrypsin (1)	-35.4	122.4
GNP@chymotrypsin (2)	-37.2	141.8
GNP@chymotrypsin (3)	-37.6	141.8
Average	-36.7 ± 1.2	135.3 ± 11.2

Hence, a sufficient reproducibility of the immobilization chemistry of GNP@trypsin and GNP@chymotrypsin can be referred.

5.1.2 Long-time stability study of GNPs

The influence of storage conditions to the long-time stability of GNPs and their conjugates was determined by monitoring of the characteristic parameters ZP, DLS and SPR spectra (q.v. 4.2.4). For this study, aliquots of citrate stabilized GNPs, ligand modified GNP (GNP-PEG₇-COOH and GNP-MHA, respectively) and GNP@trypsin were stored at 4°C and -25°C, respectively.

The samples of citrate stabilized GNPs (30 nm) (storage temperature 4°C) showed no change of consistence till day 50, not till then the color changed from intensive dark violet to grayish lilac and single particle agglomerations were visible, but soluble by ultrasonic. In contrast, the samples of citrate stabilized GNPs (30 nm) (storage temperature -25°C) turned to light gray to very bright purple after a storage time of one week. A dark gray, not soluble precipitate was apparent.

The solution of GNP-PEG₇-COOH (storage temperature 4°C) retained an intensive dark violet color over the total storage time. The solution was transparent at any time and no particle agglomerations were visible. As well, there was no change of consistence of the samples of GNP-PEG₇-COOH (storage temperature -25°C) until day 90, henceforward a decoloration to purple took place. Equally, these observances were done for GNP@trypsin (storage temperature 4°C) and GNP@trypsin (storage temperature -25°C), respectively.

For the samples of GNP-MHA (storage temperature 4°C) no change of appearance was observed till day 90. From then the dark violet transparent solution was more and more decolorated to a grayish color and single particle agglomerations were visible. However, the samples of GNP-MHA (storage temperature -25°C) were decolorated after one week, the solution was light gray and a not soluble precipitate was apparent.

In Figure 24 the maximal absorbance determined by the SPR measurements of the sample aliquots, stored at a temperature of 4°C, are depicted. While the maximal absorbance of GNP-PEG₇-COOH, GNP-MHA and GNP@trypsin stayed almost constant over the total storage time of 140 days, the maximal absorbance of the citrate stabilized GNPs decreased from day 50 to approximately sixth of the original value. This absorbance reduction is in accordance to the occurring decoloration of the solution from day 50.

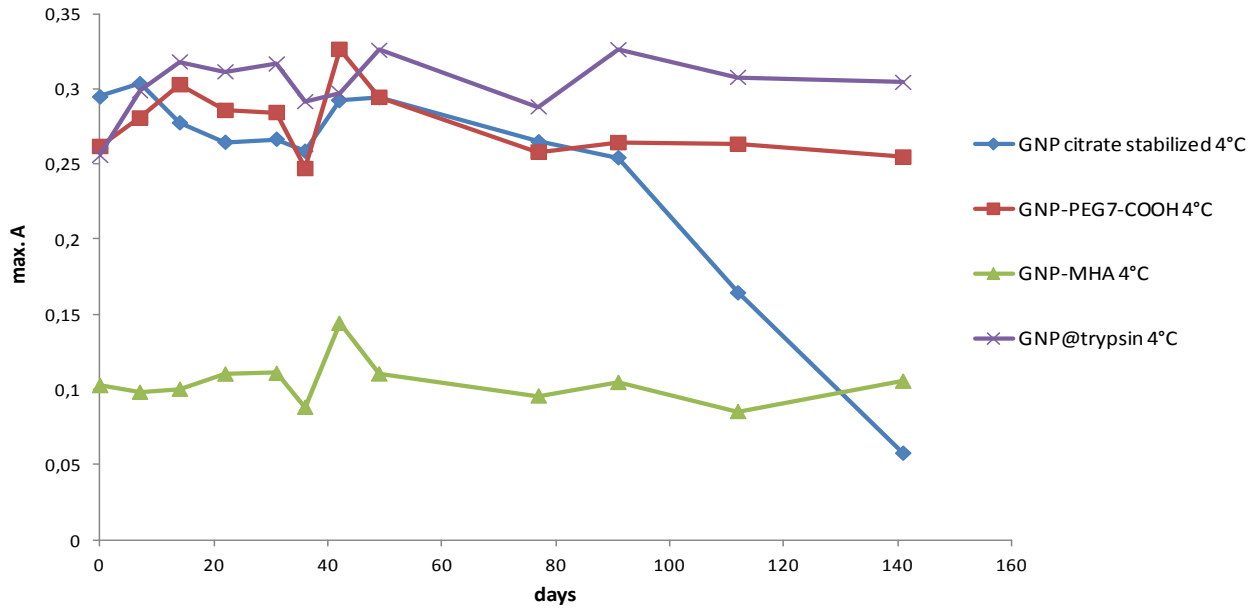


Figure 24: Maximal absorbance of SPR measurements of GNP citrate stabilized, GNP-PEG₇-COOH, GNP-MHA and GNP@trypsin with a storage temperature of 4°C and a total storage time of 141 days.

Figure 25 shows the maximal absorbance of the sample aliquots with a storage temperature of -25°C. For the citrate stabilized GNPs as well as GNP-MHA a formidable decline of the maximal absorbance was observed after a storage time of one week, corresponding to the loss of color and change of appearance. However, there was no absorbance decrease observable for GNP@trypsin and only a slight decrease for GNP-PEG₇-COOH.

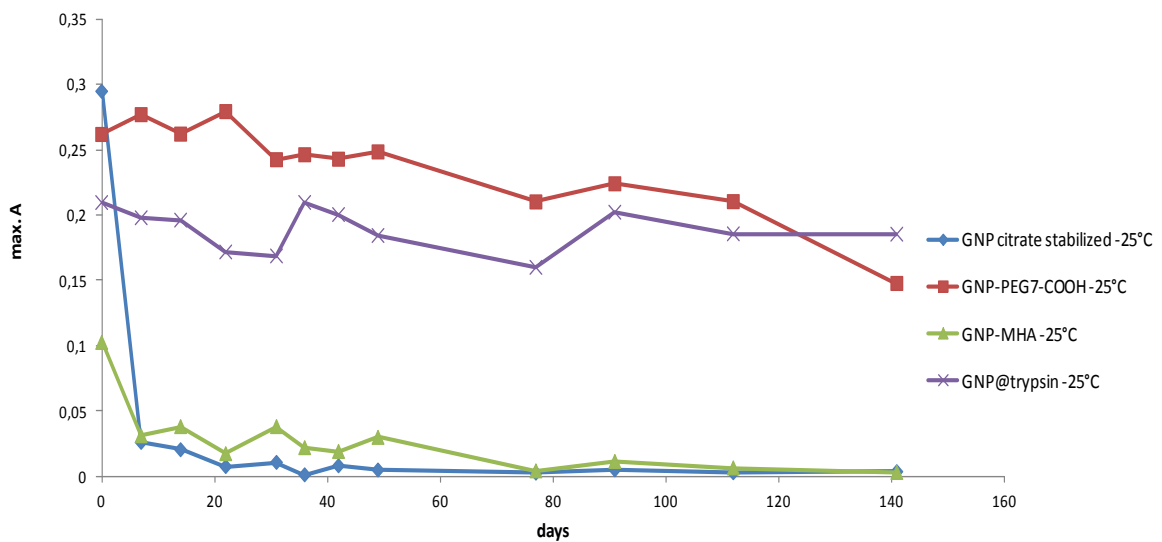


Figure 25: Maximal absorbance of SPR measurements of GNP citrate stabilized, GNP-PEG₇-COOH, GNP-MHA and GNP@trypsin with a storage temperature of -25°C and a total storage time of 141 days.

The ZP values of the aliquots stored at a temperature of 4°C are given in Figure 26. For both, GNP-PEG7-COOH and GNP@trypsin the measurement yielded similar ZP values and no distinct increase of the ZP was observed. Though, for the citrate stabilized GNPs an increase of the ZP with storage time was monitored. After a storage time of about 50 days, the ZP values of approximately -10 mV indicated an unstable colloidal system (see Characterization of GNPs by SPR, DLS and ZP 3.4.2). For GNP-MHA the ZP values show an abrupt rise after a storage time of more than 112 days. With a ZP around 0 mV, the colloidal system could not be considered as stable any more (q.v. 3.4.2).

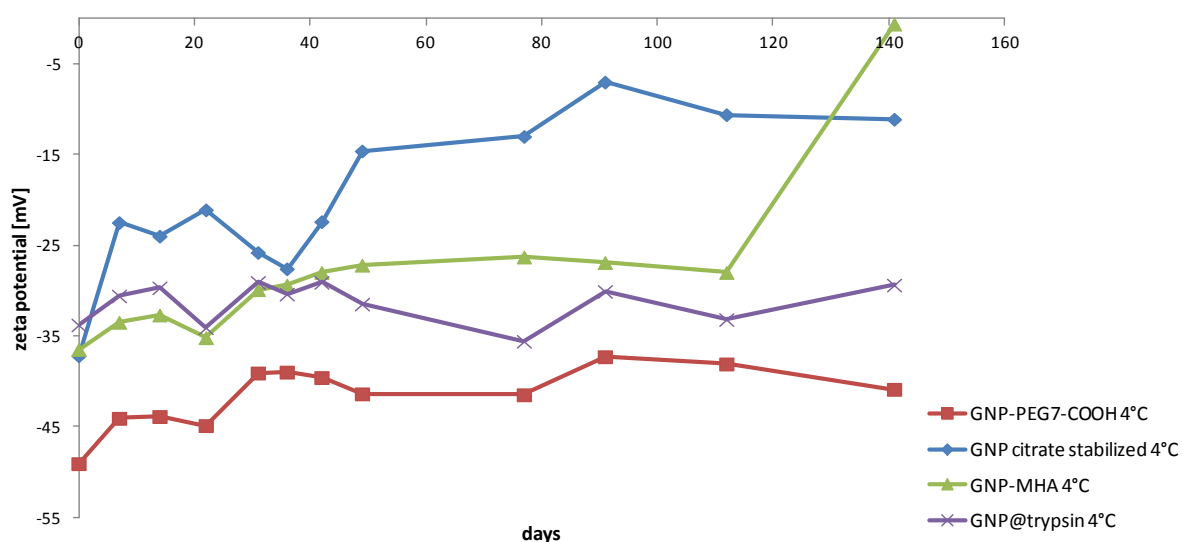


Figure 26: ZP values [mV] of GNP citrate stabilized, GNP-PEG₇-COOH, GNP-MHA and GNP@trypsin with a storage temperature of 4°C and a total storage time of 141 days.

Figure 27 depicts the ZP values of the aliquotes stored at -25°C. While the ZP values of GNP-PEG₇-COOH and GNP@trypsin are more or less constant and, the values around -30 mV still indicate stable colloidal systems for the total storage time. Likewise, the ZP value of the GNP-MHA aliquots slightly increase with the time, however a rise up to values about -20 mV after more than 100 days of storage was observed. For the citrate stabilized GNPs an immediate gain of the ZP to values about -10 mV is shown from the beginning of the storage. Therefore, the ZP of GNP-MHA and citrate stabilized GNPs attained values above the boundary to stable colloidal systems (q.v. 3.4.2) and may be regarded as unstable.

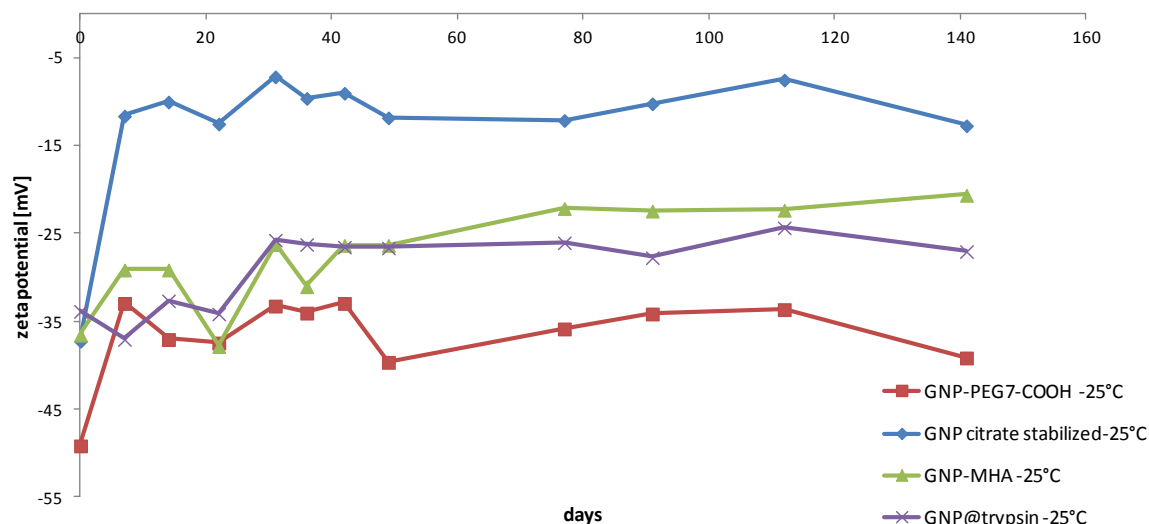


Figure 27: ZP values [mV] of GNP citrate stabilized, GNP-PEG₇-COOH, GNP-MHA and GNP@trypsin with a storage temperature of -25°C and a total storage time of 141 days.

The size distributions, determined by DLS, for the sample aliquots stored at a temperature of 4°C are given in Figure 28. Here, the size of the GNP-PEG7-COOH, GNP-MHA and GNP@trypsin stayed constant over the total storage time. However, for the citrate stabilized GNPs an increase of the size distribution with the time may be noticed, more precisely incipient with the 50th day of storage which is in accordance to data obtained from ZP and SPR spectra.

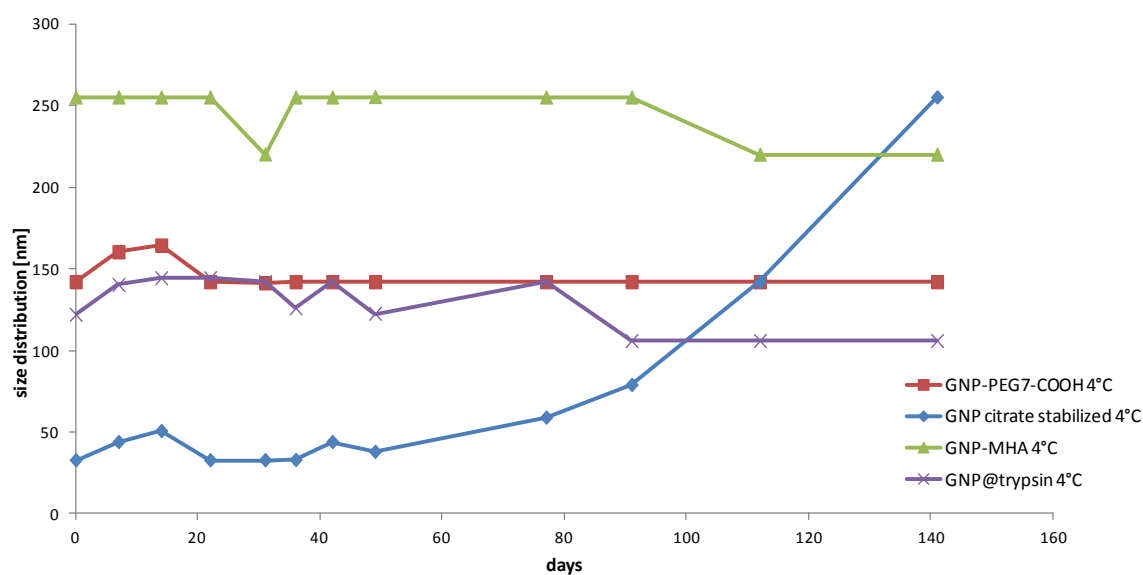


Figure 28: Size distribution [nm] of GNP citrate stabilized, GNP-PEG₇-COOH, GNP-MHA and GNP@trypsin with a storage temperature of 4°C and a total storage time of 141 days.

Figure 29 depicts the size distributions for the GNPs with a storage temperature of -25°C . While for both, GNP@trypsin and GNP-PEG₇-COOH the size decreased slightly with the storage time, for the citrate stabilized GNPs an increase of size with advancing periods of storage was observed. Furthermore, an additional peak in the range from 200 to 350 nm was detected for citrate stabilized GNPs for almost all samples, which indicates an aggregation of the citrate stabilized particles. For GNP-MHA an immediate decline of size was indicated after the first week of storage.

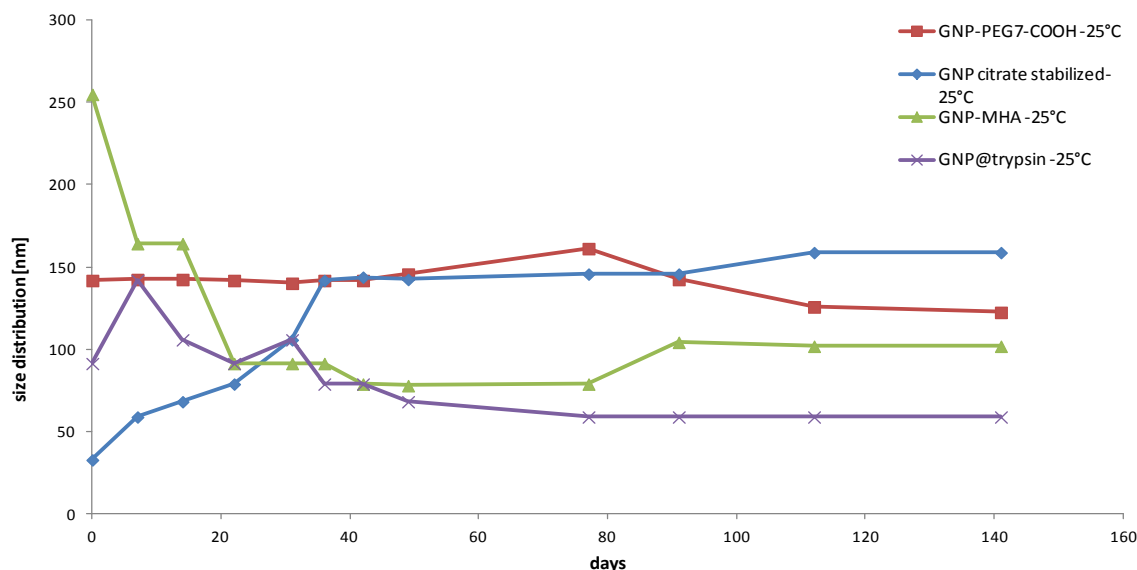


Figure 29: Size distribution [nm] of GNP citrate stabilized, GNP-PEG₇-SH, GNP-MHA and GNP@trypsin with a storage temperature of -25°C and a total storage time of 141 days.

Concluding, a long-term storage at a storage temperature of 4°C is possible without major changes of the characteristics for either, GNP@trypsin and GNP-PEG₇-COOH for almost 5 months (total storage time: 141 days). Aside, GNP-MHA can be stored for about 3 months at 4°C largely without changing properties. In contrast, the unproblematic storage time of citrate stabilized GNPs amounts to about one month. Accordingly, a destabilization of the colloidal systems takes place, as well as an increase of particle size and particle agglomerations.

Both, GNP@trypsin and GNP-PEG₇-COOH endure at least a storage time of 3 months at a storage temperature of -25°C , whereat only slight changes in ZP, size distribution and maximal absorbance may be observed. However, GNP-MHA as well as citrate stabilized GNPs are not appropriate for a storage under these temperature conditions. An immediate change of characteristics can be expected.

Figure 30 shows D,L-BApNA ($c = 1 \text{ mM}$) digestion assays (q.v. 4.2.3.2) accomplished with aliquots of GNP@trypsin stored at -25°C and 4°C for the total storage time of 141 days. As a reference, GNP@trypsin prepared directly before the assay was used. Despite the long storage time under different temperature conditions, the concentration of converted pNA of the GNP@trypsin 4°C and -25°C assays was only slightly below the concentration of the reference assay. Thus, one may suggest no substantial loss of activity due to the storage time and conditions.

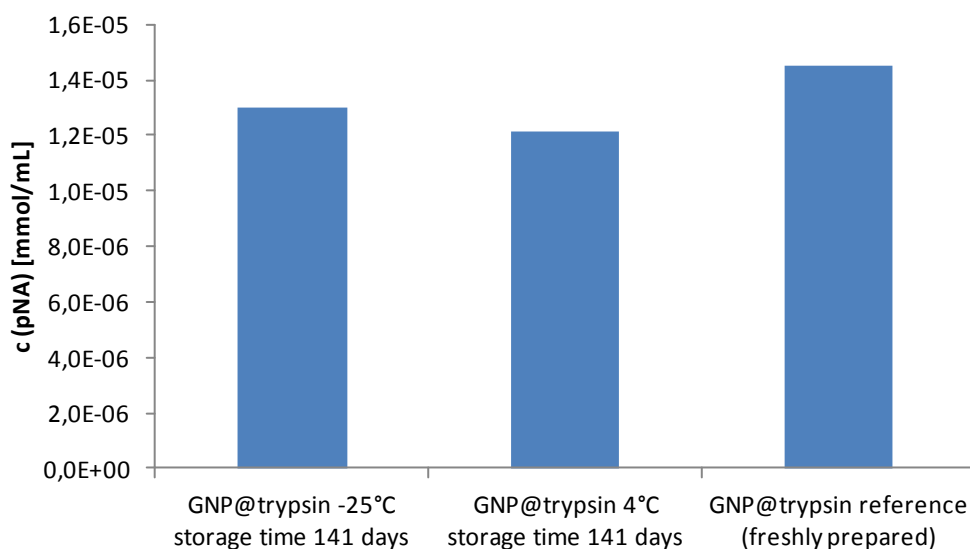


Figure 30: D,L-BApNA ($c = 1 \text{ mM}$) assay of GNP@trypsin -25°C (storage time 141 days), GNP@trypsin 4°C (storage time 141 days) and GNP@trypsin reference (freshly prepared). The reaction time amounted to 60 minutes, the absorbance was measured at 410 nm.

5.1.3 Reuseability of GNP@enzyme

Figure 31 gives the results of the D,L-BApNA assay, either accomplished with or without 0.1 (v/v) % Tween20, to determine the possibility of a reuse of GNP@trypsin (q.v. 4.2.5). Here, for the assay without Tween20 a rapid decrease of activity after the first reuse was observed. Accordingly, for reuse 2 and 3 the concentration of the converted pNA persisted at an approximately consistent low level. However, the addition of 0.1 (v/v) % Tween20 yielded a much less decrease of activity. Moreover, the activity decreased slightly with each reuse, but still remained at a higher level than without Tween20.

The reduced loss of activity and hence the higher reuseability of the assay accomplished with

0.1 (v/v) % Tween20 arises from the depletion stabilization of the colloids, caused by created steric barrier between the approaching particles. Consequently, the addition of the nonionic tenside Tween20 enables a reuse of the GNP@trypsin, however one must consider a constant loss of activity with increasing number of reuses.

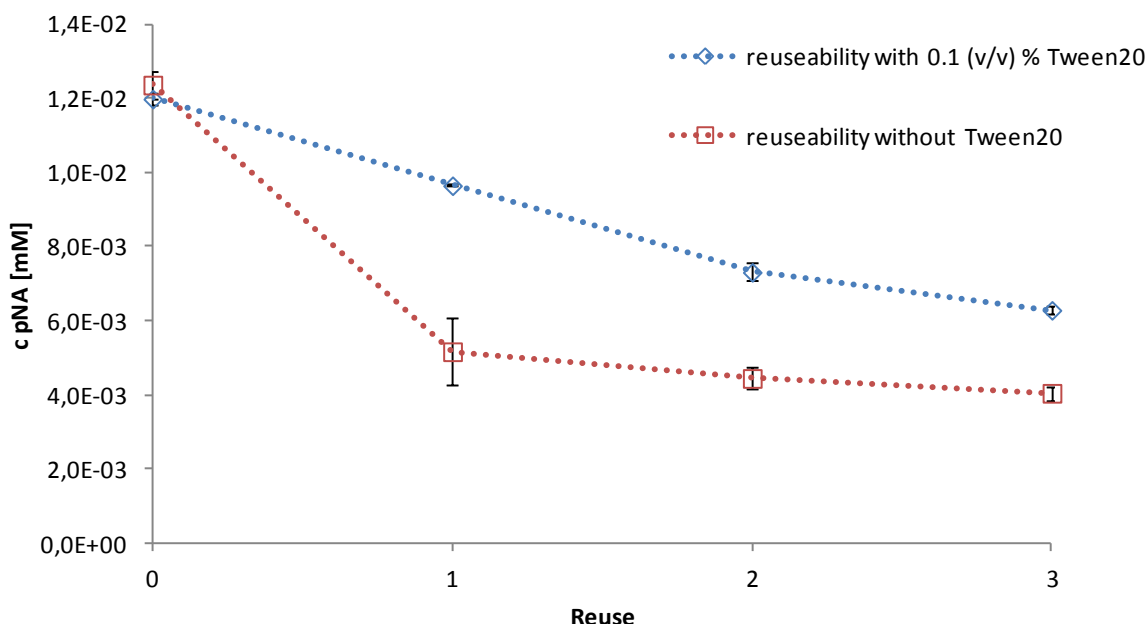


Figure 31: D,L-BApNA ($c = 1.5 \text{ mM}$) digestion assay to determine the reuseability of GNP@trypsin, accomplished without Tween20 as well as with 0.1 (v/v) % Tween20 with a reaction time of 60 min. 3 reuses were done and the absorbance was measured at 410 nm.

Furthermore, the GNP@trypsin concentration of the solution was characterized before each reuse (q.v. 4.2.5) to correlate the decrease of activity with the loss of GNP@trypsin concentration. Figure 32 shows the correlation between the concentration of converted pNA and consequently the activity and the concentration of residual GNP@trypsin in the solution. Thereby, a direct relation between the decrease of the activity and the decrease of the GNP@trypsin concentration with each reuse step may be observed. Hence, the minor conversion of D,L-BApNA to p-NA is not ascribed to the minor activity of the reused GNP@trypsin, but can be explained by the reduced GNP@trypsin concentration in the solution aroused due to the washing steps between the reuses. To achieve consistent values for the activity, one must consider a correction factor to adjust the volume of the reused GNP@trypsin solution.

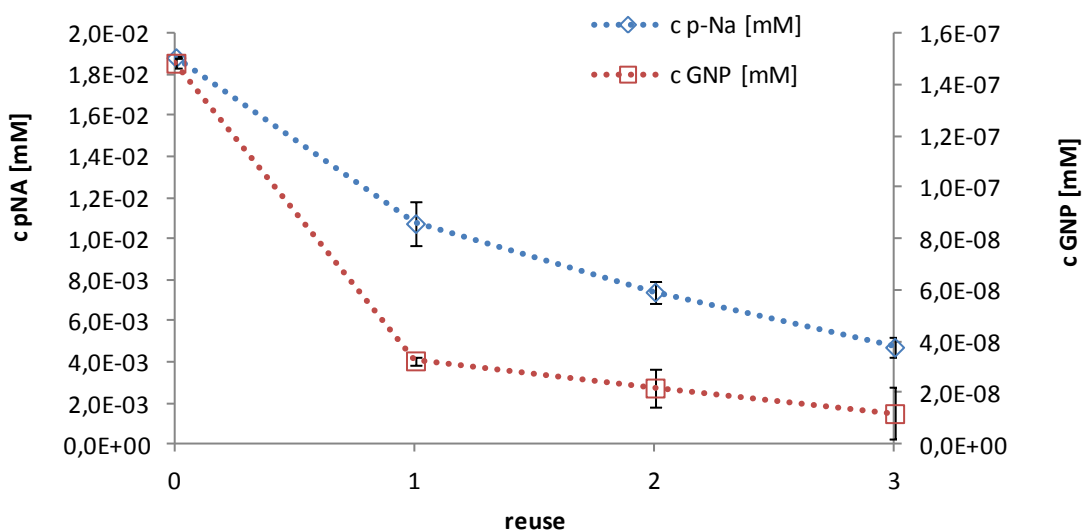


Figure 32: D,L-BApNA (c= 1.5 mM) digestion assay to determine the reuseability of GNP@trypsin, accomplished with 0.1 (v/v) % Tween20 with a reaction time of 60 min. 3 reuses were done and the absorbance was measured at 410 nm. Moreover, the GNP@trypsin concentration was determined before each reuse.

5.2 Determination of enzyme activity – Stereoselectiv and nonstereoselectiv D,L-BApNA digestion assay

5.2.1 Solubility of BApNA

As already observed in foregoing experiments, in higher concentrations the substrate D,L-BApNA is not soluble in higher concentrations and falls out of suspension after a few hours. To determine the soluble concentration and to figure out the influence of temperature for solubility, standard solutions were prepared and stored at different temperatures (q.v. 4.2.3.2 Precipitation of D,L-BApNA). After storage at 25°C and 4°C, respectively, a precipitate in the sample solutions with 2, 3 and 5 mM D,L-BApNA was formed. However, the solutions with a concentration of 0.5 and 1 mM were found to be stable.

Figure 33 shows the absorbance of the sample solutions measured immediately after preparation and after 1 day of storage, respectively. While the sample solutions exhibit a linear increase with the D,L-BApNA concentration when freshly prepared, the stored samples above 1 mM showed a decrease in the concentration. Due to the precipitation of D,L-BApNA in the solution, the absorbances were much lower than expected. Between the different storage temperatures, only a slight difference was observed.

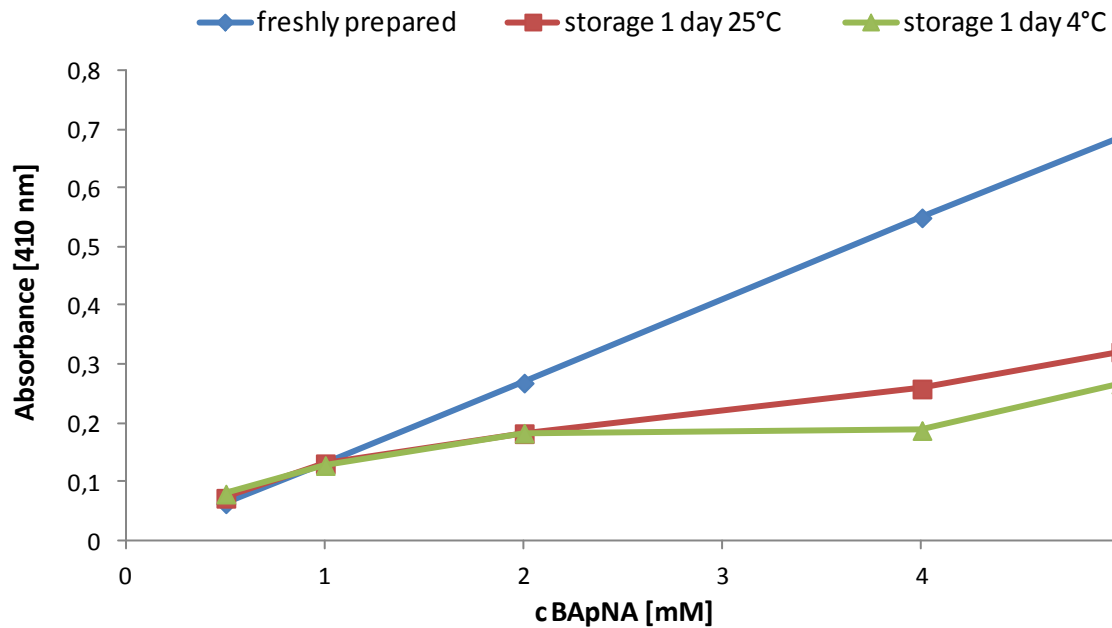


Figure 33: UV/vis detection of D,L-BApNA solutions with a concentration of 0.5 to 5 mM with 10% DMSO, detected at $\lambda = 410$ nm before and after storage. The storage time was 1 day at a temperature of 25°C and 4°C, respectively.

5.2.2 Determination of M. M. constants K_m , v_{max} and specific enzyme activity

The M. M. constants v_{max} , K_M , K_M/v_{max} and specific activity of trypsin (1mg mL^{-1}) and α -chymotrypsin (1mg mL^{-1}) in solution as well as of GNP@trypsin and GNP@ α -chymotrypsin were determined with BApNA digestion assay (4.2.3.1) using substrate concentrations in a range from 0.5 to 4 mM. Figure 34 a) shows the M.M. diagram of the assay of trypsin (1mg mL^{-1}) in solution. Corresponding, Figure 34 b) shows the Lineweaver-Burk diagram of the assay.

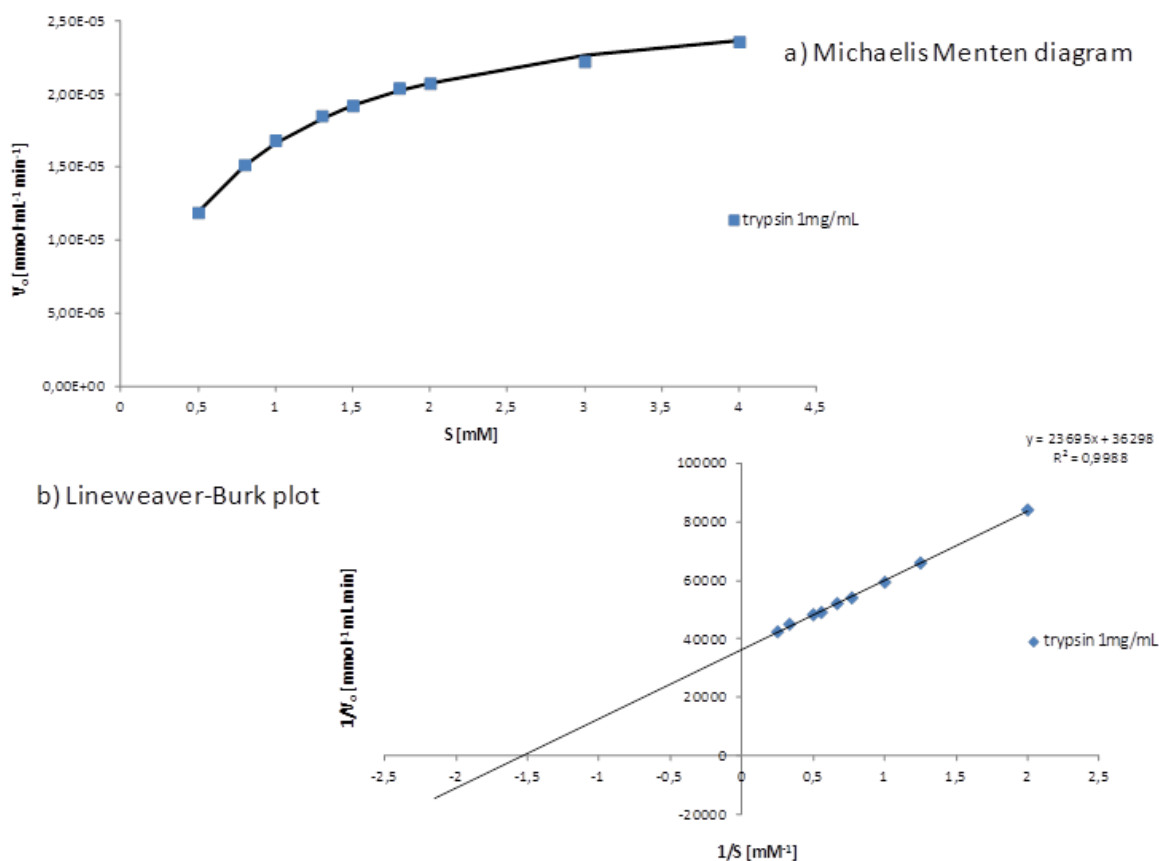


Figure 34: a) M.M. diagram of BApNA digestion assay ($c = 0.5 - 4 \text{ mM}$) for trypsin (1 mg mL^{-1}) in solution b) Lineweaver-Burk diagram of BApNA digestion assay ($c = 0.5 - 4 \text{ mM}$) for trypsin in solution (1 mg mL^{-1}), both with a digestion time of 15 minutes, measured at $\lambda = 410 \text{ nm}$.

Table 7: Michaelis-Menten constants V_{\max} , K_M , specific activity and K_M/V_{\max} for trypsin in solution (1 mg mL^{-1}), α -chymotrypsin (1 mg mL^{-1}), GNP@trypsin and GNP@ α -chymotrypsin shows the Michaelis-Menten constants V_{\max} , K_M , specific activity and K_M/V_{\max} for trypsin in solution (1 mg mL^{-1}), α -chymotrypsin (1 mg mL^{-1}), GNP@trypsin and GNP@ α -chymotrypsin. The K_M value of trypsin in solution was determined with 0.66 mM . This is in accordance to the literature, where under the same or similar conditions, such as pH value and temperature, K_M values in the range from $0.43 - 0.88$ were obtained [101], [102]. A considerably higher K_M value, 7.52 mM , and therefore a lower enzyme affinity was determined for α -chymotrypsin in solution. This result can be explained by the not ideal cleavage opportunities of the substrate D,L -BApNA for α -chymotrypsin [103], which cleaves preferentially peptide bonds next to the carbonylic group of an aromatic amino acid (q.v. 3.5.1). Equally, a higher V_{\max} and specific activity was observed for the trypsin in solution. With a K_M value of 3.06 mM GNP@trypsin shows a lower enzyme activity to the substrate D,L -BApNA than trypsin in solution. For GNP@ α -chymotrypsin a considerably lower enzyme

affinity with a K_M value of 11.31 mM was determined.

Table 7: Michelis Menten constants V_{max} , K_M , specific activity and K_M/V_{max} for trypsin in solution (1 mg mL^{-1}), α -chymotrypsin (1 mg mL^{-1}), GNP@trypsin and GNP@ α -chymotrypsin of a BApNA assay ($c = 0.5 - 4 \text{ mM}$) with a digestion time of 15 min.

	V_{max} [mmol mL ⁻¹ min ⁻¹]	K_M [mM]	specific activity [mmol ml ⁻¹ mg ⁻¹]	K_M/V_{max} [min ⁻¹]
trypsin	2.78E-05	0.66	1.39E-03	2.37E+01
α-chymotrypsin	3.61E-06	7.52	1.81E-04	2.08E+03
GNP@trypsin	1.20 E-06	3.06	1.17E-05	1.06E+03
GNP@α-chymotrypsin	1.79E-06	11.31	1.79E-05	6.57E+03

5.3 D,L-BApNA hydrolysis – Determination of enantioselectivity of GNP@enzyme

5.3.1 Enantioselective cleavage of D,L-BApNA

The enantioselectivity of GNP@trypsin and GNP@ α -chymotrypsin was determined by HPLC separation with an Htau-QD silica column (q.v. 4.1.3.1) of D,L-BApNA digestion assay samples (q.v. 4.2.3.2).

Figure 35 shows the HPLC enantioseparation of the substrate D,L-BApNA and the product D,L-Bz-Arg for the GNP@trypsin BApNA assay with substrate concentrations in the range of 1.0 to 5.0 mM with 10 (v/v) % DMSO and a digestion time of 30 minutes. Both cleavage products of D,L-BApNa, L-Bz-Arg and D-Bz-Arg, were detected separately. A distinct increase of L-Bz-Arg and a considerably lower increase of D-Bz-Arg with increasing substrate concentration were obtained.

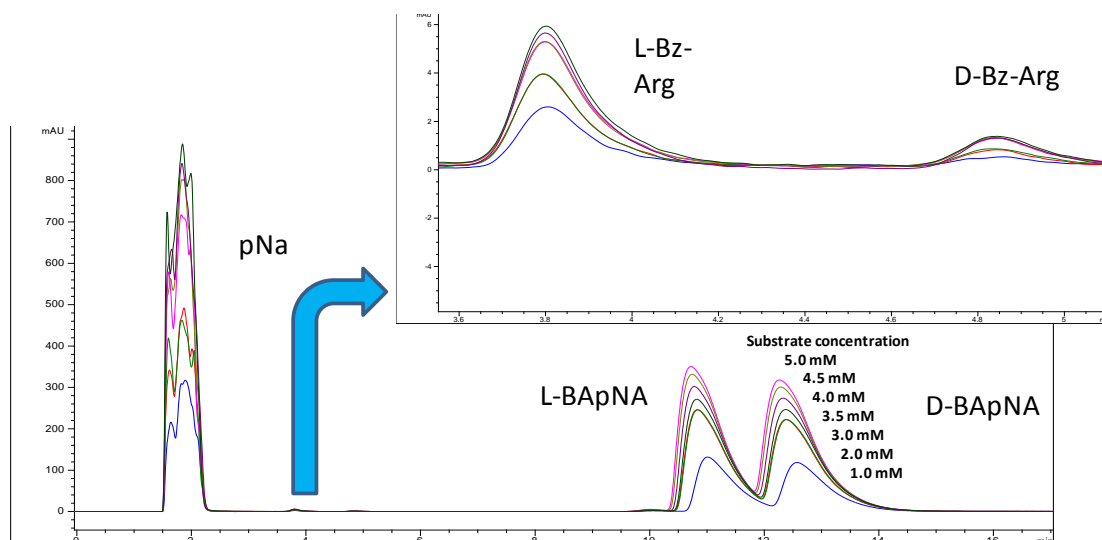


Figure 35: HPLC chromatogram of GNP@trypsin BApNA assay ($c = 1.0 - 5.0$ mM with 10 (v/v) % DMSO and a digestion time of 30 min). The separations of the substrate D,L- BApNA and the products D and L-Bz-Arg (insert) are depicted. Mobile Phase: MeOH 50 mM FA 25 mM DEA 1 ml min^{-1} , UV detection.

In Figure 36 the areas of the products L-Bz-Arg and D-Bz-Arg, respectively, of the GNP@trypsin and GNP@ α -chymotrypsin BApNA assay are depicted. While for GNP@ α -chymotrypsin the formation of L-Bz-Arg and D-Bz-Arg was approximate the same, for GNP@trypsin a preferred formation of L-Bz-Arg compared to D-Bz-Arg was detected. Here, the increase of concentration of formed L-Bz-Arg was correlated to the increase of substrate concentration.

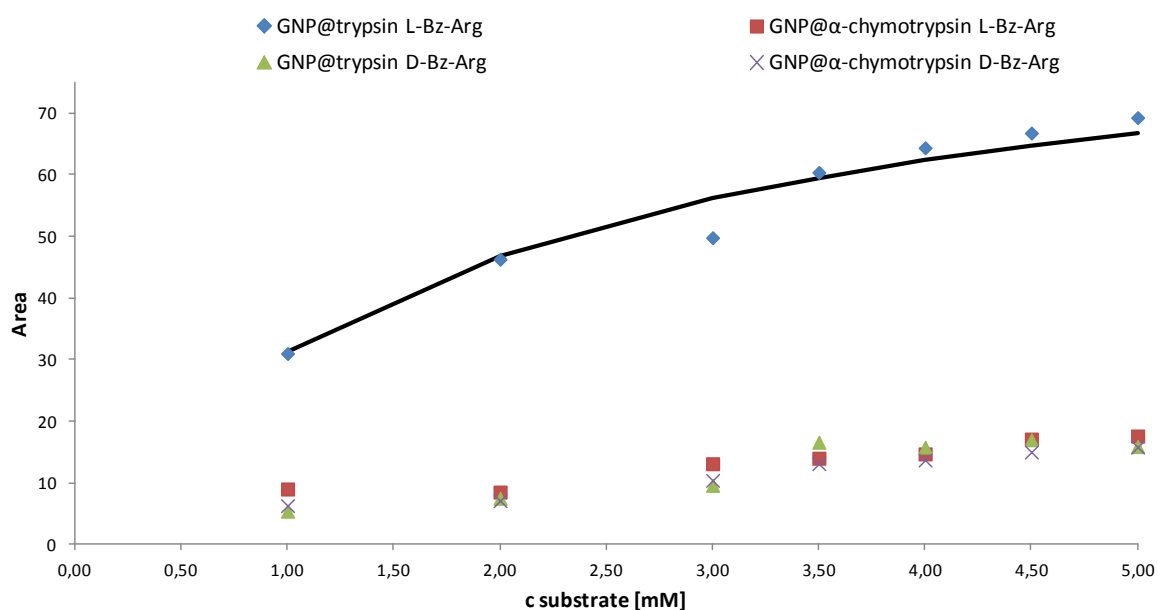


Figure 36: Plot of area of the products D-Bz-Arg and L-Bz-Arg of GNP@trypsin BApNA assay and GNP@ α -chymotrypsin BApNA assay ($c = 1.0 - 5.0$ mM with 10 (v/v) % DMSO with a digestion time of 30 min). Mobile Phase: MeOH 50 mM FA 25 mM DEA 1 ml min^{-1} , UV detection.

To determine the reason for the not enantioselective cleavage of D,L-BApNA, a GNP@trypsin BApNa assay with a constant substrate concentration of 0.45 mM without DMSO, but different digestion times in a range from 30 to 1740 min was done. Figure 37 illustrates the HPLC separation data of this assay. Here, an increase of L-Bz-Arg (Insert 1) with time was observed, while the area of the L-enantiomer (Insert 2) of the substrate was decreasing with the time due to conversion. Neither D-Bz-Arg, nor a consumption of D-BApNA was detected.

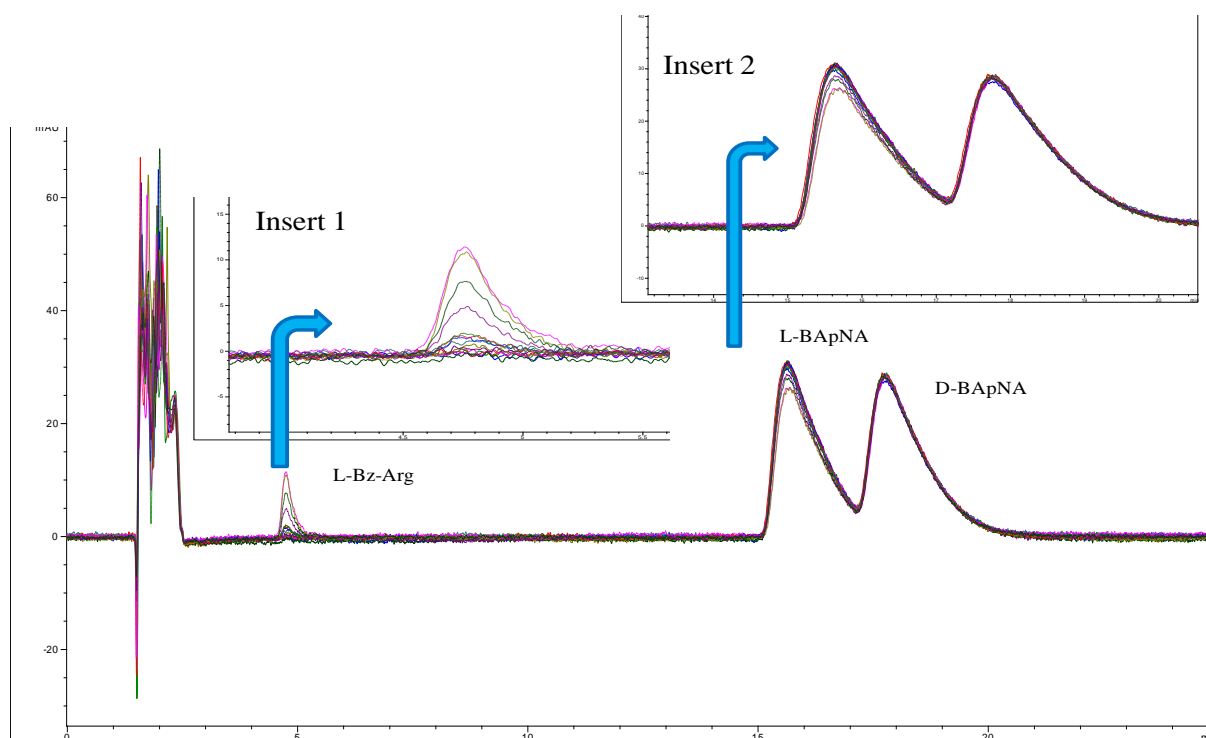


Figure 37: HPLC chromatogram of GNP@trypsin BApNA assay ($c = 0.45$ mM without DMSO and digestion times from 0 – 1740 min). The separations of the substrate D,L- BApNA shows a decrease of L-BApNa with digestion time (insert 2) and the product L-Bz-Arg (insert 1) an increase. Mobile Phase: MeOH 50 mM FA 25 mM DEA 1ml min^{-1} , UV detection.

Figure 38 a) depicts the HPLC detection of the area increase of L-Bz-Arg with digestion time for the GNP@trypsin BApNA assay and Figure 38 b) shows the increase of absorbance due to pNa formation, detected with UV/Vis. In both cases, an increase of product formation, either pNA (b) or L-Bz-Arg (a) was observed. In Table 8 the L-Bz-Arg areas correlating to the digestion times are given, while no formation of the product D-Bz-Arg was detected.

Table 8: Increase of L-Bz-Arg with time of GNP@trypsin BApNA assay (c= 0.45 mM without DMSO with digestion times from 30 – 1740 min).

Digestion time [min]	L-Bz-Arg Area	D-Bz-Arg
30	18.4	-
45	21.1	-
60	25.9	-
120	31.7	-
180	43.5	-
240	56.5	-
300	66	-
1440	103.9	-
1740	133.8	-

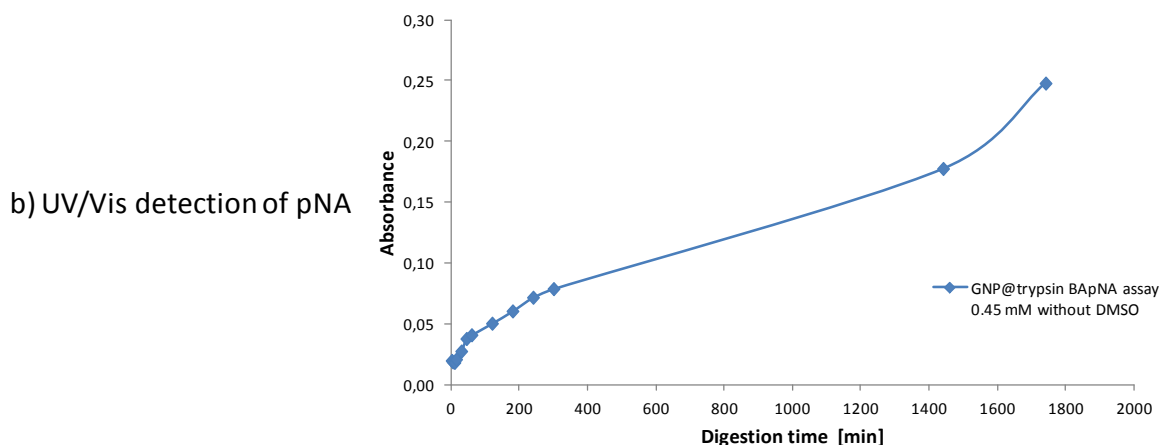
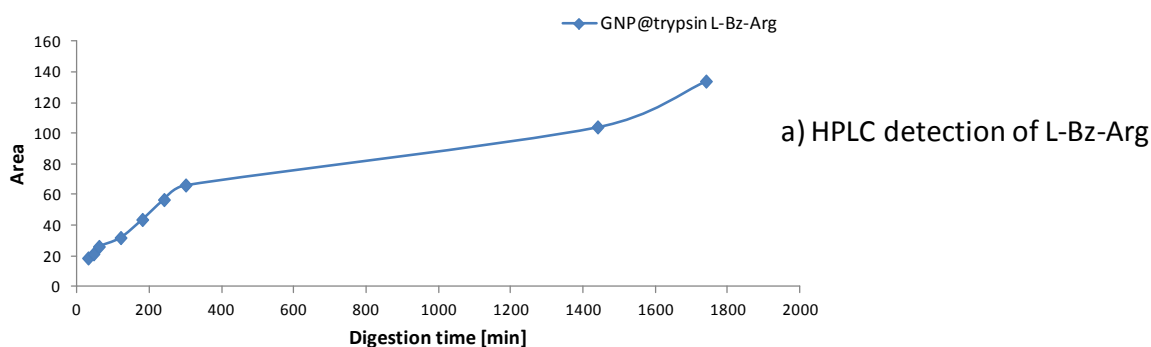


Figure 38: GNP@trypsin BApNA assay (c= 0.45 mM without DMSO with digestion times from 30 – 1740 min): a) HPLC detection of the increase of the product L-Bz-Arg. Mobile Phase: MeOH 50 mM FA 25 mM DEA 1ml min⁻¹, UV detection. b) UV/Vis detection of p-NA at $\lambda=410$ nm.

Since in this GNP@trypsin BApNA assay without DMSO and lower substrate concentrations no D-Bz-Arg was detected, one may assume a correlation between the enantioselectivity and either the substrate concentrations or the deployed solvents. To investigate their effect on the enantioselective formation of the product, further assays with different solvents were

required (q.v. 5.3.2). Furthermore, a GNP@trypsin BApNA assay with 10 (v/v) % DMSO and substrate concentration in a range of 0.05 to 5 mM and digestion times from 15 to 1440 minutes was done.

In Table 9 the M. M. constants V_{max} , K_M , specific activity and K_M/V_{max} are given. While the K_M of the digestion times between 15 and 300 min were coincident with the values obtain for GNP@trypsin BApNa assays in 5.2.2, the value for the assay with a digestion time of 1440 min was twice as high.

Table 9: M. M. constants V_{max} , K_M , specific activity and K_M/V_{max} for GNP@trypsin of a BApNA assay ($c = 0.05 - 5$ mM) with digestion times of 15 to 1440 min.

Digestion time [min]	V_{max} [mmol mL ⁻¹ min ⁻¹]	K_M [mM]	specific activity [mmol ml ⁻¹ mg ⁻¹]	K_M/V_{max} [min ⁻¹]
15	8.35E-07	1.82	4.18E-06	2.18E+06
30	3.85E-07	1.94	1.93E-06	5.04E+06
60	2.47E-07	1.98	1.24E-06	8.01E+06
300	6.38E-08	2.04	3.19E-07	3.20E+07
1440	6.91E-08	3.94	3.46E-07	5.70E+07

Figure 39 shows exemplarily the HPLC separation for all substrate concentrations of the D,L-BApNA assay at a digestion time of 1440 min. Even for long digestion times, one may observe the formation of the product D-Bz-Arg only at substrate concentrations higher than 1 mM, while a formation of L-Bz-Arg was detected for all concentrations. The border of concentration, from which a formation of D-Bz-Arg was detectable, was decreasing with increasing digestion time. For the digestion times 15 to 300 minutes, a formation of D-Bz-Arg was observable not until a substrate concentration of 2.5 mM (see Figure 40). Moreover, an increase of the formed products D-Bz-Arg with increasing digestion times was detected. In Figure 41 the formation of L-Bz-Arg is depicted. As well as for D-Bz-Arg an increase with increasing digestion times and substrate concentrations was observed, however a considerably higher formation, incipient at substantial lower substrate concentrations and digestion times, was detected. For instance, while at a digestion time of 1440 min and a substrate concentration of 5 mM for the formed D-Bz-Arg an Area of 51.6 was measured, the formation of L-Bz-Arg achieved an area of 260.2.

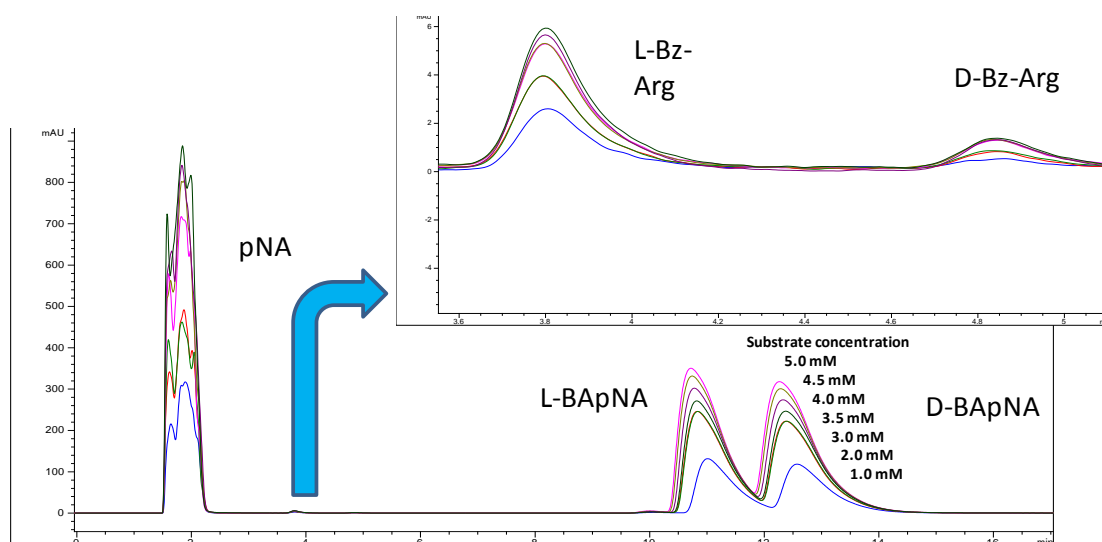


Figure 39: HPLC chromatogram of GNP@trypsin BApNA assay ($c = 0.05 - 5 \text{ mM}$ with 10 (v/v) % DMSO and digestion times from 0 – 1440 min). The separations of the substrate D and L- BApNA and the products D and L- Bz-Arg (insert) are depicted. Mobile Phase: MeOH 50 mM FA 25 mM DEA 1ml/min, UV detection.

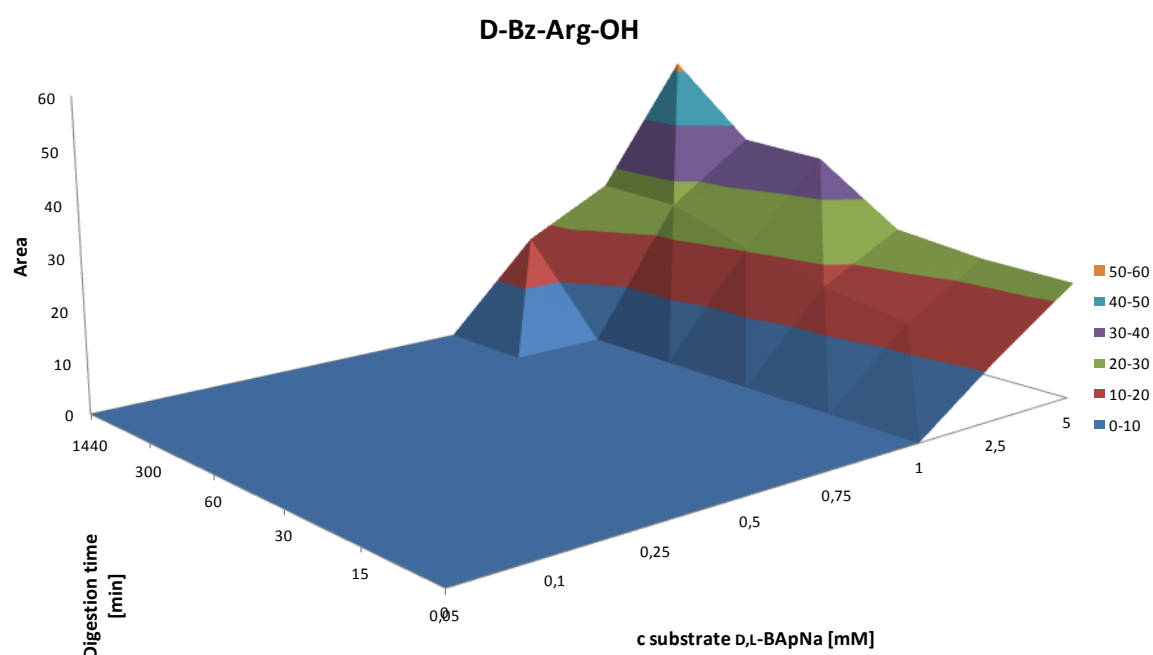


Figure 40: HPCL detection of area increase of the product D-Bz-Arg with digestion time (30 – 1440 min) and substrate concentration (0.05 – 5 mM with 10 (v/v) % DMSO). Mobile Phase: MeOH, 50 mM FA, 25 mM DEA, 1 mg mL^{-1} , UV- detection.

Indeed, a completely enantioselectivity in favor of the L-enantiomer was determined for substrate concentrations below 2.5 mM and 1 mM, respectively, for digestion times in time domains of over 1140 min (equates to one day). Beyond that, also a conversion of the D-enantiomer was affected, even though in a distinct minor degree. Hence, enantioselectivity was correlated to concentration of the substrate and the digestion time.

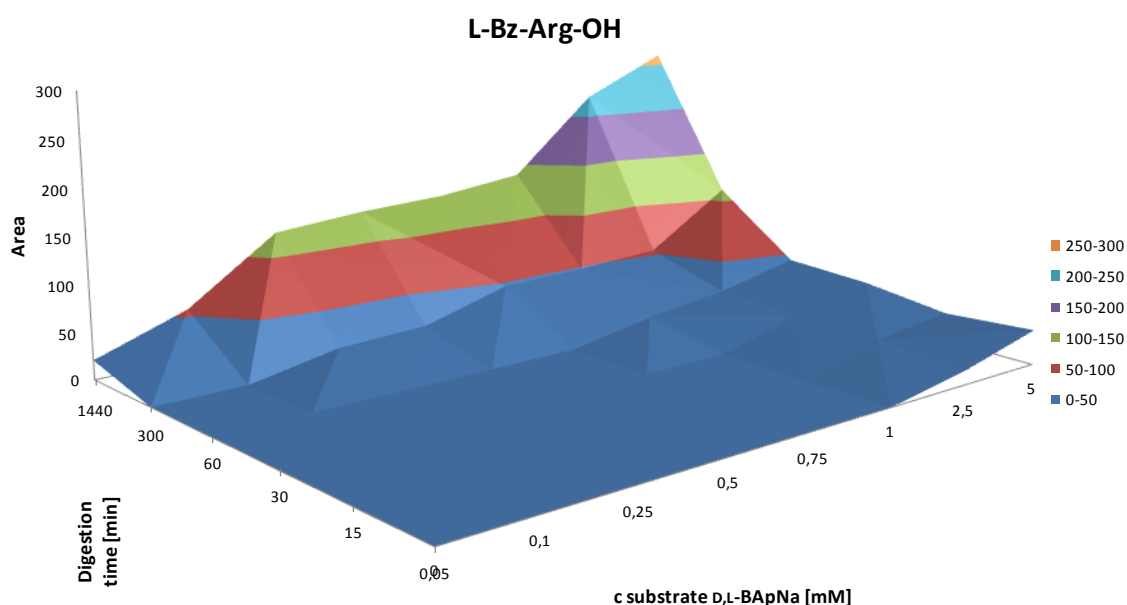


Figure 41: HPLC detection of increase of the product L-Bz-Arg with digestion time (30 – 1440 min) and substrate concentration (0.05 – 5 mM with 10 (v/v) % DMSO). Mobile Phase: MeOH, 50 mM FA, 25 mM DEA, 1 mg mL^{-1} , UV- detection.

5.3.1.1 Enantioselectivity after total consumption of L-enantiomer

To determine the enantioselectivity of the cleavage of D,L- BApNA after completely consumption of the L-enantiomer, a GNP@trypsin BApNa assay with a substrate concentration of 0.05 mM without DMSO and digestion times between 30 min and 29 h was performed.

After the total cleavage of L-BApNA of a racemic D,L-BApNA substrate sample to L-Bz-Arg (17h), also D-BApNa was cleaved to D-Bz-Arg, but below the limit of detection, and with a much slower conversion rate. Even after 29 h reaction time less than one third of D-BApNA was cleaved. Figure 42 shows the UV/Vis detection of the digested samples. After a digestion time of more than 1000 min (equates to 17 h) no further increase of the absorbance and hence no further pNA formation was detected.

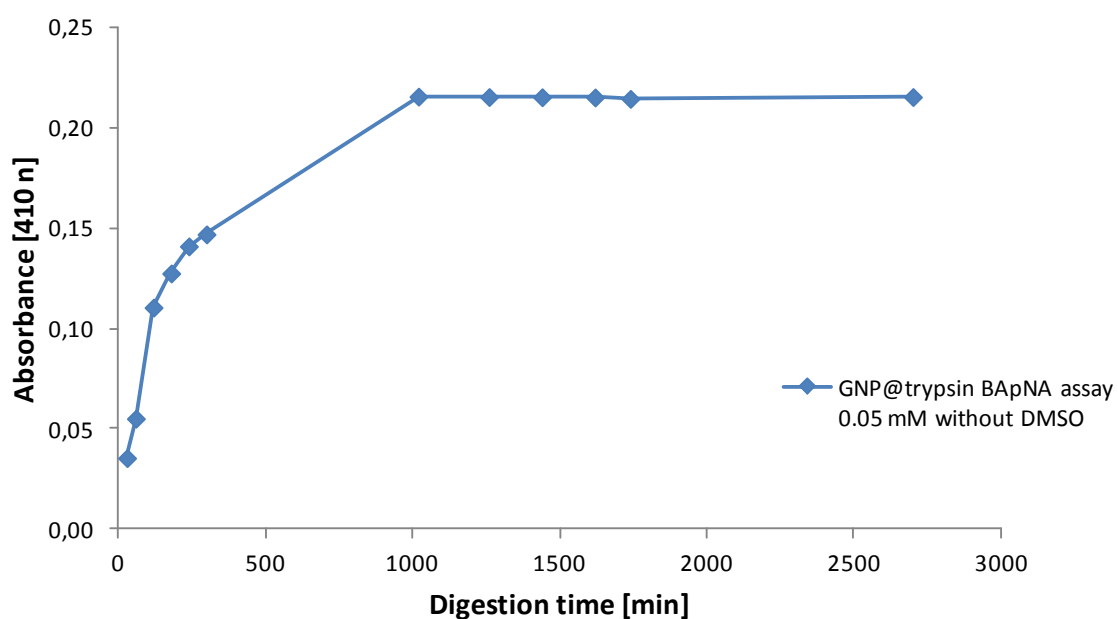


Figure 42: UV/Vis detection of GNP@trypsin BApNA assay (c = 0.05 mM without DMSO with digestion times from 30 – 1740 min) at $\lambda=410$ nm.

Table 10: Increase of L-Bz-Arg and respectively decrease of the substrate with time of GNP@trypsin D,L-BApNA assay (c= 0.05 mM without DMSO with digestion times from 30 – 1740 min).

Digestion time [h]	L-Bz-Arg Area	L-BApNA Area	D-Bz-Arg Area	D-BApNA Area
0.5	24	213.5	-	277.2
1	40.2	204.2	-	277.5
2	71.9	128.1	-	276
3	73.4	93.4	-	273.4
4	88.3	76.1	-	264.5
5	91.2	0	-	245.5
17	129.3	0	-	247.1
21	131.7	0	-	232.5
24	133.6	0	-	232.4
27	131.3	0	-	232.9
29	131.9	0	-	232.3

Table 10 gives the areas of the substrates L-BApNA and D-BApNA, respectively, as well as the formation of the product L-Bz-Arg. After a digestion time of 5 hours, the L-enantiomer was totally consumed, subsequently a final increase of L-Bz-Arg was observed, followed by a perpetuation of the product concentration (see Figure 43). Simultaneously, after the total consumption of L-BApNa, a slight decrease of D-BApNA was detected. However, at neither time a product (D-Bz-Arg) of the possible D-BApNa cleavage was detected. One assumption may be that the formed product D-Bz-Arg was yet below the limit of detection (LOD) (q.v. 5.6). Otherwise, the slight decrease of D-BApNA can be ascribed to a faint, not visible to the naked eye precipitate of the substrate due to the waiting period aroused by the high sample throughput during the HPLC analysis.

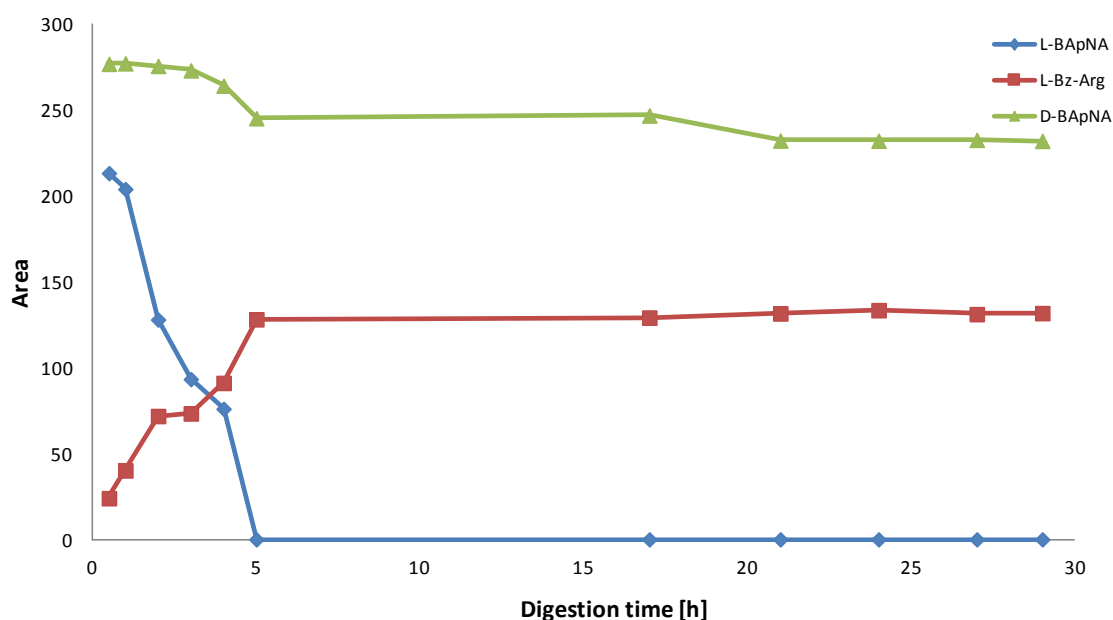


Figure 43: Increase of L-Bz-Arg and respectively decrease of the substrate with time of GNP@trypsin BApNA assay (c= 0.05 mM without DMSO with digestion times from 30 – 1740 min). Mobile Phase: MeOH, 50 mM FA, 25 mM DEA, 1mg mL⁻¹, UV- detection.

5.3.2 Enantioselectivity – influence of different solvents

An eventual effect of different solvents to the enantioselectivity of GNP@trypsin was determined with D,L-BApNA assays, either with 5 (v/v) % or 10 (v/v) % DMSO, EtOH, MeOH and AmBic-buffer, respectively. The D,L BApNA digestion assays were performed with a constant substrate concentration of 0.05 mM, whereof 0.025 mM are L- and 0.025 mM are D-enantiomer. The digestion times ranged from 1 to 7 h.

The Figure 44 a) and b) shows the UV/Vis-detection of the pNA formation for 5 (v/v) % and 10 (v/v) % solvent addition to the aqueous buffer, respectively. Neither for 5 (v/v) % solvent nor for 10 (v/v) % substantial differences between the used solvents in the concentration of the formed product pNA were observed.

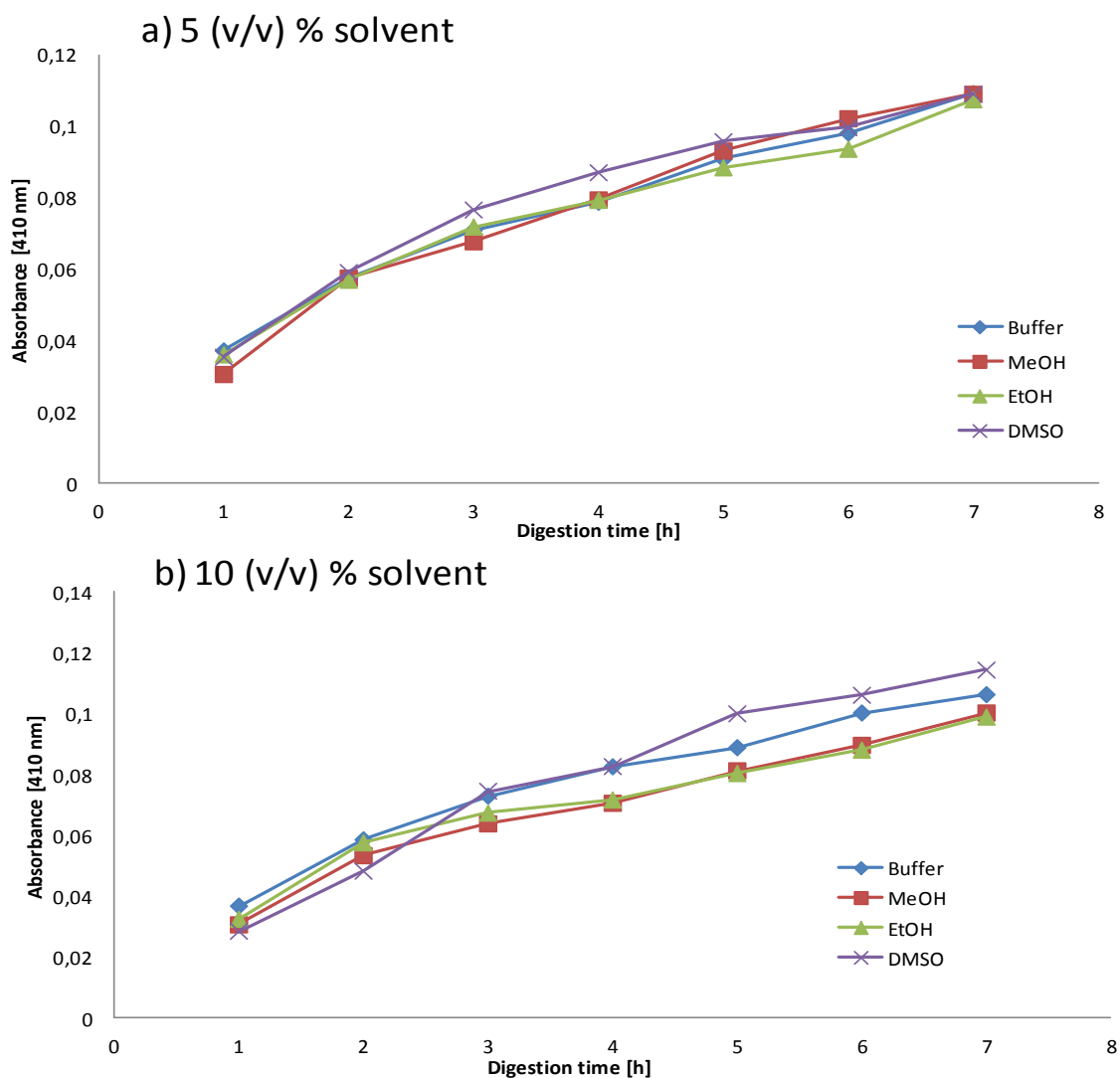


Figure 44: UV/Vis detection of GNP@trypsin D,L-BApNA digestion assay ($c = 0.05 \text{ mM}$) a) 5 (v/v) % solvent, b) 10 (v/v) % solvent, both with digestion times from 1 – 7 h) at $\lambda = 410 \text{ nm}$.

The Figure 45 depicts the increase of L-Bz-Arg with increasing digestion times with a) 5 (v/v) % and b) 10 (v/v) % solvent, respectively. For both assays, only very slight differences between the used solvents related to the product formation were detectable. Moreover, in neither of the assays a formation of D-Bz-Arg was observed. Hence, for the tested solvents no influence of enantioselectivity was established.

Furthermore, neither a significant increase in speed of the pNA formation (Figure 44) nor of the L-Bz-Arg formation (Figure 45) was observed.

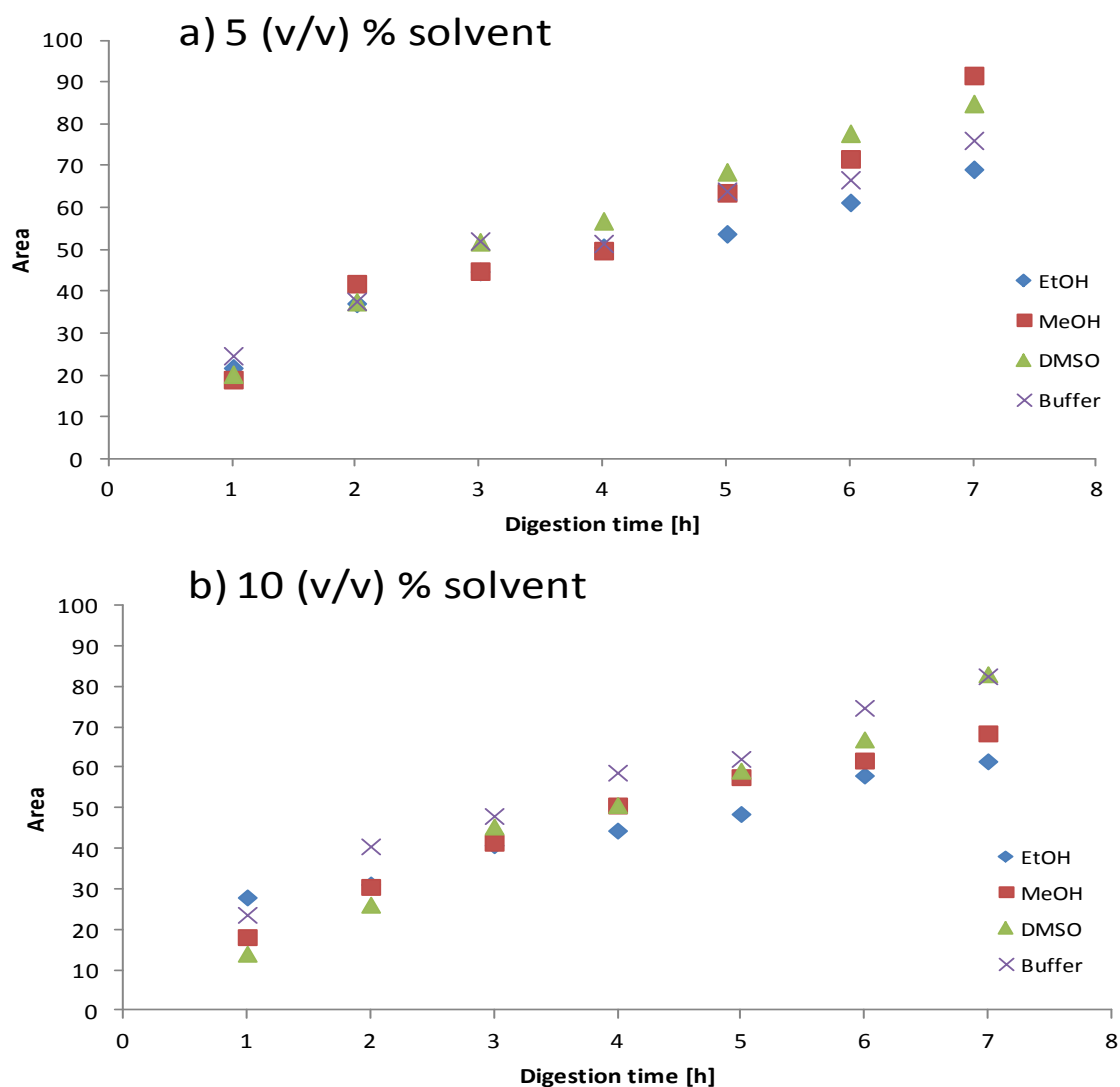


Figure 45: Increase of L-Bz-Arg with time of GNP@trypsin D,L-BApNA digestion assay ($c = 0.05 \text{ mM}$) a) 5 (v/v) % solvent, b) 10 (v/v) % solvent, with digestion times from 1 – 7 h). Mobile Phase: MeOH, 50 mM FA, 25 mM DEA, 1 mg mL^{-1} , UV- detection.

5.4 Acetylation of trypsin and GNP@trypsin to improve enzyme activity

To verify the activity of self-made AANHS, D-Phe was acetylated analogue to 4.2.3.3 and then detected with HPLC (q.v. 4.1.3.2). Standard samples of not acetylated D-Phe and already acetylated bought AA-D-Phe (Sigma Aldrich, Germany) were injected. Thereby, the acetylation reagent AANHS could shown to be reactive (Figure 46) and was used for further studies to acetylate trypsin in-solution and immobilized onto GNPs, respectively.

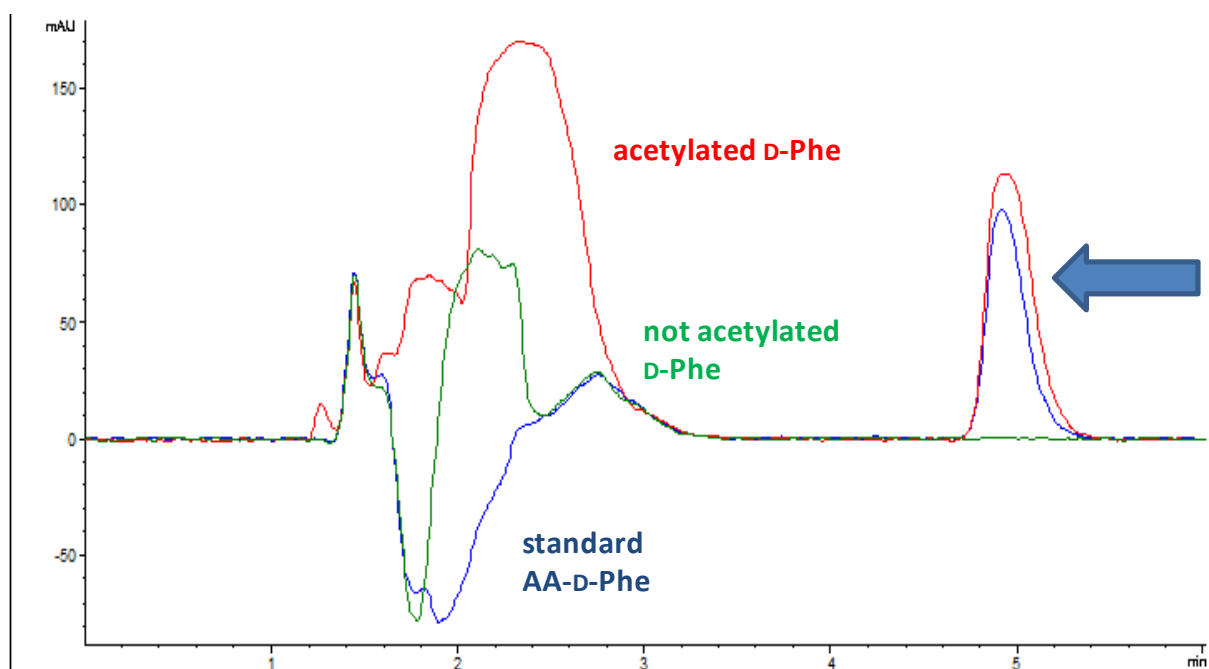


Figure 46: HPLC detection of standard AA-D-Phe (blue), acetylated D-Phe (red) and not acetylated D-Phe (green). Mobile phase MeOH, 25 mM FA, 12.5 NH₄FA, 0.55 mL min⁻¹. Column: QN-AX type, 390 μmol immobilized selector per g of 3-SHproyl modified Daisogel 5 μm 120 Å poresize (SH covered 840 μg/g silica).

5.4.1 Comparison of acetylated and not acetylated trypsin in-solution

As discussed in 3.5.3 (Enzym modifications (Acetylation)) Freije *et al.*[83] predicted not only an enhancement of trypsin stability towards autolysis, but also at least preserved or even improved digestion efficiencies towards cytochrome C. To observe the influence on the trypsin activity with the substrate D,L-BApNA, D,L-BApNA digestion assays with substrate concentrations from 0.1 to 6 mM with 10 (v/v) % DMSO and a digestion time of 30 minutes

were performed for trypsin in-solution acetylated and not acetylated.

Figure 47 shows the Lineweaver-Burk diagram of the D,L BApNA assays of trypsin in-solution acetylated and not acetylated. The M.M. constants K_M , V_{max} , specific activity and K_M/V_{max} of acetylated and not acetylated trypsin are given in Table 11. For the acetylated trypsin in-solution, no variation of the K_M value was determined, but V_{max} was increased due to acetylation for one order in magnitude. Hence, the prediction of Freije *et al.* was confirmed also for the substrate D,L-BApNA. The thesis of Murphy *et al.* [95] that no acetylation-dependent enhancement was obtained, is only valid for the K_M value, but not for V_{max} .

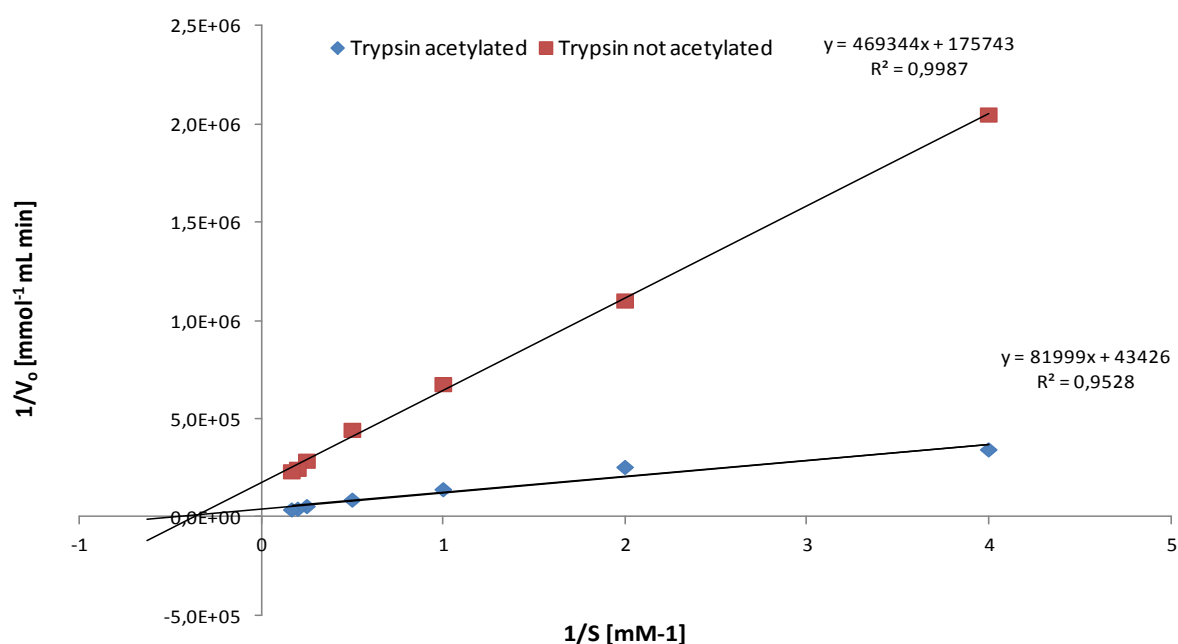


Figure 47: Lineweaver-Burk diagram of D,L-BApNA assay ($c = 0.1$ to 6 mM with 10 (v/v) % DMSO with a digestion time of 30 min) with trypsin in-solution acetylated and not acetylated, respectively.

Table 11: M. M. constants V_{max} , K_M , specific activity and K_M/V_{max} for trypsin in-solution acetylated and not acetylated BApNA assays ($c = 0.1 - 6$ mM with 10 (v/v) % DMSO and a digestion time of 30 min).

	V_{max} [mmol mL ⁻¹ min ⁻¹]	K_M [mM]	specific activity [mmol ml ⁻¹ mg ⁻¹]	K_M/V_{max} [min ⁻¹]
Trypsin not acetylated	2.59E-06	0.65	1.30E-05	2.52E+02
Trypsin acetylated	1.91E-05	0.62	9.54E-05	3.25E+01

5.4.2 Comparison of acetylated and not acetylated GNP@trypsin

The influence of acetylation was studied by acetylation of trypsin before and after immobilization onto GNP-PEG₇-COOH, respectively. Subsequently, the activity was determined with a D,L-BApNA solution with a concentration of 0.05 mM without DMSO and a digestion time of 30 min. Figure 48 shows the determined activity of GNP@trypsin acetylated before immobilization, GNP@trypsin acetylated after immobilization and not acetylated GNP@trypsin.

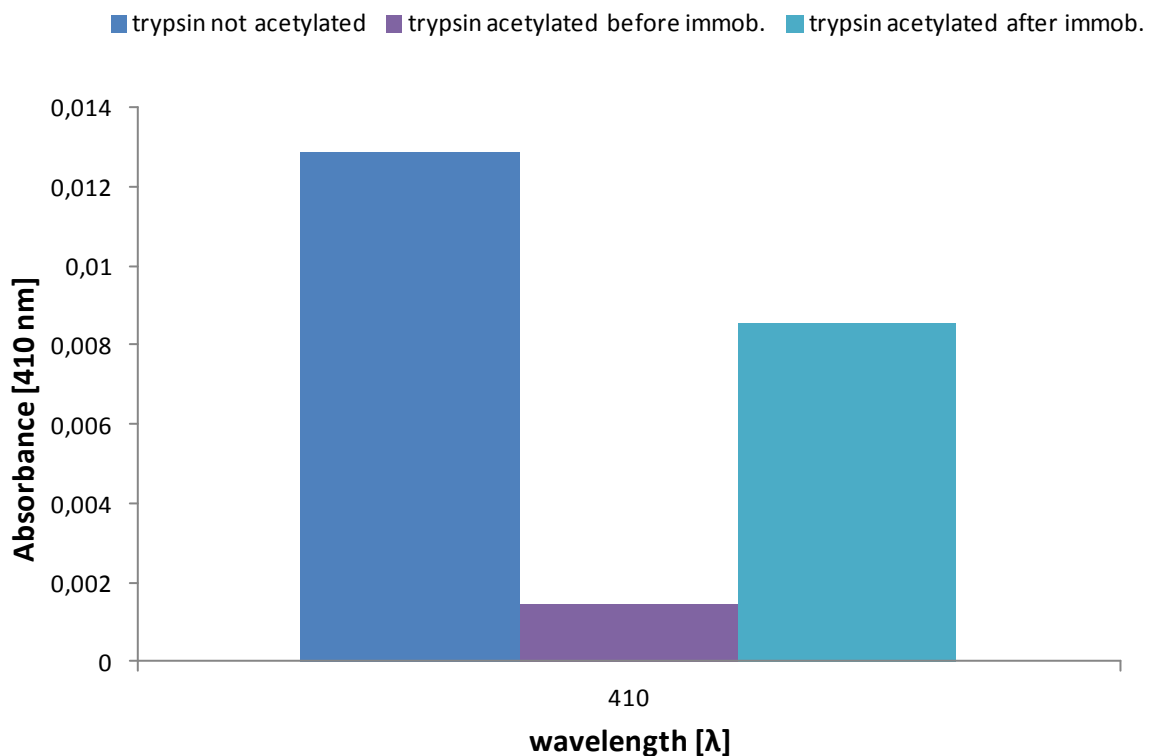


Figure 48: Determination of activity of trypsin not acetylated, trypsin acetylated before immobilization and trypsin acetylated after immobilization with a substrate concentration of 0.05 mM D,L-BApNA and a digestion time of 30 min.

Due to the acetylation before immobilization, the accessible amino groups are already blocked and therefore less trypsin can be linked onto the GNPs. Considering these results, the acetylation after immobilization onto the GNPs can be considered as more favourable than before the acetylation. Thus the following acetylation experiments were done with particles acetylated after trypsin-immobilization.

Analogue to 5.4.1 the M.M constants of GNP@trypsin acetylated and not acetylated were determined (Figure 49). Table 12 gives the values for K_M , specific activity and K_M/V_{max} . Due to an increased K_M value and decreased V_{max} as well as specific activity of GNP@trypsin acetylated, one may consider the acetylation as not favorable for trypsin immobilized onto GNPs referring to the activity, although an increase of activity was referred for other immobilization materials [83].

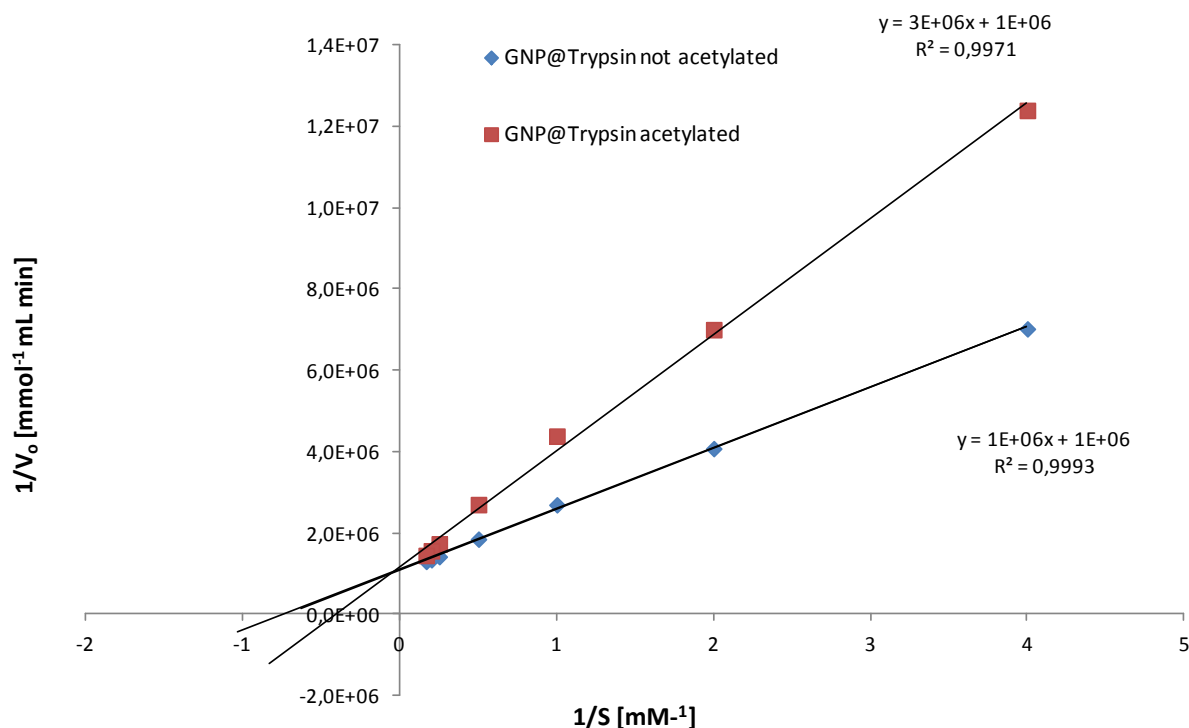


Figure 49: Lineweaver-Burk diagram of D,L-BApNA assay ($c = 0.1$ to 6 mM with 10 (v/v) % DMSO with a digestion time of 30 min) with GNP@trypsin acetylated and not acetylated, respectively.

Table 12: M. M. constants V_{max} , K_M , specific activity and K_M/V_{max} GNP@trypsin acetylated and not acetylated D,L-BApNA assays ($c = 0.1 - 6$ mM with 10 (v/v) % DMSO and a digestion time of 30 min).

	V_{max} [mmol mL ⁻¹ min ⁻¹]	K_M [mM]	specific activity [mmol ml ⁻¹ mg ⁻¹]	K_M/V_{max} [min ⁻¹]
GNP@trypsin not acetylated	1.15E-06	1.98	5.74E-06	1.72E+03
GNP@trypsin acetylated	8.58E-07	2.45	4.29E-06	2.86E+03

In Figure 50 the increase of D-Bz-Arg and L-Bz-Arg, respectively, with increasing substrate concentration of the GNP@trypsin acetylated and not acetylated BApNA assays are depicted. One may observe no noticeable differences in the enantioselective formation of

the products between the acetylated and not acetylated GNP@trypsin.

No significant enhancement of the activity of GNP@trypsin due to acetylation was obtained.

Furthermore, the results indicate no noteworthy influence to the enantioselectivity.

To eventually obtain more clearly differences between acetylated and not acetylated GNP@trypsin, further research higher digestion times may be done.

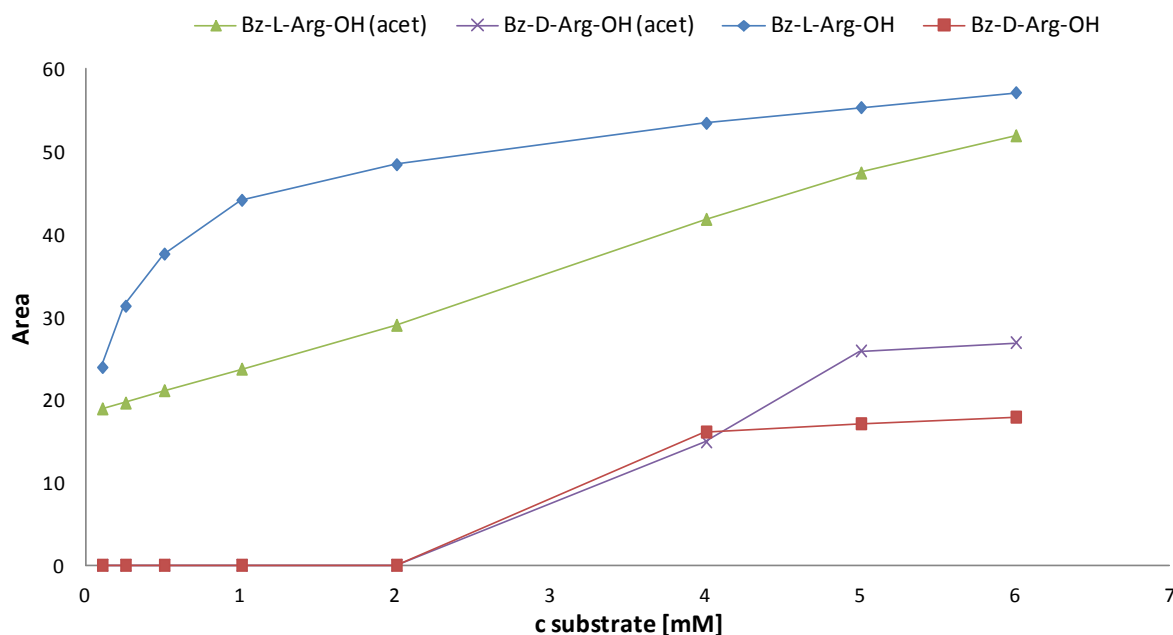


Figure 50: Increase of the area of D,L-Bz-Arg with substrate concentration of the GNP@trypsin acetylated and not acetylated BApNA assays ($c = 0.1$ to 6 mM with 10 (v/v) % DMSO with a digestion time of 30 min). Mobile Phase: MeOH, 50 mM FA, 25 mM DEA, 1 mL min^{-1} , UV- detection.

5.5 Digestion of mimic peptides – Development of a new enzyme assay

5.5.1 Optimization of HPLC separation

Due to separation problems with the commonly used mobile phase for all BApNA assays (MeOH, 50 mM FA, 25 mM DEA), various runs with different mobile phase compositions were done. A sufficient separation was necessary to enable multicomponent-analysis (q.v. 5.5.3).

Figure 51 shows the separation of the used peptides α -N-benzoyl-D,L-lysine-glycine (α -N-benzoyl-D,L-Lys-Gly-OH) and N-benzoyl-D,L-arginine-glycine (N-benzoyl-D,L-Arg-Gly-OH) with the mobile phase MeOH, 50 mM FA, 25 mM DEA. Besides a not baseline separation, due to

an overlapping of the formed products D-Bz-Arg and L-Bz-Arg with the substrate peptides a meaningful analysis was prevented. To optimize the separation a new mobile phase (MeOH, 50 mM FA, 25 mM NH₄FA) was prepared and the ion strength was modified due to addition of MeOH and ACN, respectively, in various percentages (Table 13).

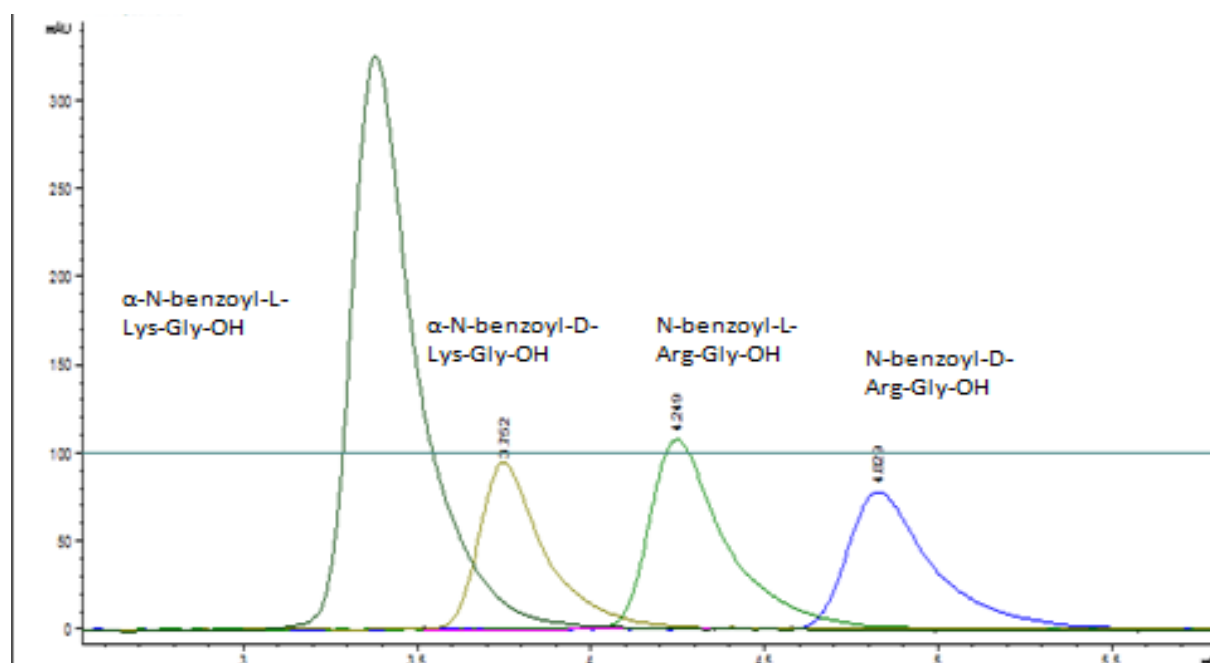


Figure 51: Separation of the peptides α -N-Bz-D,L-Lys-Gly and N-Bz-D,L-Arg-Gly with standard mobile phase MeOH, 50 mM FA, 25 mM DEA 1mL min⁻¹, UV-detection.

Table 13: Various compositions of the used mobile phases with different ion strength.

	MeOH 50 mM FA 25 mM NH ₄ FA %	MeOH %	ACN %
MP 1	75	25	-
MP 2	50	50	-
MP 3	25	75	-
MP 4	75	-	25
MP 5	50	-	50
MP 6	25	-	75

Figure 52 shows the different retention factors k of the substrates and, if detectable due to sufficient separation the standards of the products D-Bz-Arg and L-Bz-Arg, according to the ion strength [%] as depicted. For the different compositions with MeOH, 50 mM FA, 25 mM NH_4FA (mobile phase A) (Figure 52 a) an increase of the retention time with increasing MeOH (mobile phase B) and therefore an improvement of the separation was observed. Hence, in this case mobile phase MP 3 with 25 % MeOH, 50 mM, FA 25 mM NH_4FA and 75 % MeOH was the most favorable. Figure 52 b) shows the retention factors with increasing amount of ACN (mobile phase C). The mobile phase MP 5 with 50 % MeOH 50 mM FA 25 mM NH_4FA and 50 % ACN yielded the best separation results, while further increase of ACN (see MP 4) caused a decline of the separation.

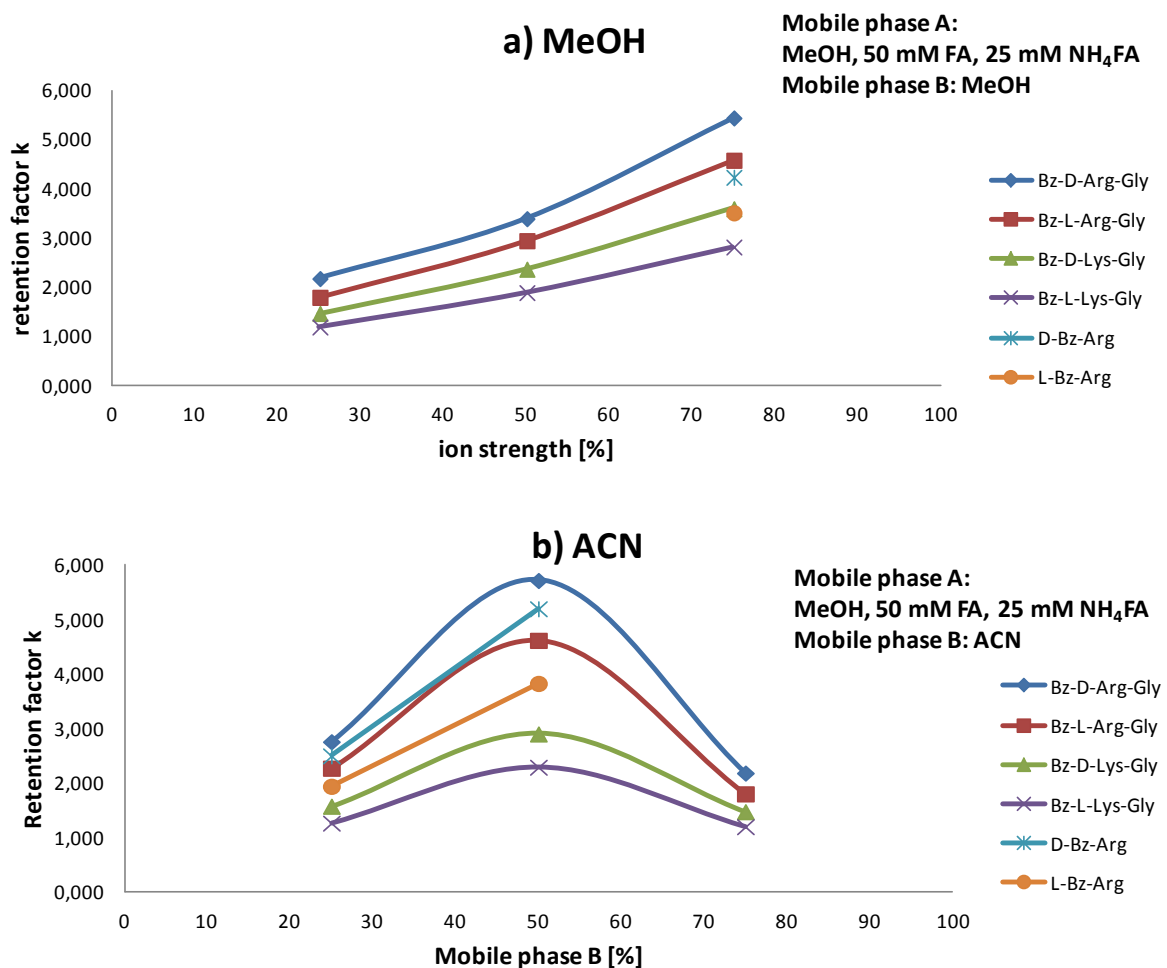


Figure 52: Used mobile phases with various compositions according to Table 13. a) MeOH, 50 mM FA, 25 mM NH_4FA with different percentages of MeOH. b) MeOH, 50 mM FA, 25 mM NH_4FA with different percentages of ACN.

Furthermore, mobile phases with different percentages of MeOH, 50 mM FA, 25 mM NH₄FA [A] and ACN, 50 mM FA [B] and Millipore water 50 mM FA, 25 mM NH₄FA [C], respectively, were tested. Table 14 gives the different used compositions in percentages. Mobile phases consisting of [A] and [C] showed a constant amount of NH₄FA, while the phases with the component [B] showed a slight increase of NH₄FA concentration with increasing percentage of ingredient [B], because NH₄FA is not soluble in pure ACN.

Table 14: Various compositions of the used mobile phases with different percentages of components.

	MeOH 50 mM FA 25 mM NH ₄ FA % [A]	ACN 50 mM FA % [B]	Millipore water 50 mM FA 25 mM NH ₄ FA % [C]
MP 7	75	25	-
MP 8	70	30	-
MP 9	50	50	-
MP 10	40	60	-
MP 11	35	65	-
MP 12	30	70	-
MP 13	25	75	-
MP 14	75	-	25
MP 15	50	-	50
MP 16	25	-	75

Figure 53 a) shows the retention factors of the separations with with different percentages of mobile phase A and mobile phase B. With increasing content of ACN till 70%, an improvement of the separation was observed. However, an increase to 75 % bred an overlay of the substrate peptide Bz-D-Arg-Gly and the standard of the possible product D-Bz-Arg. Figure 53 b) depicts the separation for the compound of mobile phase A and mobile phase C. Just as well, with increasing amount of Millipore water the retention factors enhanced, but there were still some peak overlays.

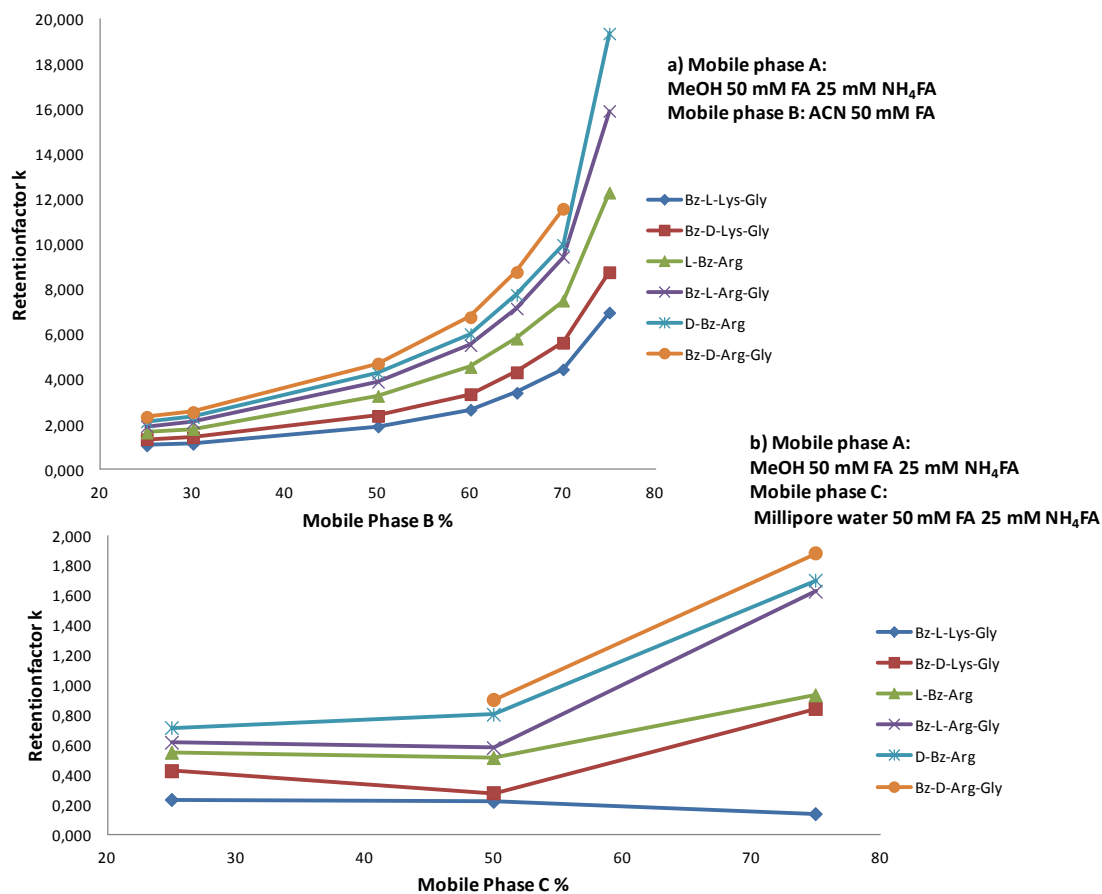


Figure 53: Used mobile phases with various compositions according to Table 13. a) MeOH, 50 mM FA, 25 mM NH₄FA with different percentages of ACN, 50 mM FA. b) MeOH, 50 mM FA, 25 mM NH₄FA with different percentages of millipore water, 50 mM FA, 25 mM NH₄FA.

As the separation with a mobile phase mix of MeOH, 50 mM FA, 25 mM NH₄FA and ACN 50 mM FA was considered as most favourable, further experiments were done. Besides a reduction of the ion strength in mobile phase A (MeOH 25 mM FA 12.5 mM NH₄FA [A₂]) a mobile phase with ACN 90 (v/v) %, MeOH 10 (v/v) %, 25 mM FA, 12.5 mM NH₄FA [D] and one with ACN 95 (v/v) %, MeOH 5 (v/v) %, 25 mM FA, 12.5 mM NH₄FA [E] was prepared. The MeOH content serves the purpose to dissolve the NH₄FA before the addition of ACN.

Table 15 gives the different used compositions in percentages.

Corresponding, Figure 54 depicts the retention factors increasing with the percentage of [D] (Figure 54 a) and [E] (Figure 54b), respectively. Mobile Phase MP 19 was proved to be the most favorable for a satisfying separation.

Table 15: Various compositions of the used mobile phases with different percentages of components.

	MeOH 25 mM FA 12.5 mM NH ₄ FA % [A ₂]	ACN 90 (v/v) % MeOH 10 (v/v) % 25 mM FA 12.5 mM NH ₄ FA [D]	ACN 95 (v/v) % MeOH 5 (v/v) % 25 mM FA 12.5 mM NH ₄ FA [E]
MP 17	75	25	-
MP 18	50	50	-
MP 19	25	75	-
MP 20	75	-	25
MP 21	50	-	50
MP 22	25	-	75

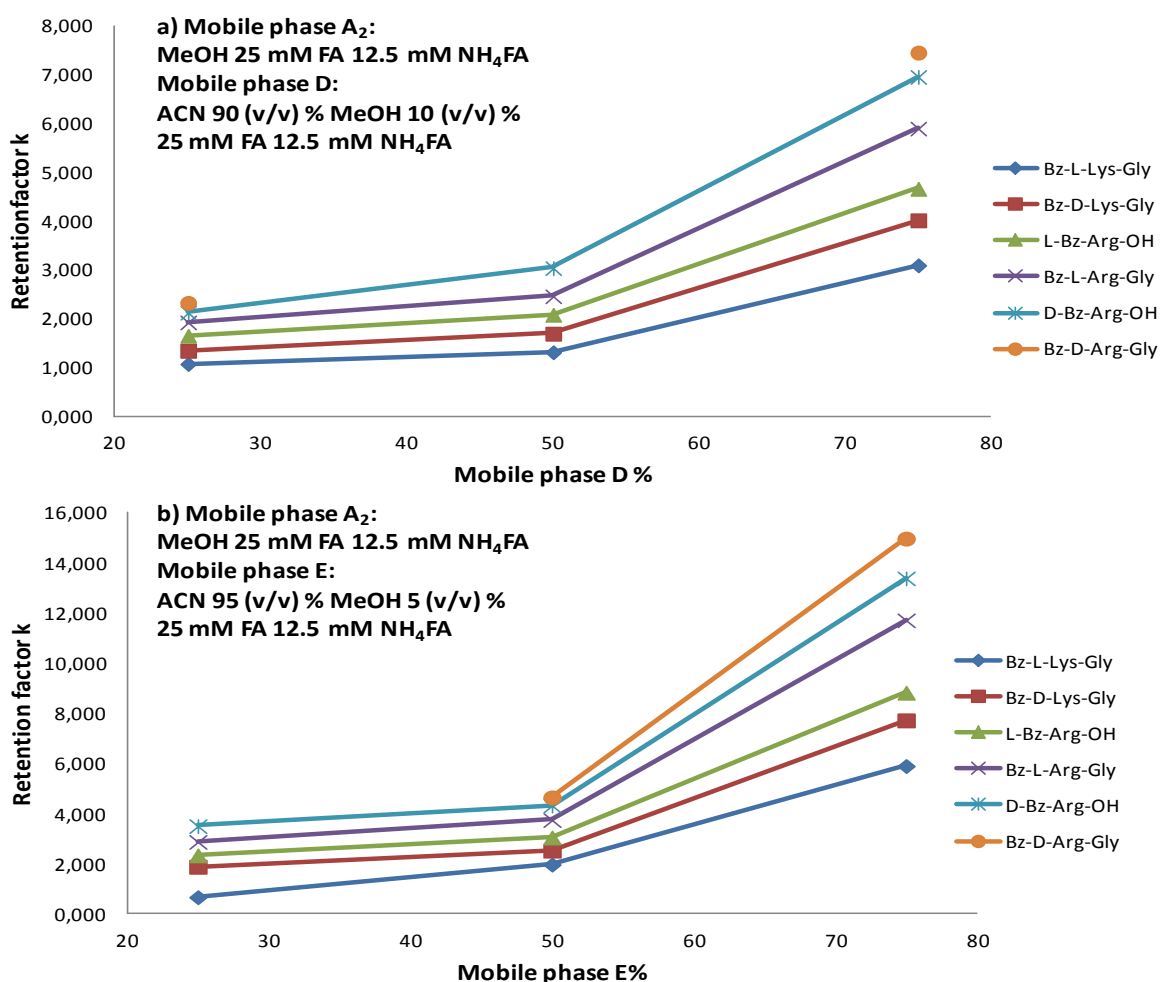


Figure 54: Used mobile phases with various compositions according to Table 13. a) MeOH, 25 mM FA, 12.5 mM NH₄FA with different percentages of ACN 90 (v/v) %, MeOH 10 (v/v) %, 25 mM FA, 12.5 mM NH₄FA. b) MeOH, 25 mM FA, 12.5 mM NH₄FA with different percentages of ACN 90 (v/v) %, MeOH 10 (v/v) %, 25 mM FA, 12.5 mM NH₄FA.

Figure 55 depicts the separation on a Htau-QD 150 x 4 mm, 5 μ m material, SO coverage 188 μ mol/g silica column with the finally used mobile phase MP 19. A baseline separation of the used peptides α -N-Bz-D-Lys-Gly and α -N-Bz-L-Lys-Gly and N-Bz-D-Arg-Gly, and N-Bz-L-Arg-Gly, respectively, as well as the standards of the possible formed products D-Bz-Arg-OH and L-Bz-Arg-OH was obtained.

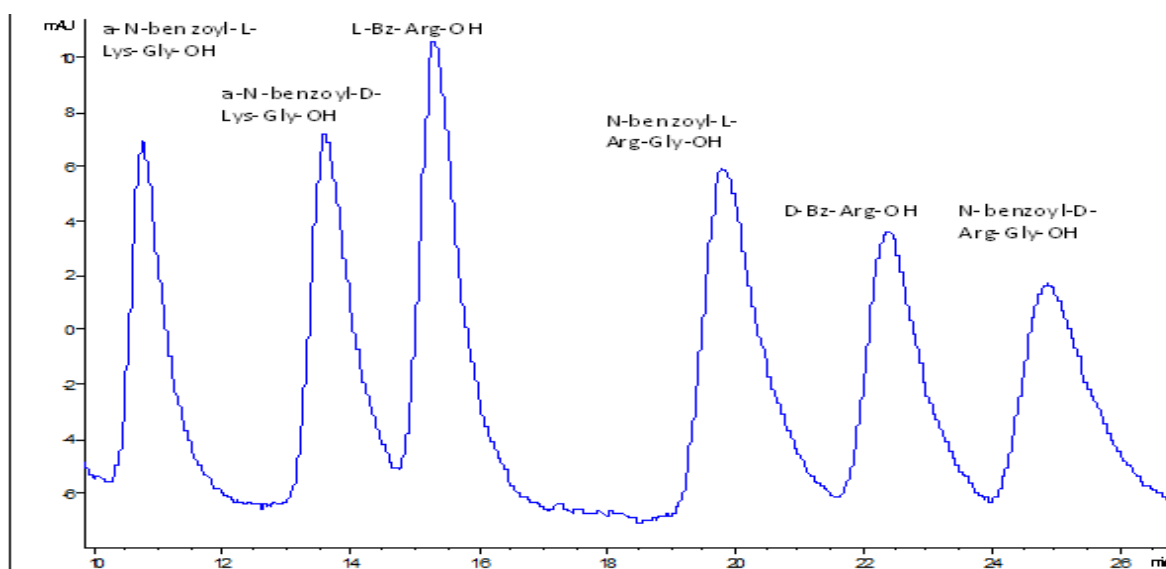


Figure 55: Separation of the peptides α -N-Bz-D,L-Lys-Gly, N-Bz-D,L-Arg-Gly and the products D,L-Bz-Arg with finally used mobile phase 75 % MeOH 25 mM FA 12.5 mM NH₄FA / 25% ACN 90 (v/v) %, MeOH 10 (v/v) %, 25 mM FA 12.5 mM NH₄FA 1mL min⁻¹, UV-detection. Column: Htau-QD 150 x 4 mm, 5 μ m material, SO coverage 188 μ mol g⁻¹ silica column.

5.5.2 Determination of M.M. constants

The enzyme-substrate affinity of the peptides N-benzoyl-L-Arg-Gly-OH and α -N-benzoyl-L-Lys-Gly-OH were determined by enzyme assays digested with GNP@trypsin (q.v. 4.2.3.1) with substrate concentrations of 0.298 – 2.98 mM (N-benzoyl-L-Arg-Gly-OH) and 0.324 – 3.24 mM (α -N-benzoyl-L-Lys-Gly-OH), respectively.

Figure 56 a) shows the M.M. diagram for N-benzoyl-L-Arg-Gly-OH and Figure 56 b) depicts the digestion assay for α -N-benzoyl-L-Lys-Gly-OH. However, the determination of the formed product via photometry similar to the D,L-BAPNA digestion assays (q.v. 4.2.3.4) was not possible for N-benzoyl-L-Arg-Gly-OH and α -N-benzoyl-L-Lys-Gly-OH and their digestion products. All measurement were done with HPLC and V_{max} was calculated via the determination of the maximal area. The M.M. constants were determined by dint of a

Lineweaver-Burk diagram (Figure 57). K_M and V_{max} , specified as maximal area, are given in Table 16.

It appears there was only a slightly higher enzyme-substrate affinity for *N*-benzoyl-L-Arg-Gly-OH due to a lower K_M value than for α -*N*-benzoyl-L-Lys-Gly-OH. Nevertheless, both values were in the same dimension and so there is no considerable difference of enzyme-substrate affinity of GNP@trypsin to *N*-benzoyl-L-Arg-Gly-OH and α -*N*-benzoyl-L-Lys-Gly-OH. Compared with the K_M values from 5.2.2, both enantiomerically pure peptides appear to be a better substrate for GNP@trypsin than the racemic D,L-BApNA.

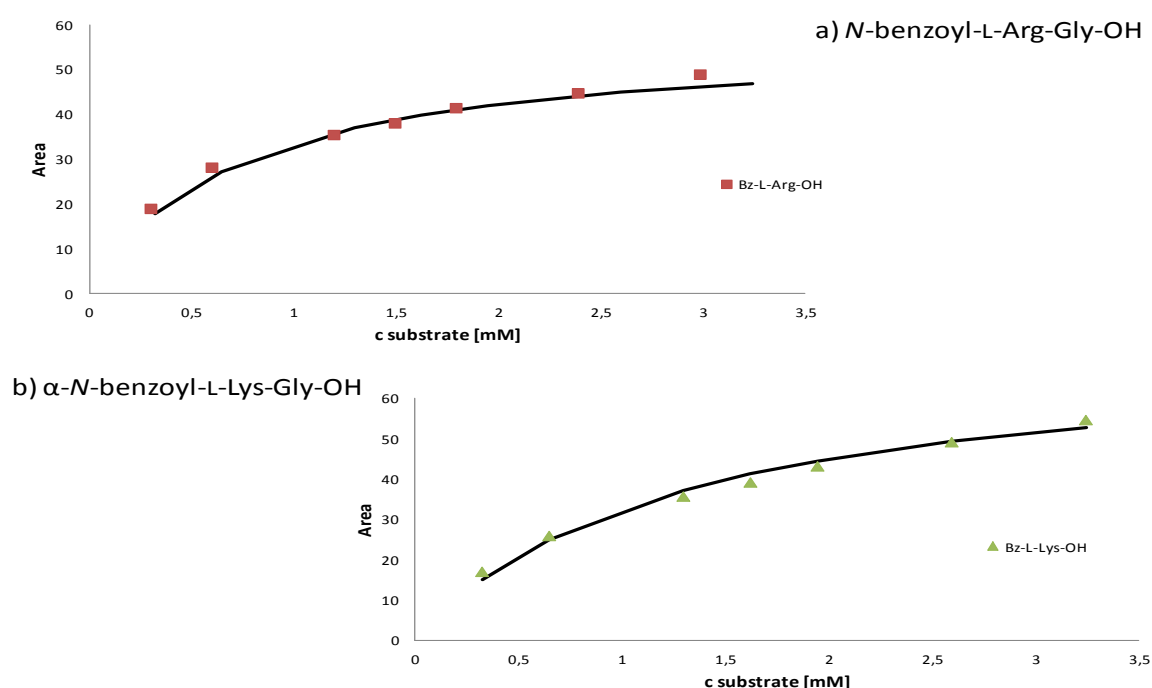


Figure 56: M. M. diagram for GNP@trypsin peptide assays ($c = 0.298 - 2.98$ mM (*N*-benzoyl-L-Arg-Gly-OH) and $0.324 - 3.24$ mM (α -*N*-benzoyl-L-Lys-Gly-OH), respectively and a digestion time of 3.5 h). Mobile phase 75 % MeOH, 25 mM FA, 12.5 mM NH_4FA / 25% ACN 90 (v/v) %, MeOH 10 (v/v) %, 25 mM FA, 12.5 mM NH_4FA 1mL min^{-1} , UV-detection.

Table 16: M. M. constants V_{max} and K_M for GNP@trypsin peptide assays ($c = 0.298 - 2.98$ mM (*N*-benzoyl-L-Arg-Gly-OH) and $0.324 - 3.24$ mM (α -*N*-benzoyl-L-Lys-Gly-OH), respectively and a digestion time of 3.5 h).

	V_{max} [Area]	K_M [mM]
<i>N</i>-benzoyl-L-Arg-Gly-OH	54.28	0.55
α-<i>N</i>-benzoyl-L-Lys-Gly-OH	63.66	0.89

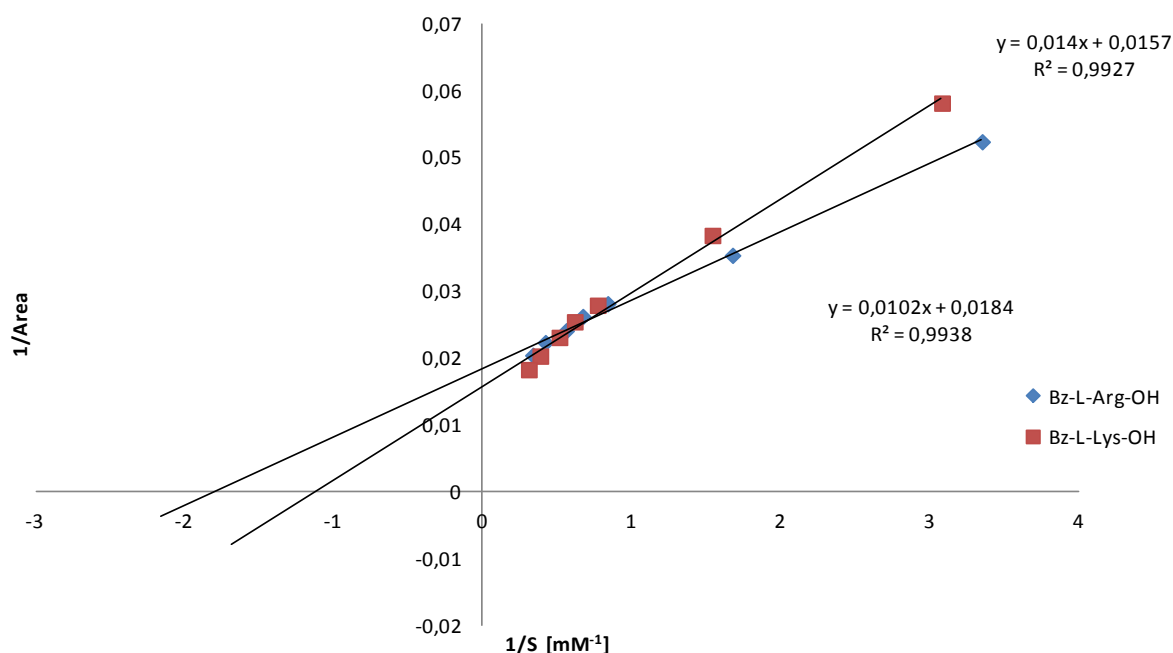


Figure 57: Lineweaver-Burk diagram for GNP@trypsin peptide assays ($c = 0.298 - 2.98$ mM (*N*-benzoyl-L-Arg-Gly-OH) and $0.324 - 3.24$ mM (α -*N*-benzoyl-L-Lys-Gly-OH), respectively and a digestion time of 3.5 h). Mobile phase 75 % MeOH, 25 mM FA, 12.5 mM NH_4FA / 25% ACN 90 (v/v) %, MeOH 10 (v/v) %, 25 mM FA, 12.5 mM NH_4FA 1 mL min^{-1} , UV-detection.

5.5.3 Enantioselectivity of tryptic digestion of enantiomeric peptides with GNP@trypsin

To estimate the influence of present enantiomers to enantioselectiv digestion, the peptides were first digested separately (α -*N*-benzoyl-D-Lys-Gly-OH, α -*N*-benzoyl-L-Lys-Gly-OH, *N*-benzoyl-D-Arg-Gly-OH, *N*-benzoyl-L-Arg-Gly-OH), each pair of enantiomers together in a racemic mixture and all 4 peptides together in a mix each with same concentration ratio than the others. The enantioselectivity of the GNP@trypsin digest was observed due to peptide assays analogue to 4.2.3.2 (Digestion of peptides). The assays were done with 1 mg mL^{-1} peptide standard solutions and digestion times from 0 to 24 h.

Figure 58 shows the digestion of α -*N*-benzoyl-D-Lys-Gly-OH and α -*N*-benzoyl-L-Lys-Gly-OH, each enantiomer digested seperatly with GNP@trypsin under the same conditions. Thereby, α -*N*-benzoyl-D-Lys-Gly-OH as well as the product Bz-D-Lys-OH showed an invariant area. On the other hand, a decrease of the area of α -*N*-benzoyl-L-Lys-Gly-OH and an increase of the product Bz-L-Lys-OH was observed. The same results were obtained for *N*-benzoyl-L-Arg-Gly-

OH and *N*-benzoyl-D-Arg-Gly-OH. While the L-enantiomer of the peptide decreased, an increase of the product Bz-L-Arg-Gly was observed. The areas of *N*-benzoyl-D-Arg-Gly-OH as well as the product Bz-D-Arg-Gly were invariant (Figure 59). Because Bz-D-Lys-Gly and Bz-D-Arg-Gly were also present in the undigested reference samples in the already in the same amount and no further increase was observed, one may assume their presence is ascribable to hydrolysis of the peptide solution samples during the storage. Consequently, an entire enantioselectivity in favor of the L-enantiomer was observed for both peptides for separately digested enantiomers of the peptides.

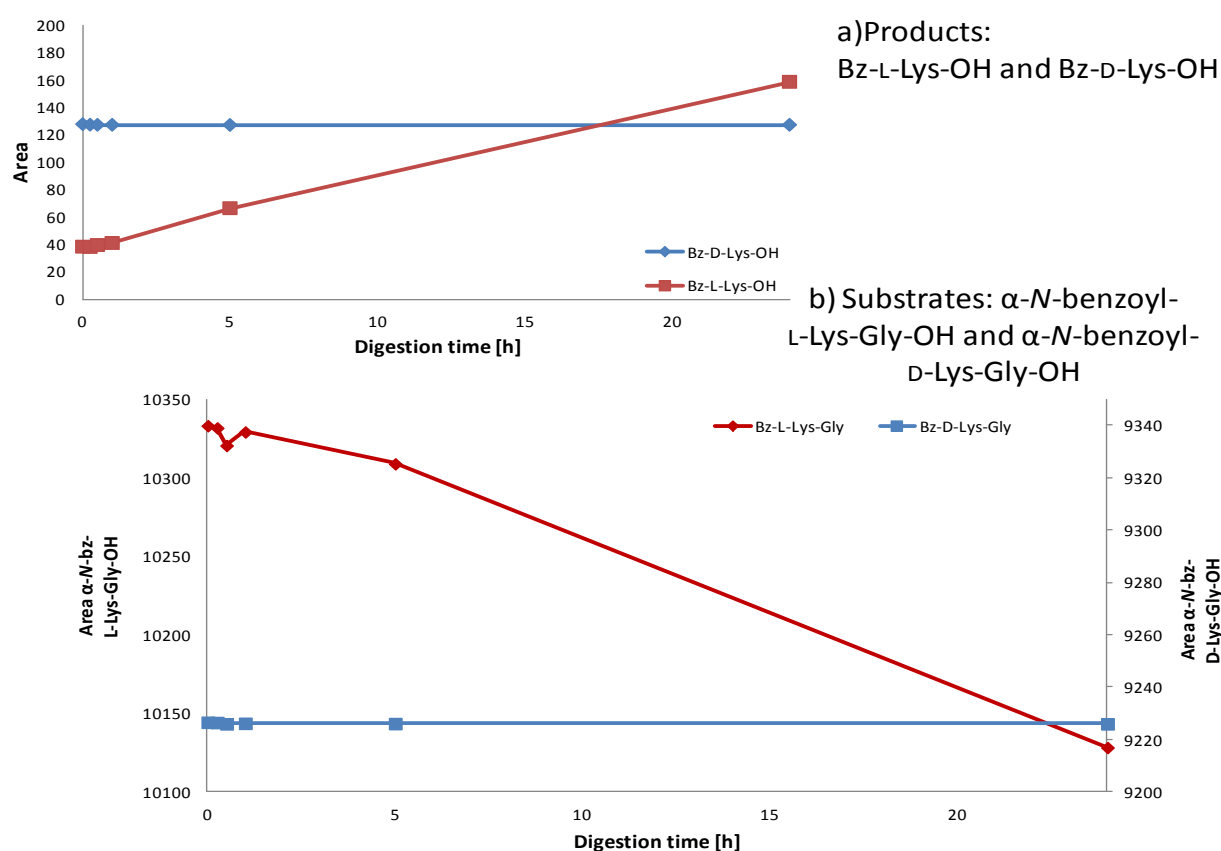


Figure 58: Digestion of α -N-benzoyl-L-Lys-Gly-OH and α -N-benzoyl-D-Lys-Gly-OH, digested separately ($c = 1.0 \text{ mg mL}^{-1}$ each, digestion time 0 – 24 h). a) Products b) Substrates. Analysis: Mobile phase 75 % MeOH 25 mM FA 12.5 mM NH_4FA / 25% ACN:MeOH 9:1 25 mM FA 12.5 mM NH_4FA 1 mL min^{-1} , UV-detection.

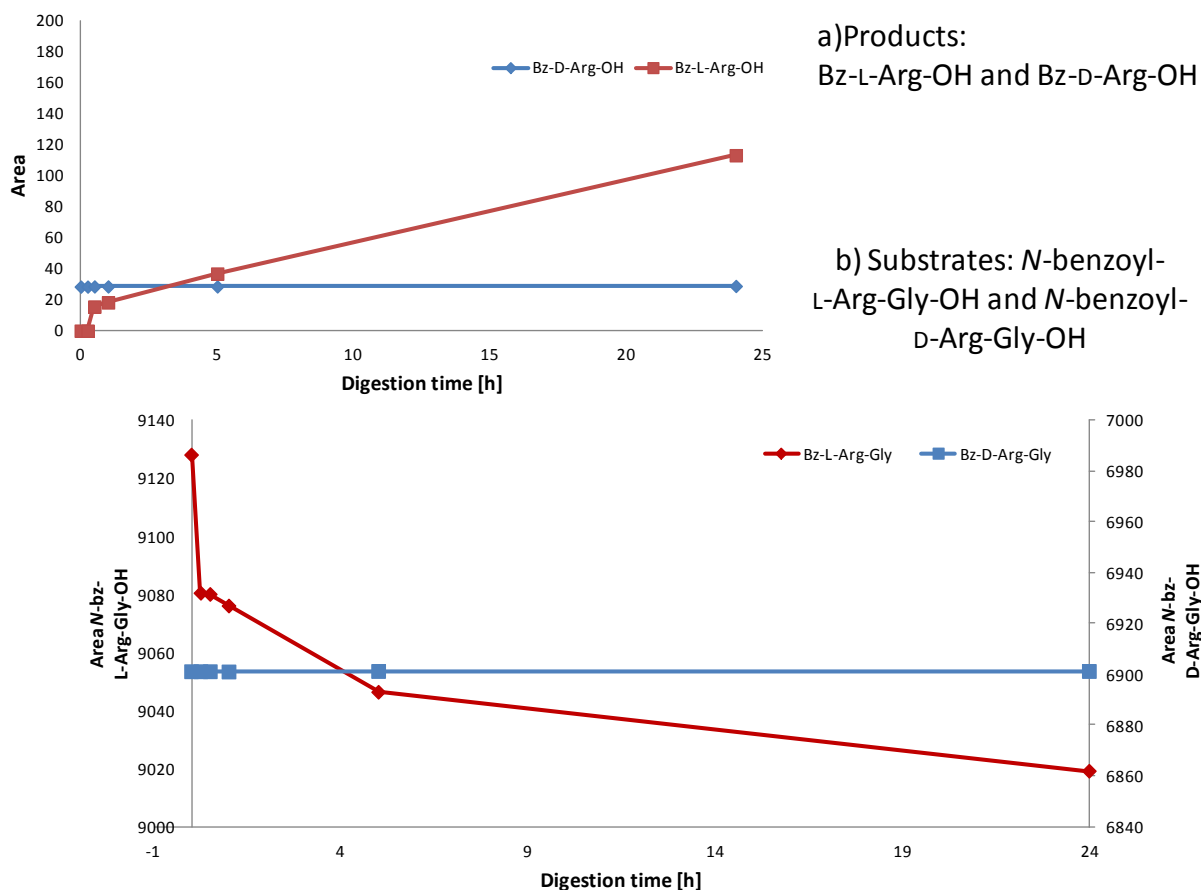


Figure 59: Digestion of *N*-benzoyl-D-Arg-Gly-OH and *N*-benzoyl-L-Arg-Gly-OH, digested separately ($c = 1.0 \text{ mg mL}^{-1}$ each, digestion time 0 – 24 h). a) Products b) Substrates. Analysis: Mobile phase 75 % MeOH 25 mM FA 12.5 mM NH_4FA / 25% ACN:MeOH 9:1 25 mM FA 12.5 mM NH_4FA 1 mL min^{-1} , UV-detection.

The same results as for the separately digested enantiomerically pure peptides were observed for the digestion of both enantiomers in a racemic mixture. The area α -*N*-benzoyl-L-Lys-Gly-OH was decreasing with time, while for α -*N*-benzoyl-D-Lys-Gly-OH a constant area was detected (Figure 60). The product of α -*N*-benzoyl-L-Lys-Gly-OH, Bz-L-Lys-OH was increasing with time. Although an eventually formed product of digested α -*N*-benzoyl-D-Lys-Gly-OH would have been beyond the peak of α -*N*-benzoyl-L-Lys-Gly-OH, due to the constant area of the substrate a product formation cannot be assumed.

Figure 60 shows the decrease of *N*-benzoyl-L-Arg-Gly-OH while no change of area was detected for *N*-benzoyl-D-Arg-Gly-OH. Simultaneously an increase of the product Bz-L-Arg-OH was observed, but not for Bz-D-Arg-OH.

Hence, there was no influence on the enantioselectivity due to digestion of racemic mixtures of both enantiomers compared to separate digestion of enantiomerically pure peptides observed.

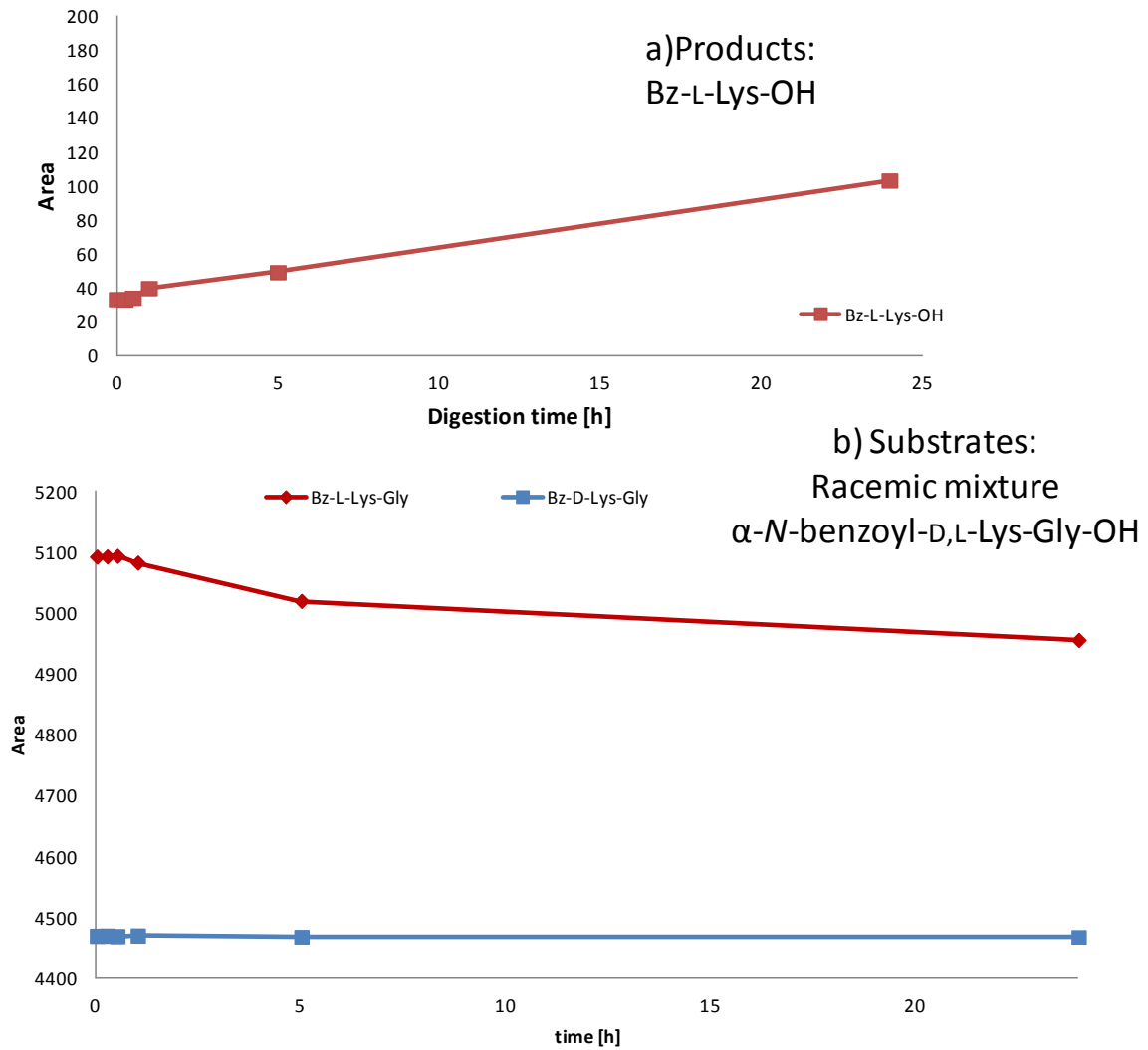


Figure 60: Digestion of α -N-benzoyl-D,L-Lys-Gly-OH, digested together in a racemic mixture ($c = 0.5 \text{ mg mL}^{-1}$ each, digestion time 0 – 24 h). a) Products b) Substrates. Analysis: Mobile phase 75 % MeOH 25 mM FA 12.5 mM NH_4FA / 25% ACN:MeOH 9:1 25 mM FA 12.5 mM NH_4FA 1 mL min^{-1} , UV-detection.

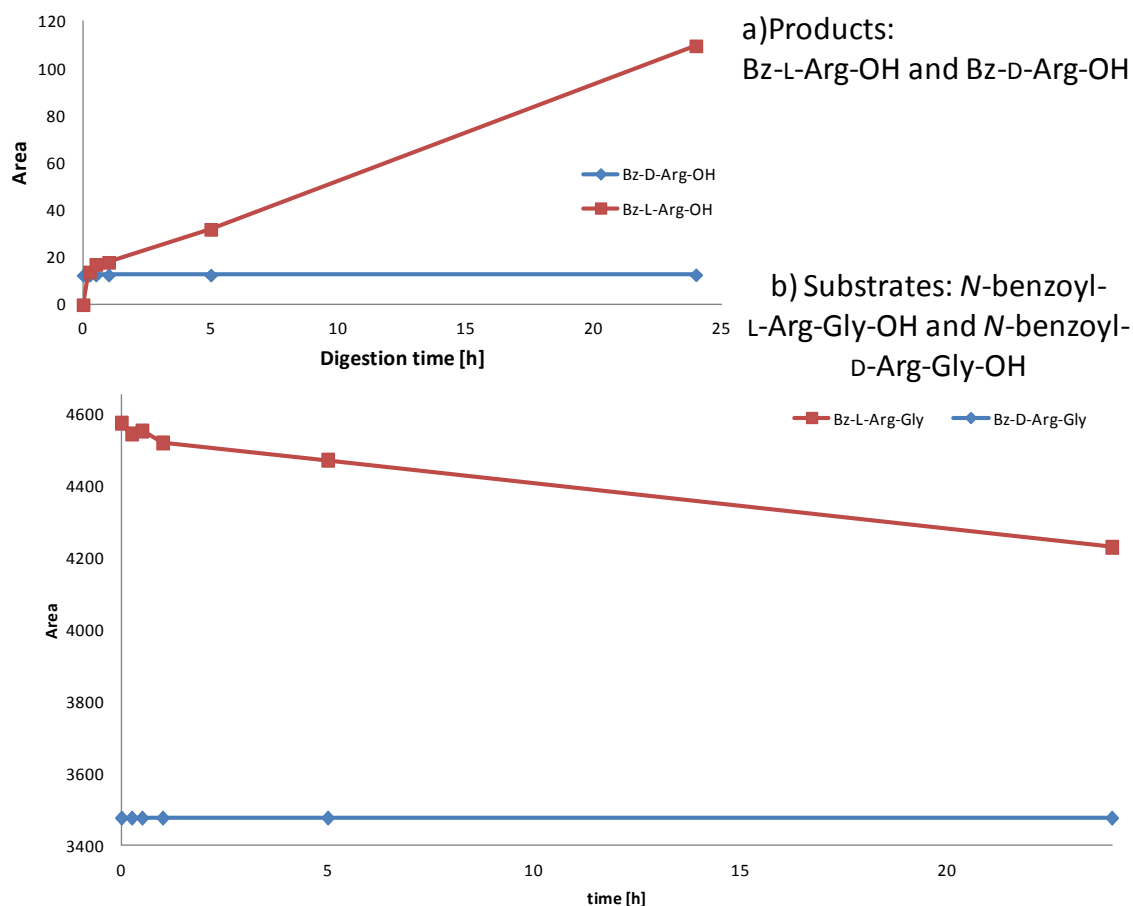


Figure 61: Digestion of *N*-benzoyl-D,L-Arg-Gly-OH, digested together in a racemic mixture ($c = 0.5 \text{ mg mL}^{-1}$ each, digestion time 0 – 24 h). a) Products b) Substrates. Analysis: Mobile phase 75 % MeOH 25 mM FA 12.5 mM NH_4FA / 25% ACN:MeOH 9:1 25 mM FA 12.5 mM NH_4FA 1 mL min^{-1} , UV-detection.

When digesting both peptides, α -*N*-benzoyl-D,L-Lys-Gly-OH and *N*-benzoyl-D,L-Arg-Gly-OH together, for neither of the D-enantiomers a decrease of area was detected, though for α -*N*-benzoyl-L-Lys-Gly-OH and *N*-benzoyl-L-Arg-Gly-OH (Figure 62). Corresponding, as anticipated, an increase of Bz-L-Lys-OH and Bz-L-Arg-OH with digestion time was observed. No formation of Bz-D-Lys-OH and Bz-D-Arg-OH, respectively, was detectable. Hence, the observed enantioselectivity in favor of the L-enantiomer for separate digestion can also be applied for digestion of both peptides together in a multicomponent mix.

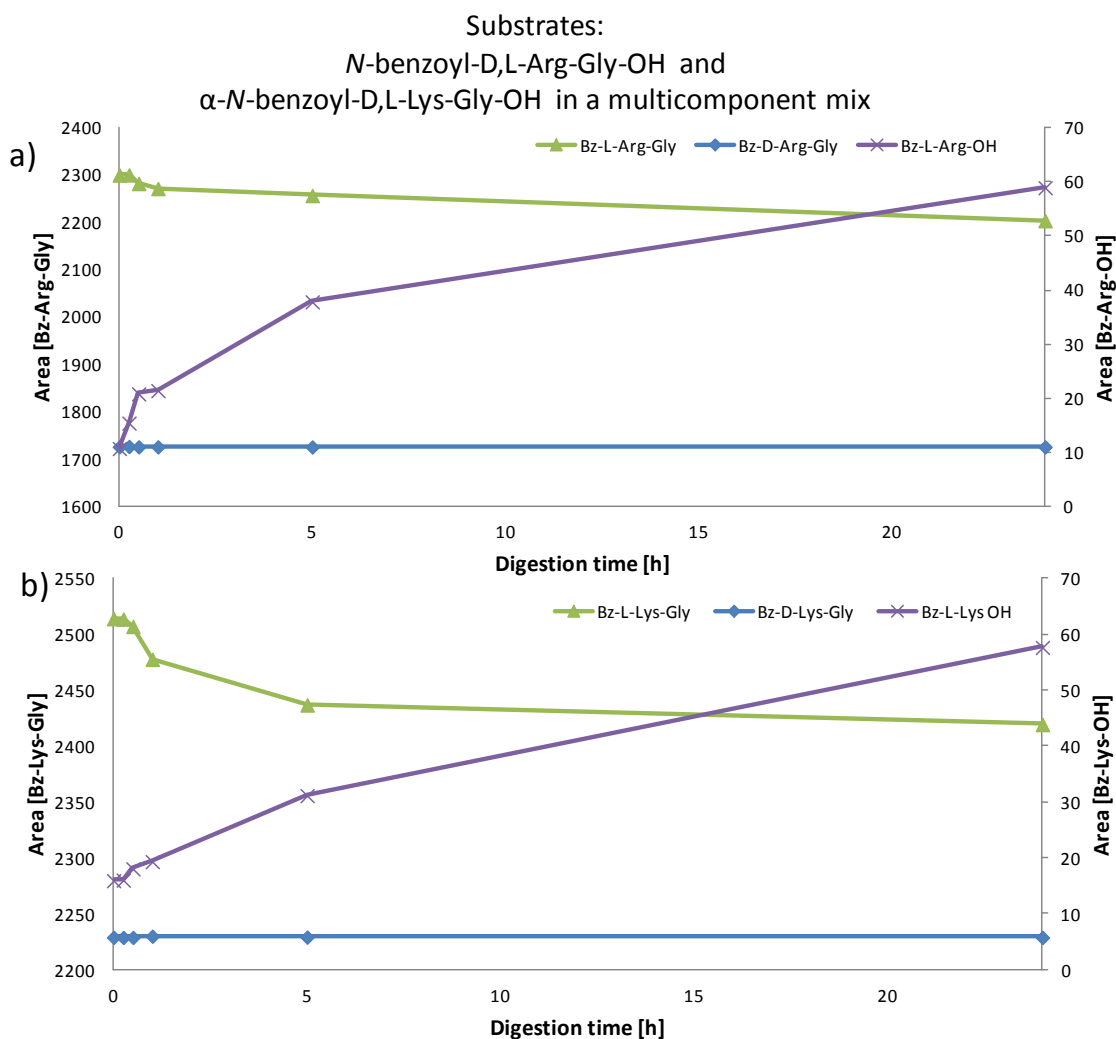


Figure 62: Digestion of α -*N*-benzoyl-D,L-Lys -Gly-OH and *N*-benzoyl-D,L-Arg -Gly-OH, digested together in a multicomponent mix ($c = 0.25 \text{ mg mL}^{-1}$ each, digestion time 0 – 24 h). a) Increase of Bz-L-Lys-OH with decreasing α -*N*-benzoyl-L-Lys-Gly-OH b) Increase of Bz-L-Arg-OH with decreasing *N*-benzoyl-L-Arg-Gly-OH. Analysis: Mobile phase 75 % MeOH 25 mM FA 12.5 mM NH_4FA / 25% ACN:MeOH 9:1 25 mM FA 12.5 mM NH_4FA 1 mL min^{-1} , UV-detection.

To determine a dependency of the enantioselectivity on the substrate concentration, related to the one observed for the substrate D,L-BApNA (q.v. 5.3.1), peptide assays of α -*N*-benzoyl-D,L-Lys-Gly-OH and *N*-benzoyl-D,L-Arg-Gly-OH with same digestion times, but concentrations of 2.5 mg/mL were performed. Figure 63 depicts that there was neither for the substrates, nor for Bz-D-Arg-OH and Bz-D-Lys-OH, respectively, a change of area detectable. Hence, one cannot assume a digestion of the D-enantiomers of the substrate peptides. For this reason, no correlation of the enantioselectivity and the substrate concentration was observed for the used peptides.

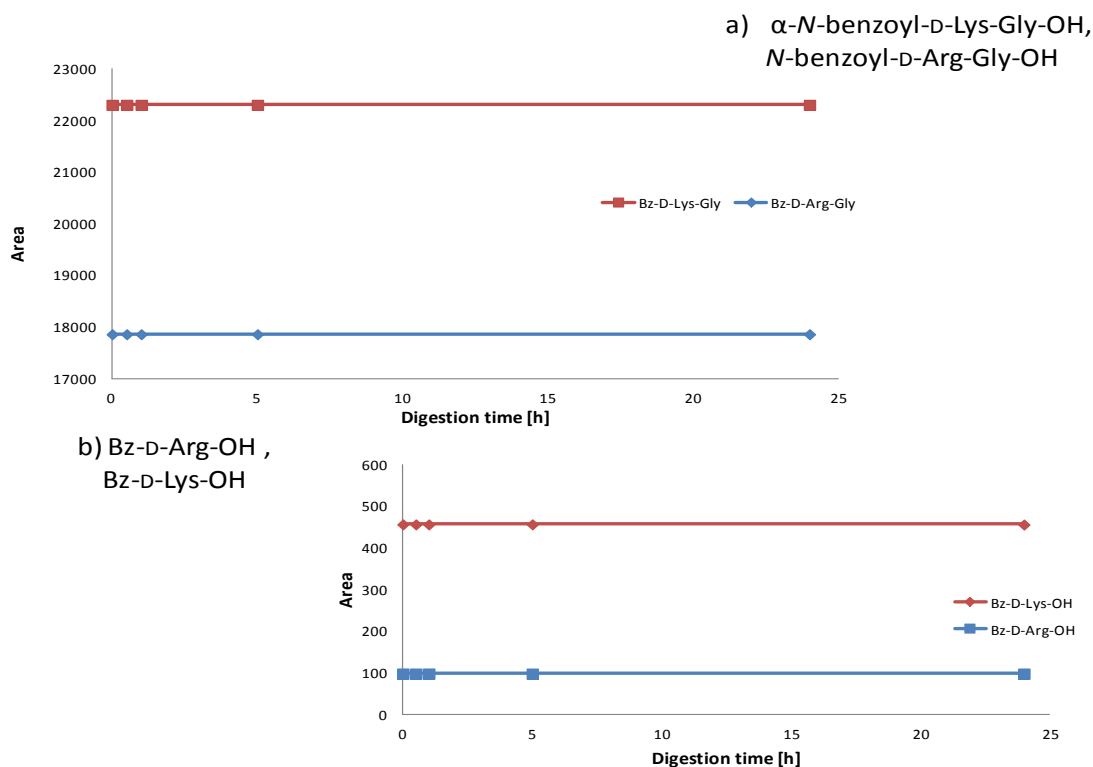


Figure 63: Digestion of α -N-benzoyl-D-Lys -Gly-OH and N-benzoyl-D-Arg -Gly-OH, digested separately ($c = 2.5 \text{ mg mL}^{-1}$ each, digestion time 0 – 24 h). a) Invariant area of substrates b) Invariant area of Bz-D-Lys-OH and Bz-D-Arg-OH, respectively. Analysis: Mobile phase 75 % MeOH 25 mM FA 12.5 mM NH_4FA / 25% ACN:MeOH 9:1 25 mM FA 12.5 mM NH_4FA 1 mL min^{-1} , UV-detection.

5.5.4 Digestion of peptides containing the amino acid arginine

To observe a possible further digestion of the cleavage products Bz-L-Arg-OH or Bz-D-Arg-OH, respectively, Bz-Arg-OH digestion assays with GNP@trypsin were accomplished (q.v. 4.2.3.2). Figure 64 shows the Bz-Arg-OH assay with a concentration of 0.5 mg mL^{-1} and digestion times from 0 to 48 h. Neither for the L-enantiomer nor for the D-enantiomer, a decrease of area was detectable, as well as any possible digestion products. Hence, a further digestion of Bz-Arg-OH and tryptic cleavage between Bz and Arg may be excluded.

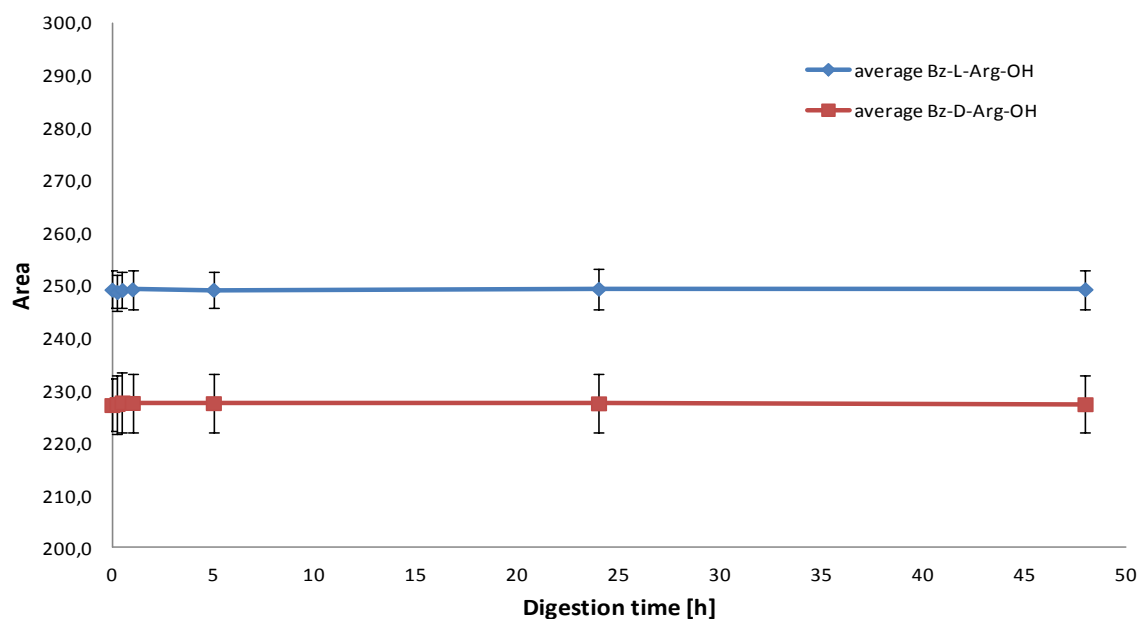


Figure 64: Digestion of Bz-D,L-Arg-OH ($c = 0.5 \text{ mg mL}^{-1}$ and a digestion time of 0 – 48 h), including standard deviation (measurement done in triplicate). Mobile phase: MeOH, 50 mM FA, 25 mM DEA, 1 mL min^{-1} , UV-detection.

Furthermore, the digestion of L-phenylalanine-L-arginine (L-Phe-L-Arg) and L-arginine-L-phenylalanine (L-Arg-L-Phe) with substrate concentrations of 1 mg mL^{-1} and digestion times from 0 – 5 h was accomplished (q.v. 4.2.3.2). However, there was no decrease of both, L-Phe-L-Arg and L-Arg-L-Phe observed, as well as any possible digestion products (Figure 65). In accordance to literature, due to the voluminous Phenylalanin-moiety at the C-terminus there is a stereochemical shielding which prevents a tryptic digest [77, 104].

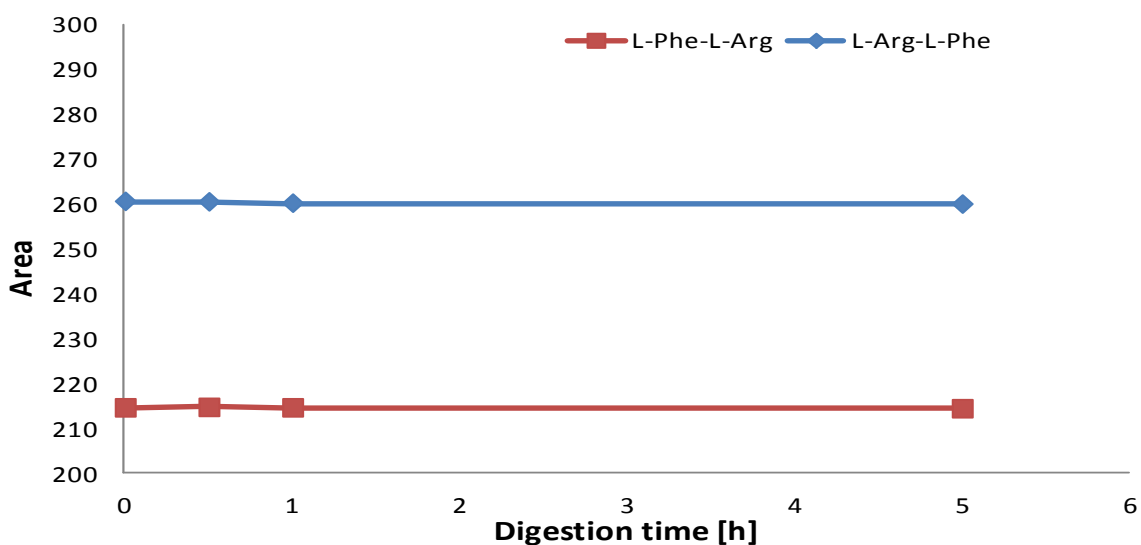


Figure 65: Digestion of L-Phe-L-Arg and L-Arg-L-Phe ($c = 1.0 \text{ mg mL}^{-1}$ and a digestion time of 0 – 5 h). Mobile phase: MeOH, 50 mM FA, 25 mM DEA, 1 mL min^{-1} , UV-detection.

5.6 Determination of limit of detection (LOD)

The determination of the LOD of pNA was measured with standard solutions with concentrations from 0.5 μM to 0.1 mM and the dilution series was measured at 410 nm with UV/Vis-spectroscopy.

The LOD of D,L-BApNA was determined by standard solutions, prepared analogue 4.2.3.1, with concentration ranges from 0.005 to 5 mM. The measurements were done with HPLC detection (q.v. 4.1.3.1).

Standard solutions with concentrations in a range from 0.05 to 1 mg mL^{-1} of the peptides α -N-Bz-D,L-Lys-Gly and N-Bzl-D,L-Arg-Gly were prepared to determined the LOD with HPLC detection (q.v. 4.1.3.3)

The LODs for D,L-BApNA, the peptides α -N-benzoyl-D,L-Lys-Gly-OH and N-benzoyl-D,L-Arg-Gly-OH and pNA were calculated analogue to 4.2.6. (eq.19) and the results are given in Table 17.

Table 17: LOD of D,L-BApNA, α -N-benzoyl-D,L-Lys-Gly-OH, N-benzoyl-D,L-Arg-Gly-OH and p-Na.

LOD of:	$[\mu\text{M}]$	$[\mu\text{g mL}^{-1}]$
D-BApNA	4.13	
L-BApNA	4.55	
pNA	0.198	
N-benzoyl-L-Arg-Gly-OH		1.8192
N-benzoyl-D-Arg-Gly-OH		1.8264
α -N-benzoyl,L-Lys-Gly-OH		1.3044
α -N-benzoyl-D-Lys-Gly-OH		1.3181

6 Conclusion

The used method for GNP preparation as well as the immobilization of trypsin via a spacer showed a satisfying reproducibility. Due to SPR, DLS and ZP measurement the characteristics of the produced GNPs were monitored fast and reliable. The long-time study disclosed the possibility of long storage times at 4°C of at least 3 months for all GNPs stabilized by immobilization, either of only the spacer or spacer and enzyme. Storage temperatures of -25°C were endured only by GNP@trypsin and GNP-PEG₇-COOH. Hence, in general the storage at 4°C can be considered as more advantageous. Enzyme activity test of GNP@trypsin stored at both, -25° and 4°C, for about 5 months showed no significant loss of activity compared to freshly prepared GNP@trypsin.

The development of an assay to review the enantioselectivity of enzyme conjugated nanoparticles for the chiral substrate D,L-BApNA was achieved. The determination of the M.M. constants K_m , V_{max} and specific activity indicated only slightly decreases of the enzyme-substrate affinity and the maximal reaction velocity compared to trypsin in-solution. However, GNP@trypsin shows not only the advantage of easy removal of the enzyme due to centrifugation, but also the possibility of a reuse, even though a certain loss of activity has to be considered. GNP@trypsin showed in the BApNA assays an enantioselectivity in favor of the L-enantiomer, also for the tested solvents MeOH, EtOH and DMSO up to 10 (v/v) % in buffered solution there was no influence compared to the commonly used aqueous buffer. Though, an influence of the used substrate concentration on the enantioselectivity was observed. In the D,L-BApNA determination assays with GNP@trypsin, from concentration of over 2.5 mM, the completely enantioselectivity in favor of the L-enantiomer was reversed. Beyond that, also a conversion of the D-enantiomer was affected, even though in a distinct minor degree and long digestion times. For high digestion times of at least one day, small amounts of Bz-D-Arg-OH were also detected for substrate concentrations of 1 mM. Hence, a correlation of the enantioselectivity and the substrate concentration as well as the digestion time was observed.

For all BApNA assays with concentrations above 2 mM an eventual precipitation of the substrate has to be considered. Therefore, the solution should be prepared near-term before use and storage times over 1 day should be avoided.

The modification of trypsin due to acetylation showed different results for trypsin in-solution and immobilized trypsin. Though for the enzyme in-solution the enzyme-substrate affinity showed hardly any noteworthy differences between acetylated and not acetylated, there were changes observed for GNP@trypsin acetylated and not acetylated. The enzyme-substrate affinity decreased after acetylation, as well as the maximal reaction velocity. However, no influence on the enantioselectivity was observed. Hence, modification due to acetylation was not considered as favorable for trypsin immobilized on GNPs for D,L-BApNA assays. Furthermore, the point in time of acetylation affected different enzyme activities. The immobilization of trypsin onto the GNPs followed by the acetylation of the enzyme resulted in considerably higher enzyme activity compared to acetylation of trypsin before its immobilization onto the GNPs.

For the peptide assays with α -N-benzoyl-D,L-Lys-Gly-OH and N-benzoyl-D,L-Arg-Gly-OH a complete enantioselectivity in favor of the L-enantiomer was observed, for both, separate digestion as well as digestion of both enantiomers coevally. Also for high substrate concentrations and long digestion times, no cleavage of D-enantiomers was detected. The enzyme-substrate affinity was evaluated for the α -N-benzoyl-L-Lys-Gly-OH and N-benzoyl-L-Arg-Gly-OH. Here, values for the Michaelis Menten constants in the same order of magnitude were obtained. Hence, no significant preference of GNP@trypsin to one of the substrate was observed. To determine a possible further cleavage of Bz-D,L-Arg-OH, assays with this substrate were done. However, no digestion was detectable, as well as for the other tested arginine containing peptides L-Phe-L-Arg and L-Arg-L-Phe.

Recently, members of the Lindner/Lämmerhofer group published research in the field of bioconjugation of trypsin onto gold nanoparticles and the effect of surface chemistry on bioactivity. Various linkers differing in lipohilicity and hydrophilicity as well as spacer lengths were investigated to observe their influence on the bioactivity of the conjugated trypsin. Moreover, the applicability of the new heterogenous nanostructured biocatalyst was reviewed by the digestion of a standard protein mixture (cytochrome C, bovine serum albumin, myoglobin), followed by analysis with LC-ESI-MS and successful MASCOT search.

In the future, similar experiments with GNP@ α -chymotrypsin, as already initiated in this thesis, are conceivable with appropriate substrates. Moreover, the immobilization of other proteases and hydrolysis would be an interesting starting point for further research.

7 Chemicals and Materials

7.1 Buffers

All buffers were stored at 4°C.

50 mM phosphate buffered saline (PBS): 0.170 mL o-phosphoric acid (85%) were dissolved in 50 mL distilled H₂O. The pH was adjusted to pH 7 with NaOH.

50 mM ammonium bicarbonate buffer (AmBic buffer, pH 8.5): 0.198 g ammonium hydrogen carbonate were dissolved in 50 mL distilled H₂O. The pH was adjusted to pH 8.5 with ammonium hydroxid solution.

20 mM potassium diphosphate buffer (KH₂PO₄ buffer):

0.1361 g KH₂PO₄ were dissolved in 50 mL H₂O dest.

20 mM dipotassium phosphate buffer (K₂HPO₄ buffer):

0.1742 g K₂HPO₄ were dissolved in 50 mL H₂O dest. The pH was adjusted to pH 8.0 with a 20 mM KH₂PO₄ buffer.

1 M Tris(hydroxymethyl)aminomethane hydrochloric buffer (Tris/HCl buffer, pH 8.5):

6.057 g Tris were dissolved in 50 mL distilled H₂O. The pH was adjusted to pH 8.5 with HCl.

50 mM Tris(hydroxymethyl)aminomethane hydrochloric buffer (Tris/HCl buffer, pH 8.5):

0.3029 g Tris were dissolved in 50 mL H₂O dest. The pH was adjusted to pH 8.5 with HCl.

7.2 Source of Supply

N-(3-Dimethylaminopropyl)-*N'*-ethylcarbodiimide hydrochloride (*EDC*) CAS 1892-57-5 Fluka

1-Hydroxy-2.5-pyrrolidinedione/ *N*-hydroxy-succinimide (*NHS*) CAS 6066-82-6 Fluka

16-mercaptohexadecanoic acid (MHA) CAS 69839-68-5 Sigma Aldrich

Ammonium formiate (NH₄FA) CAS 540-69-2 Sigma Aldrich

Ammonium hydrogencarbonate CAS 1066-33-7 Fluka

Benzoyl-D,L-arginine-4-nitroanilide (*D,L*-BApNA) CAS 911-77-3 Aldrich Chemistry

Benzoyl-D,L-arginine (Bz-D,L-Arg-OH) Bachem

N-Benzoyl-D-arginine-glycine (*N*-benzoyl-D-Arg-Gly-OH) HPLC purity 95% GenScript

N-Benzoyl-L-arginine-glycine (*N*-benzoyl-L-Arg-Gly-OH) HPLC purity 95% GenScript

α -*N*-Benzoyl-D-lysine-arginine (α -*N*-benzoyl-D-Lys-Gly-OH) HPLC purity 95% GenScript

α -*N*-Benzoyl-L-lysine-arginine (α -*N*-benzoyl-L-Lys-Gly-OH) HPLC purity 95% GenScript

Diethylamine (DEA) CAS 109-89-7 Sigma-Aldrich

Formic acid (FA) 98-100% puriss. CAS 64-18-6 Riedel de Haen

Gold(III)chloride trihydrate (HAuCl_4) CAS 16961-25-4 Sigma-Aldrich

O-(2-carboxyethyl)-O'-(2-mercaptoethyl)heptaethylene glycol Sigma-Aldrich

o-phosphoric acid CAS 7664-38-2 Fisher Scientific

Sodium citrate tribasic dehydrate CAS 6132-04-3 Sigma-Aldrich

(Tris-2-carboxyethyl)phosphine hydrochloride (TCEP) CAS 5961-85-3 Sigma-Aldrich

Trypsin (*hog pancreas*) E.C. 3.4.21.4. foreign activities chymotrypsin $\leq 0.2\%$. 13.644 U mg⁻¹.
Sigma-Aldrich

8 Abbreviations

AFM.....atomic force microscope

Arg.....amino acid arginine

CE.....capillary electrophoresis

CEC.....cation-exchange capacity

CMP.....chiral mobile phase

CSP.....chiral stationary phase

Da.....Dalton, standard unit for atomic mass

DAD.....diode array detector

DLS.....dynamic light scattering

E_Aactivation energy

ee.....enantiomeric excess

er.....enantiomeric ratio

ESI.....electrospray ionization

Gly.....amino acid glycine

GC.....gas chromatography

GNP.....gold nanoparticle

GNP@enzyme.....gold nanoparticles immobilized enzyme

HPLC..... high pressure liquid chromatography

Htau-QD..... Homotau-quinidin

LC.....liquid chromatography

LOD.....limit of detection

Lys.....amino acid lysine

M.M.....Michaelis Menten

mL.....milliliter

mV.....millivolt

MS.....mass spectrometry

nm.....nanometer

op.....optical purity

OPA..... ortho-phthalaldehyde

pNA.....para-nitroaniline

Phe.....amino acid phenylalanine

QD.....(S)-(6-methoxyquinolin-4-yl)((2R,4S,8R)-8-vinylquinuclidin-2-yl)methanol

QN.....(R)-(6-methoxyquinolin-4-yl)((2S,4S,8R)-8-vinylquinuclidin-2-yl)methanol

RP.....reversed-phase

SA.....selectand

SAM.....self assembling monolayer

SCX.....strong cation exchanger

SEM.....scanning electron microscope

SH-PEG₇-COOH.....O-(2-carboxyethyl)-O'-(2-mercaptoethyl)heptaethylene glycol

SO.....selector

SPR.....surface plasmon resonance

TEM..... transmission electron
microscopyUV/Vis.....ultraviolet-visible (spectroscopy)

WAX.....weak anion exchanger

ZP.....	zeta potential
ZWIX.....	zwitter-ionic exchangers
K_M	Michaelis constant
V_{max}	maximum reaction rate
v_0	initial reaction rate

9 List of Tables

Table 1: Classification of enzymes by their catalyzed reaction type, adapted from [69].	36
Table 2: Overview of the subclassification of endopeptidases according to their active sites and functional amino acids, respectively, modified after [76].	40
Table 3: Zeta potential of GNP citrate stabilized (30 nm), GNP-PEG ₇ -COOH and GNP@trypsin of manufacturing batch 1 – 8 and the respective averaged ZP values.	61
Table 4: Size distribution of GNP citrate stabilized (30 nm), GNP-PEG ₇ -COOH and GNP@trypsin of manufacturing batch 1 – 8 and the corresponding ZP values.	62
Table 5: Size distribution and ZP of GNP@trypsin (batch1-3).	65
Table 6: Size distribution and ZP of GNP@trypsin 1-3.	65
Table 7: Michelis Menten constants V_{max} , K_M , specific activity and K_M/V_{max} for trypsin in solution (1 mg mL ⁻¹), α -chymotrypsin (1 mg mL ⁻¹), GNP@trypsin and GNP@ α -chymotrypsin of a BApNA assay ($c = 0.5 - 4$ mM) with a digestion time of 15 min.	76
Table 8: Increase of L-Bz-Arg with time of GNP@trypsin BApNA assay ($c = 0.45$ mM without DMSO with digestion times from 30 – 1740 min).	79
Table 9: M. M. constants V_{max} , K_M , specific activity and K_M/V_{max} for GNP@trypsin of a BApNA assay ($c = 0.05 - 5$ mM) with digestion times of 15 to 1440 min.	80
Table 10: Increase of L-Bz-Arg and respectively decrease of the substrate with time of GNP@trypsin D,L-BApNA assay ($c = 0.05$ mM without DMSO with digestion times from 30 – 1740 min).	83
Table 11: M. M. constants V_{max} , K_M , specific activity and K_M/V_{max} for trypsin in-solution acetylated and not acetylated BApNA assays ($c = 0.1 - 6$ mM with 10 (v/v) % DMSO and a digestion time of 30 min).	88
Table 12: M. M. constants V_{max} , K_M , specific activity and K_M/V_{max} GNP@trypsin acetylated and	

not acetylated D,L-BApNA assays (c = 0.1 – 6 mM with 10 (v/v) % DMSO and a digestion time of 30 min).	90
Table 13: Various compositions of the used mobile phases with different ion strength.	92
Table 14: Various compositions of the used mobile phases with different percentages of components.	94
Table 15: Various compositions of the used mobile phases with different percentages of components.	96
Table 16: M. M. constants V_{max} and K_M for GNP@trypsin peptide assays (c = 0.298 – 2.98 mM (N-benzoyl-L-Arg-Gly-OH) and 0.324 – 3.24 mM (α -N-benzoyl-L-Lys-Gly-OH), respectively and a digestion time of 3.5 h).	98
Table 17: LOD of D,L-BApNA, α -N-benzoyl-D,L-Lys-Gly-OH, N-benzoyl-D,L-Arg-Gly-OH and p-Na.	107

10 List of Figures

Figure 1: Both possible configurations of the stereogenic center of lactic acid, ligands numbered according to the CIP system from highest priority (a) to lowest priority (d).	10
Figure 2: (S)-(6-methoxyquinolin-4-yl)((2R,4S,8R)-8-vinylquinuclidin-2-yl)methanol, commonly known as quinidine (QD) and the pseudo-enantiomer (R)-(6-methoxyquinolin-4-yl)((2S,4S,8R)-8-vinylquinuclidin-2-yl)methanol (quinine, QN).	10
Figure 3: Classification of diastereomers and enantiomers and their characteristic properties.	12
Figure 4: Main principle of indirect and direct approach in enantiomeric separation, adapted from [2].	16
Figure 5: 3-point interaction model according to Dalgliesh, illustrating the "ideal fit" and the "non-ideal fit" [2]. Within this example, the (S)-SA is preferred due to a perfect spatial match of the interaction sites of SA and SO.	18
Figure 6: Overview of common commercially available CSPs and their classification, modified after [2]	19
Figure 7: Homotau-QD (8R, 9S), an aminosulfonic acid- <i>cinchona</i> -based SCX-WAX/ZWIX-type	

CSP.....	21
Figure 8: Electric double layer, consisting of three parts: The surface charge, the stern layer and the diffuse layer [49].	24
Figure 9: Illustration of the operating forces on two particles interacting with each other in the DLVO theory [49].	25
Figure 10:Two approaches of polymeric stabilization of colloids, either by steric or by depletion stabilization [49].	27
Figure 11: SPR spectra of GNPs with different immobilization states. The characteristic absorbance maximum (SPR band) at 520 nm is most distinct for the citrate stabilized 30 nm GNPs and decreases for ligand modified GNPs (GNP-PEG ₇ -COOH) and enzyme immobilized GNPs (GNP@enzyme).	28
Figure 12: Constituent parts of a typical DLS system: Laser, attenuator, cell, detector, correlator and computer, modified after [61].	31
Figure 13: Synthesis of citrate stabilized GNPs with subsequent dative binding and self-assembling of the thiol containing bifunctional linker SH-PEG ₇ -COOH to yield carboxylic acid functionalized GNPs. In a final step, trypsin is immobilized using EDC/NHS as coupling agents for linkage of carboxylic acid and amino group, adapted from [68].	35
Figure 14: Influence of enzymes on the activation energy and therefore on the progress of a reaction [70].	37
Figure 15: Lock-key model for enzymes and their substrates: The active site of the enzyme is preformed for the corresponding substrates, after substrate binding further adaption of the binding site takes place for ideal fit. After enzyme catalysis, the active site of the enzyme turns back to the originally preformed shape [72].	38
Figure 16: Enantiospecificity of enzymes pertaining to chiral substrates [73].	39
Figure 17: Active site of trypsin [78].	41
Figure 18: a) Hyberbolic function given by the Michaelis-Menten equation (eq. 15) [96] and b) double reciprocal Lineweaver-Burk plot [97] with the plotted parameters K_M , V_{max} and K_M/V_{max}	47
Figure 19: Cleavage of the substrate benzoyl-Arg-p-nitronanilide by trypsin. The enzyme activity can be determinated by the release of p-nitroanilide with an extinction coefficient of $8800 \text{ M}^{-1} \text{ cm}^{-1}$ at the absorbance wavelength of 410 nm.	48
Figure 20: SPR spectra in a range from 200 – 800 nm of GNP citrate stabilized (size ~ 30 nm),	

GNP-PEG ₇ -COOH and GNP@trypsin, each 1:20 diluted with distilled water. The average data of all SPR measurements (batch 1-8) was plotted.	60
Figure 21: Zeta potential of GNP citrate stabilized (30 nm) , GNP-PEG ₇ -COOH and GNP@trypsin of manufacturing batch 1 – 8 and the corresponding ZP values.	62
Figure 22: Size distribution of GNP citrate stabilized (30 nm), GNP-PEG ₇ -COOH and GNP@trypsin of manufacturing batch 1 – 8 and the respective averaged ZP values.	63
Figure 23: a) Typical ZP measurement of GNP@trypsin (manufacturing batch 5) with a ZP of -37 mV. b) Size distribution of 32.7 nm citrate stabilized GNPs with frequently occurring false additional peaks in the range of 1-5 nm.	64
Figure 24: Maximal absorbance of SPR measurements of GNP citrate stabilized, GNP-PEG ₇ -COOH, GNP-MHA and GNP@trypsin with a storage temperature of 4°C and a total storage time of 141 days.	67
Figure 25: Maximal absorbance of SPR measurements of GNP citrate stabilized, GNP-PEG ₇ -COOH, GNP-MHA and GNP@trypsin with a storage temperature of -25°C and a total storage time of 141 days.	67
Figure 26: ZP values [mV] of GNP citrate stabilized, GNP-PEG ₇ -COOH, GNP-MHA and GNP@trypsin with a storage temperature of 4°C and a total storage time of 141 days.	68
Figure 27: ZP values [mV] of GNP citrate stabilized, GNP-PEG ₇ -COOH, GNP-MHA and GNP@trypsin with a storage temperature of -25°C and a total storage time of 141 days.	69
Figure 28: Size distribution [nm] of GNP citrate stabilized, GNP-PEG ₇ -COOH, GNP-MHA and GNP@trypsin with a storage temperature of 4°C and a total storage time of 141 days.	69
Figure 29: Size distribution [nm] of GNP citrate stabilized, GNP-PEG ₇ -SH, GNP-MHA and GNP@trypsin with a storage temperature of -25°C and a total storage time of 141 days.	70
Figure 30: D,L-BApNA (c= 1 mM) assay of GNP@trypsin -25°C (storage time 141 days), GNP@trypsin 4°C (storage time 141 days) and GNP@trypsin reference (freshly prepared). The reaction time amounted to 60 minutes, the absorbance was measured at 410 nm.	71
Figure 31: D,L-BApNA (c= 1.5 mM) digestion assay to determine the reuseability of GNP@trypsin, accomplished without Tween20 as well as with 0.1 (v/v) % Tween20 with a reaction time of 60 min. 3 reuses were done and the absorbance was measured at 410 nm.	72
Figure 32: D,L-BApNA (c= 1.5 mM) digestion assay to determine the reuseability of GNP@trypsin, accomplished with 0.1 (v/v) % Tween20 with a reaction time of 60 min. 3	

reuses were done and the absorbance was measured at 410 nm. Moreover, the GNP@trypsin concentration was determined before each reuse.....	73
Figure 33: UV/vis detection of D,L-BApNA solutions with a concentration of 0.5 to 5 mM with 10% DMSO, detected at $\lambda = 410$ nm before and after storage. The storage time was 1 day at a temperature of 25°C and 4°C, respectively.....	74
Figure 34: a) M.M. diagram of BApNA digestion assay ($c = 0.5 - 4$ mM) of trypsin (1 mg mL^{-1}) in solution b) Lineweaver-Burk diagram of BApNA digestion assay ($c = 0.5 - 4$ mM) of trypsin in solution (1 mg mL^{-1}), both with a digestion time of 15 minutes, measured at $\lambda = 410$ nm.	75
Figure 35: HPLC chromatogram of GNP@trypsin BApNA assay ($c = 1.0 - 5.0$ mM with 10 (v/v) % DMSO and a digestion time of 30 min). The separations of the substrate D,L- BApNA and the products D and L-Bz-Arg (insert) are depicted. Mobile Phase: MeOH 50 mM FA 25 mM DEA 1 ml min^{-1} , UV detection.....	77
Figure 36: Plot of area of the products D-Bz-Arg and L-Bz-Arg of GNP@trypsin BApNA assay and GNP@ α -chymotrypsin BApNA assay ($c = 1.0 - 5.0$ mM with 10 (v/v) % DMSO with a digestion time of 30 min). Mobile Phase: MeOH 50 mM FA 25 mM DEA 1 ml min^{-1} , UV detection.	77
Figure 37: HPLC chromatogram of GNP@trypsin BApNA assay ($c = 0.45$ mM without DMSO and digestion times from 0 – 1740 min). The separations of the substrate D,L- BApNA shows a decrease of L-BApNa with digestion time (insert 2) and the product L-Bz-Arg (insert 1) an increase. Mobile Phase: MeOH 50 mM FA 25 mM DEA 1 ml min^{-1} , UV detection.....	78
Figure 38: GNP@trypsin BApNA assay ($c = 0.45$ mM without DMSO with digestion times from 30 – 1740 min): a) HPLC detection of the increase of the product L-Bz-Arg. Mobile Phase: MeOH 50 mM FA 25 mM DEA 1 ml min^{-1} , UV detection. b) UV/Vis detection of p-NA at $\lambda = 410$ nm.....	79
Figure 39: HPLC chromatogram of GNP@trypsin BApNA assay ($c = 0.05 - 5$ mM with 10 (v/v) % DMSO and digestion times from 0 – 1440 min). The separations of the substrate D and L- BApNA and the products D and L-Bz-Arg (insert) are depicted. Mobile Phase: MeOH 50 mM FA 25 mM DEA 1 ml/min , UV detection.....	81
Figure 40: HPCL detection of area increase of the product D-Bz-Arg with digestion time (30 – 1440 min) and substrate concentration (0.05 – 5 mM with 10 (v/v) % DMSO). Mobile Phase: MeOH, 50 mM FA, 25 mM DEA, 1 mg mL^{-1} , UV- detection.	81
Figure 41: HPCL detection of increase of the product L-Bz-Arg with digestion time (30 – 1440	

min) and substrate concentration (0.05 – 5 mM with 10 (v/v) % DMSO). Mobile Phase: MeOH, 50 mM FA, 25 mM DEA, 1mg mL ⁻¹ , UV- detection.	82
Figure 42: UV/Vis detection of GNP@trypsin BApNA assay (c = 0.05 mM without DMSO with digestion times from 30 – 1740 min) at $\lambda=410$ nm.....	83
Figure 43: Increase of L-Bz-Arg and respectively decrease of the substrate with time of GNP@trypsin BApNA assay (c= 0.05 mM without DMSO with digestion times from 30 – 1740 min). Mobile Phase: MeOH, 50 mM FA, 25 mM DEA, 1mg mL ⁻¹ , UV- detection.	84
Figure 44: UV/Vis detection of GNP@trypsin D,L-BApNA digestion assay (c = 0.05 mM) a) 5 (v/v) % solvent, b) 10 (v/v) % solvent, both with digestion times from 1 – 7 h) at $\lambda=410$ nm.	85
Figure 45: Increase of L-Bz-Arg with time of GNP@trypsin D,L-BApNA digestion assay (c = 0.05 mM) a) 5 (v/v) % solvent, b) 10 (v/v) % solvent, with digestion times from 1 – 7 h). Mobile Phase: MeOH, 50 mM FA, 25 mM DEA, 1mg mL ⁻¹ , UV- detection.	86
Figure 46: HPLC detection of standard AA-D-Phe (blue), acetylated D-Phe (red) and not acetylated D-Phe (green). Mobile phase MeOH, 25 mM FA, 12.5 NH ₄ FA, 0.55 mL min ⁻¹ . Column: QN-AX type, 390 μ mol immobilized selector per g of 3-SHproyl modified Daisogel 5 μ m 120 Å poresize (SH covered 840 μ g/g silica).....	87
Figure 47: Lineweaver-Burk diagram of D,L-BApNA assay (c = 0.1 to 6 mM with 10 (v/v) % DMSO with a digestion time of 30 min) with trypsin in-solution acetylated and not acetylated, respectively.	88
Figure 48: Determination of activity of trypsin not acetylated, trypsin acetylated before immobilization and trypsin acetylated after immobilization with a substrate concentration of 0.05 mM D,L-BApNA and a digestion time of 30 min.	89
Figure 49: Lineweaver-Burk diagram of D,L-BApNA assay (c = 0.1 to 6 mM with 10 (v/v) % DMSO with a digestion time of 30 min) with GNP@trypsin acetylated and not acetylated, respectively.	90
Figure 50: Increase of the area of D,L-Bz-Arg with substrate concentration of the GNP@trypsin acetylated and not acetylated BApNA assays (c = 0.1 to 6 mM with 10 (v/v) % DMSO with a digestion time of 30 min). Mobile Phase: MeOH, 50 mM FA, 25 mM DEA, 1mL min ⁻¹ , UV- detection.....	91
Figure 51: Separation of the peptides α -N-Bz-D,L-Lys-Gly and N-Bz-D,L-Arg-Gly with standard mobile phase MeOH, 50 mM FA, 25 mM DEA 1mL min ⁻¹ , UV-detection.	92
Figure 52: Used mobile phases with various compositions according to Table 13. a) MeOH,	

50 mM FA, 25 mM NH ₄ FA with different percentages of MeOH. b) MeOH, 50 mM FA, 25 mM NH ₄ FA with different percentages of ACN.	93
Figure 53: Used mobile phases with various compositions according to Table 13. a) MeOH, 50 mM FA, 25 mM NH ₄ FA with different percentages of ACN, 50 mM FA. b) MeOH, 50 mM FA, 25 mM NH ₄ FA with different percentages of millipore water, 50 mM FA, 25 mM NH ₄ FA.	95
Figure 54: Used mobile phases with various compositions according to Table 13. a) MeOH, 25 mM FA, 12.5 mM NH ₄ FA with different percentages of ACN 90 (v/v) %, MeOH 10 (v/v) %, 25 mM FA, 12.5 mM NH ₄ FA. b) MeOH, 25 mM FA, 12.5 mM NH ₄ FA with different percentages of ACN 90 (v/v) %, MeOH 10 (v/v) %, 25 mM FA, 12.5 mM NH ₄ FA.	96
Figure 55: Separation of the peptides α -N-Bz-D,L-Lys-Gly, N-Bz-D,L-Arg-Gly and the products D,L-Bz-Arg with finally used mobile phase 75 % MeOH 25 mM FA 12.5 mM NH ₄ FA / 25% ACN 90 (v/v) %, MeOH 10 (v/v) %, 25 mM FA 12.5 mM NH ₄ FA 1mL min ⁻¹ , UV-detection. Column: Htau-QD 150 x 4 mm, 5 μ m material, SO coverage 188 μ mol g ⁻¹ silica column.	97
Figure 56: M. M. diagram for GNP@trypsin peptide assays (c = 0.298 – 2.98 mM (N-benzoyl-L-Arg-Gly-OH) and 0.324 – 3.24 mM (α -N-benzoyl-L-Lys-Gly-OH), respectively and a digestion time of 3.5 h). Mobile phase 75 % MeOH, 25 mM FA, 12.5 mM NH ₄ FA / 25% ACN 90 (v/v) %, MeOH 10 (v/v) %, 25 mM FA, 12.5 mM NH ₄ FA 1mL min ⁻¹ , UV-detection.	98
Figure 57: Lineweaver-Burk diagram for GNP@trypsin peptide assays (c = 0.298 – 2.98 mM (N-benzoyl-L-Arg-Gly-OH) and 0.324 – 3.24 mM (α -N-benzoyl-L-Lys-Gly-OH), respectively and a digestion time of 3.5 h). Mobile phase 75 % MeOH, 25 mM FA, 12.5 mM NH ₄ FA / 25% ACN 90 (v/v) %, MeOH 10 (v/v) %, 25 mM FA, 12.5 mM NH ₄ FA 1mL min ⁻¹ , UV-detection.	99
Figure 58: Digestion of α -N-benzoyl-L-Lys -Gly-OH and α -N-benzoyl-D-Lys -Gly-OH, digested separately (c = 1.0 mg mL ⁻¹ each, digestion time 0 – 24 h). a) Products b) Substrates. Analysis:Mobile phase 75 % MeOH 25 mM FA 12.5 mM NH ₄ FA / 25% ACN:MeOH 9:1 25 mM FA 12.5 mM NH ₄ FA 1mL min ⁻¹ , UV-detection.	100
Figure 59: Digestion of N-benzoyl-D-Arg -Gly-OH and N-benzoyl-L-Arg -Gly-OH, digested separately (c = 1.0 mg mL ⁻¹ each, digestion time 0 – 24 h). a) Products b) Substrates. Analysis:Mobile phase 75 % MeOH 25 mM FA 12.5 mM NH ₄ FA / 25% ACN:MeOH 9:1 25 mM FA 12.5 mM NH ₄ FA 1mL min ⁻¹ , UV-detection.	101
Figure 60: Digestion of α -N-benzoyl-D,L-Lys -Gly-OH, digested together in a racemic mixture (c = 0.5 mg mL ⁻¹ each, digestion time 0 – 24 h). a) Products b) Substrates. Analysis:Mobile	

phase 75 % MeOH 25 mM FA 12.5 mM NH ₄ FA / 25% ACN:MeOH 9:1 25 mM FA 12.5 mM NH ₄ FA 1mL min ⁻¹ , UV-detection.....	102
Figure 61: Digestion of <i>N</i> -benzoyl-D,L-Arg -Gly-OH, digested together in a racemic mixture (c = 0.5 mg mL ⁻¹ each, digestion time 0 – 24 h). a) Products b) Substrates. Analysis: Mobile phase 75 % MeOH 25 mM FA 12.5 mM NH ₄ FA / 25% ACN:MeOH 9:1 25 mM FA 12.5 mM NH ₄ FA 1mL min ⁻¹ , UV-detection.....	103
Figure 62: Digestion of α- <i>N</i> -benzoyl-D,L-Lys -Gly-OH and <i>N</i> -benzoyl-D,L-Arg -Gly-OH, digested together in a multicomponent mix (c = 0.25 mg mL ⁻¹ each, digestion time 0 – 24 h). a) Increase of Bz-L-Lys-OH with decreasing α- <i>N</i> -benzoyl-L-Lys-Gly-OH b) Increase of Bz-L-Arg-OH with decreasing <i>N</i> -benzoyl-L-Arg-Gly-OH. Analysis: Mobile phase 75 % MeOH 25 mM FA 12.5 mM NH ₄ FA / 25% ACN:MeOH 9:1 25 mM FA 12.5 mM NH ₄ FA 1mL min ⁻¹ , UV-detection.	104
Figure 63: Digestion of α- <i>N</i> -benzoyl-D-Lys -Gly-OH and <i>N</i> -benzoyl-D-Arg -Gly-OH, digested separately (c = 2.5 mg mL ⁻¹ each, digestion time 0 – 24 h). a) Invariant area of substrates b) Invariant area of Bz-D-Lys-OH and Bz-D-Arg-OH, respectively. Analysis: Mobile phase 75 % MeOH 25 mM FA 12.5 mM NH ₄ FA / 25% ACN:MeOH 9:1 25 mM FA 12.5 mM NH ₄ FA 1mL min ⁻¹ , UV-detection.	105
Figure 64: Digestion of Bz-D,L-Arg-OH (c = 0.5 mg mL ⁻¹ and a digestion time of 0 – 48 h), including standard deviation (measurement done in triplicate). Mobile phase: MeOH, 50 mM FA, 25 mM DEA, 1mL min ⁻¹ , UV-detection.	106
Figure 65: Digestion of L-Phe-L-Arg and L-Arg-L-Phe (c = 1.0 mg mL ⁻¹ and a digestion time of 0 – 5 h). Mobile phase: MeOH, 50 mM FA, 25 mM DEA, 1mL min ⁻¹ , UV-detection.	106

11 References

1. IUPAC, *Analytical chiral separation methods* Pure and Applied Chemistry, 1997. **69**: p. 1469-1474.
2. Lämmerhofer, M. *Stereoselective liquid chromatography*. www.chromedia.org [2012-02-26].
3. Laemmerhofer, M. and W. Lindner, *Quinine and quinidine derivatives as chiral selectors. I. Brush type chiral stationary phases for high-performance liquid chromatography based on cinchonan carbamates and their application as chiral anion exchangers*. J. Chromatogr., A, 1996. **741**: p. 33-48.
4. IUPAC, *Rules for the nomenclature of organic chemistry. Section E: Stereochemistry*

- (Recommendations 1974). Pure Appl. Chem., 1976. **45**: p. 11-30.
5. Cahn, R.S., C. Ingold, and V. Prelog, *Specification of molecular chirality*. Angew. Chem., Int. Ed. Engl., 1966. **5**: p. 385-415.
 6. Testa, B., *Principles of organic stereochemistry*. Wiley-VCH, 1998.
 7. Vollhardt, *Organische Chemie* Wiley-VCH, 2005.
 8. Moss, G.P., *Basic terminology of stereochemistry*. Pure Appl. Chem., 1996. **68**: p. 2193-2222.
 9. Morrison, J.D. and H.S. Mosher, *Asymmetric Organic Reactions* 1971: Prentice-Hall. 465 pp.
 10. Gawley, R.E., *Do the terms "% ee" and "% de" make sense as expressions of stereoisomer composition or stereoselectivity?* J Org Chem, 2006. **71**: p. 2411-6.
 11. Agranat, I., H. Caner, and J. Caldwell, *Putting chirality to work: the strategy of chiral switches*. Nat. Rev. Drug Discovery, 2002. **1**: p. 753-768.
 12. Maier, N.M., P. Franco, and W. Lindner, *Separation of enantiomers: needs, challenges, perspectives*. J. Chromatogr., A, 2001. **906**: p. 3-33.
 13. Francotte, E., *Chirality in Drug Research*. Wiley-VCH, 2006. **Volume 33**: p. 189-260.
 14. Caldwell, J., *Importance of stereospecific bioanalytical monitoring in drug development*. J. Chromatogr., A, 1996. **719**: p. 3-13.
 15. Blaschke, G., *Chromatographic racemic separation of thalidomide and teratogenic activity of its enantiomers*. Arznei. Forschung, 1979. **29**: p. 1640-1642.
 16. Kelsey, F., *FDA Medical Reviewer Leaces Her Mark On History*. U.S. Food and Drug Administration Consumer Magazin, 2001.
 17. Eriksson, T., et al., *Stereospecific determination, chiral inversion in vitro and pharmacokinetics in humans of the enantiomers of thalidomide*. Chirality, 1995. **7**: p. 44-52.
 18. Ariens, E.J., *Stereochemistry, a basis for sophisticated nonsense in pharmacokinetics and clinical pharmacology*. Eur. J. Clin. Pharmacol., 1984. **26**: p. 663-8.
 19. Ariens, E.J., *Stereochemistry: a source of problems in medicinal chemistry*. Med. Res. Rev., 1986. **6**: p. 451-66.
 20. Ariens, E.J., *Implications of the neglect of stereochemistry in pharmacokinetics and clinical pharmacology*. Drug Intell. Clin. Pharm., 1987. **21**: p. 827-9.
 21. Shah, R.R. and S.K. Branch, *Regulatory requirements for the development of chirally active drugs*. Handb. Exp. Pharmacol., 2003. **153**: p. 379-399.
 22. Branch, S.K., *International Regulation on Chiral Drugs*: Wiley-VCH Weinheim 2001.
 23. ICH, *International Conference on Harmonisation; guidance on Q6A specifications: test procedures and acceptance criteria for new drug substances and new drug products: chemical substances*. Notice. Fed Regist, 2000. **65**: p. 83041-63.
 24. Yu, H.-L., et al., *Discovery and utilization of biocatalysts for chiral synthesis: an overview of Chinese scientists research and development*. Adv. Biochem. Eng./Biotechnol., 2009. **113**: p. 1-31.
 25. Grunenwald, J.-M., et al., *Diastereoselective and enantioselective preparation of bicyclic and tricyclic compounds using salt resolution*, 2011, CU Chemie Uetikon GmbH, Germany . p. 8pp.; Chemical Indexing Equivalent to 154:64358 (WO).
 26. Yang, Y., et al., *Enantioseparation in capillary electrophoresis using 6-oligo(lactic acid)cyclomaltoheptaose as a chiral selector*. Anal. Sci., 2009. **25**: p. 1315-1318.
 27. Zabka, M., P.S. Gomes, and A.E. Rodrigues, *Performance of simulated moving bed with conventional and monolith columns*. Sep. Purif. Technol., 2008. **63**: p. 324-333.
 28. Dalglish, C.E., *Optical resolution of aromatic amino acids on paper chromatograms*.

- J. Chem. Soc., 1952: p. 3940-2.
29. Francotte, E.R., *Enantioselective chromatography. An essential and versatile tool for the analytical and preparative separation of enantiomers*. *Chimia*, 1997. **51**: p. 717-725.
 30. Laemmerhofer, M., *Chiral recognition by enantioselective liquid chromatography: Mechanisms and modern chiral stationary phases*. *J. Chromatogr., A*, 2010. **1217**: p. 814-856.
 31. Hoffmann, C.V., M. Laemmerhofer, and W. Lindner, *Novel strong cation-exchange type chiral stationary phase for the enantiomer separation of chiral amines by high-performance liquid chromatography*. *J. Chromatogr., A*, 2007. **1161**: p. 242-251.
 32. Hoffmann, C.V., et al., *Synergistic effects on enantioselectivity of zwitterionic chiral stationary phases for separations of chiral acids, bases, and amino acids by HPLC*. *Anal. Chem. (Washington, DC, U. S.)*, 2008. **80**: p. 8780-8789.
 33. Hoffmann, C.V., et al., *Stationary phase-related investigations of quinine-based zwitterionic chiral stationary phases operated in anion-, cation-, and zwitterion-exchange modes*. *J. Chromatogr., A*, 2009. **1216**: p. 1147-1156.
 34. Lindner, W. and M. Laemmerhofer, *Optimization and application of quinine and quinidine derivatives as highly efficient selectors in liquid chromatography*. *Chimia*, 1996. **50**: p. 274.
 35. Mandl, A., et al., *Quinine versus carbamoylated quinine-based chiral anion exchangers. A comparison regarding enantioselectivity for N-protected amino acids and other chiral acids*. *J. Chromatogr., A*, 1999. **858**: p. 1-11.
 36. Wernisch, S., R. Pell, and W. Lindner, *Increments to chiral recognition facilitating enantiomer separations of chiral acids, bases, and ampholytes using Cinchona-based zwitterion exchanger chiral stationary phases*. *J. Sep. Sci.*, 2012. **35**: p. 1560-1572.
 37. Vidotti, M., et al., *Biosensors based on gold nanostructures*. *J. Braz. Chem. Soc.*, 2011. **22**: p. 3-20.
 38. Daniel, M.-C. and D. Astruc, *Gold Nanoparticles: Assembly, Supramolecular Chemistry, Quantum-Size-Related Properties, and Applications toward Biology, Catalysis, and Nanotechnology*. *Chem. Rev. (Washington, DC, U. S.)*, 2004. **104**: p. 293-346.
 39. Wang, Z. and L. Ma, *Gold nanoparticle probes*. *Coord. Chem. Rev.*, 2009. **253**: p. 1607-1618.
 40. Kerman, K., et al., *Gold nanoparticle-based electrochemical detection of protein phosphorylation*. *Anal. Chim. Acta*, 2007. **588**: p. 26-33.
 41. Nash, M.A., et al., *Mixed Stimuli-Responsive Magnetic and Gold Nanoparticle System for Rapid Purification, Enrichment, and Detection of Biomarkers*. *Bioconjugate Chem.*, 2010. **21**: p. 2197-2204.
 42. Faccenda, A., et al., *Gold Nanoparticle Enrichment Method for Identifying S-Nitrosylation and S-Glutathionylation Sites in Proteins*. *J. Am. Chem. Soc.*, 2010. **132**: p. 11392-11394.
 43. Zhu, S., Y. Fu, and J. Hou, *Topical review: metallic nanoparticles array for immunoassay*. *J. Comput. Theor. Nanosci.*, 2010. **7**: p. 1855-1869.
 44. Sykora, D., et al., *Application of gold nanoparticles in separation sciences*. *J Sep Sci.* **33**: p. 372-87.
 45. Wu, C.-S., F.-K. Liu, and F.-H. Ko, *Potential role of gold nanoparticles for improved analytical methods: an introduction to characterizations and applications*. *Anal. Bioanal. Chem.*, 2011. **399**: p. 103-118.

46. Lucena, R., et al., *Potential of nanoparticles in sample preparation*. J. Chromatogr., A, 2011. **1218**: p. 620-637.
47. Frens, G., *Controlled nucleation for the regulation of the particle size in monodisperse gold suspensions*. Nature (London), Phys. Sci., 1973. **241**: p. 20-2.
48. Turkevich, J., P.C. Stevenson, and J. Hillier, *The nucleation and growth processes in the synthesis of colloidal gold*. Discuss. Faraday Soc., 1951. **No. 11**: p. 55-75.
49. Kopeliovich, D. *Stabilization of colloids*. 2013-01-15]; Available from: www.subtech.com.
50. Berg, J., *An Introduction to Interfaces & Colloids: The Bridge to Nanoscience*. 2010. **1**.
51. Atkins, P., *Physical Chemistry*. Vol. 8. 2006.
52. Doane, T.L., et al., *Nanoparticle ζ -Potentials*. Acc. Chem. Res. **45**: p. 317-326.
53. Deryagin, B. and L. Landau, *Theory of the stability of strongly charged lyophobic sols and of the adhesion of strongly charged particles in solutions of electrolytes*. Acta Physicochim. URSS, 1941. **14**: p. 633-62.
54. Verwey, E.J.W. and J.T.G. Overbeek, *Theory of the Stability of Lyophobic Colloids* 1948: Elsevier Pub. Co. 216 pp.
55. Eirich, F.R. *Polymers as colloid stabilizers*. 1982. Academic.
56. Ghosh, D., et al., *A fully standardized method of synthesis of gold nanoparticles of desired dimension in the range 15 nm-60 nm*. J Nanosci Nanotechnol. **11**: p. 1141-6.
57. Haiss, W., et al., *Determination of Size and Concentration of Gold Nanoparticles from UV-Vis Spectra*. Anal. Chem. (Washington, DC, U. S.), 2007. **79**: p. 4215-4221.
58. Khlebtsov, N.G., *Determination of Size and Concentration of Gold Nanoparticles from Extinction Spectra*. Anal. Chem. (Washington, DC, U. S.), 2008. **80**: p. 6620-6625.
59. Malvern. *Application note: Characterisation of colloidal gold using dynamic light scattering*. [2012-12-10]; Available from: www.malvern.com.
60. Rawle, A., *Basic principles of particle-size analysis*. Surf. Coat. Int., Part A, 2003. **86**: p. 58-65.
61. Malvern. *Technical note: Dynamic Light Scattering*. 2012-12-10]; Available from: www.malvern.com.
62. Malvern. *Technical Note: Zeta Potential*. [2012-12-10]; Available from: www.malvern.com.
63. Srisombat, L., A.C. Jamison, and T.R. Lee, *Stability: A key issue for self-assembled monolayers on gold as thin-film coatings and nanoparticle protectants*. Colloids Surf., A, 2011. **390**: p. 1-19.
64. Kalska-Szostko, B., et al., *Enzymes immobilization on Fe₃O₄-gold nanoparticles*. Appl. Surf. Sci., 2012. **258**: p. 2783-2787.
65. Hermanson, G., *Bioconjugate Techniques*. 2nd ed, 2008: Elsevier, London, UK.
66. Prime, K.L. and G.M. Whitesides, *Self-assembled organic monolayers: model systems for studying adsorption of proteins at surfaces*. Science, 1991. **252**: p. 1164-7.
67. Ulman, A., *Formation and Structure of Self-Assembled Monolayers*. Chem. Rev. (Washington, D. C.), 1996. **96**: p. 1533-1554.
68. Hinterwirth, H., W. Lindner, and M. Laemmerhofer, *Bioconjugation of trypsin onto gold nanoparticles: Effect of surface chemistry on bioactivity*. Anal. Chim. Acta. **733**: p. 90-97.
69. Voet, D., *Lehrbuch der Biochemie*. 2nd ed, 2010: Wiley-VCH Verlag GmbH & Co. KGaA.
70. Solomon, E., *Biology, Active Learner*. 6th ed, 2002: Brooks/Cole.
71. Koshland, D.E., Jr., *Application of a theory of enzyme specificity to protein synthesis*.

- Proc. Natl. Acad. Sci. U. S. A., 1958. **44**: p. 98-105.
72. Biologyguide. *Enzymes*. [2012-01-11]; Available from: http://www.biologyguide.net/unit1/2_enzymes.htm.
 73. NPTEL. <http://nptel.iitm.ac.in>. [2013-01-10]; Available from: <http://nptel.iitm.ac.in/courses/104103018/module3/lec6>.
 74. Rasor, J.P., *Enzymes as catalysts for the manufacture of single enantiomers*. Innovations Pharm. Technol., 1998. **1**: p. 17-19.
 75. Schellenberg, A., *Enzymkatalyse: Einführung in die Chemie, Biopchemie und Technologie der Enzyme*. 1st ed 1989: Springer-Verlag.
 76. MEROPS. *The Peptidase Database*. [2013-02-01]; Available from: <http://merops.sanger.ac.uk/>.
 77. BRENDA. *The Comprehensive Enzyme Information System*. [2013-02-02]; Available from: www.brenda-enzymes.org.
 78. Williams, L., *The Catalytic Triad of Trypsin*, Georgia Tech: http://ww2.chemistry.gatech.edu/~lw26/structure/protein/serine_protease/triad_1.html.
 79. Lv, M., et al., *Trypsin-Gold Nanoparticle Conjugates: Binding, Enzymatic Activity, and Stability*. Prep. Biochem. Biotechnol., 2009. **39**: p. 429-438.
 80. Sakurai, T., et al., *Control of enzyme enantioselectivity by the reaction medium*. J. Am. Chem. Soc., 1988. **110**: p. 7236-7.
 81. Bross, J., et al., *Inversion of enantioselectivity of serine proteases*. Recl. Trav. Chim. Pays-Bas, 1995. **114**: p. 255-7.
 82. Monzo, A., E. Sperling, and A. Guttman, *Proteolytic enzyme-immobilization techniques for MS-based protein analysis*. TrAC, Trends Anal. Chem., 2009. **28**: p. 854-864.
 83. Freije, J.R., et al., *Chemically Modified, Immobilized Trypsin Reactor with Improved Digestion Efficiency*. J. Proteome Res., 2005. **4**: p. 1805-1813.
 84. Li, Y., et al., *Efficient on-chip proteolysis system based on functionalized magnetic silica microspheres*. Proteomics, 2007. **7**: p. 2330-2339.
 85. Li, S., et al., *Improvement of the enzyme performance of trypsin via adsorption in mesoporous silica SBA-15: hydrolysis of BAPNA*. Molecules, 2013. **18**: p. 1138-1149.
 86. Krenkova, J., Z. Bilkova, and F. Foret, *Characterization of a monolithic immobilized trypsin microreactor with on-line coupling to ESI-MS*. J. Sep. Sci., 2005. **28**: p. 1675-1684.
 87. Papat, A., et al., *Mesoporous silica nanoparticles for bioadsorption, enzyme immobilisation, and delivery carriers*. Nanoscale, 2011. **3**: p. 2801-2818.
 88. Zhao, L.-M., et al., *Preparation and application of chitosan nanoparticles and nanofibers*. Braz. J. Chem. Eng., 2011. **28**: p. 353-362.
 89. Davis, M.T., et al., *Microscale immobilized protease reactor columns for peptide mapping by liquid chromatography/mass spectral analyses*. Anal. Biochem., 1995. **224**: p. 235-44.
 90. Mozhaev, V.V., et al., *Protein stabilization via hydrophilization. Covalent modification of trypsin and α -chymotrypsin*. Eur. J. Biochem., 1988. **173**: p. 147-54.
 91. Zhang, Z., Z. He, and G. Guan, *Thermal stability and thermodynamic analysis of native and methoxypolyethylene glycol modified trypsin*. Biotechnol. Tech., 1999. **13**: p. 781-786.
 92. Fernandez, M., et al., *Stabilization of trypsin by chemical modification with β -cyclodextrin monoaldehyde*. Biotechnol. Lett., 2002. **24**: p. 1455-1459.

93. Murphy, A. and C.O. Fagain, *Chemically stabilized trypsin used in dipeptide synthesis*. Biotechnol. Bioeng., 1998. **58**: p. 364-373.
94. Freije, R. and R. Bischoff, *Proteolytic enzymes with modified amino acids and immobilization in a protein digestion reactor*, 2006. p. 38pp.
95. Murphy, A. and C.O. Fagain, *Stability characteristics of chemically-modified soluble trypsin*. J. Biotechnol., 1996. **49**: p. 163-171.
96. GENENGNEWS. *Using Isothermal Titration Calorimetry*. 2006 [2013-02-01]; Available from: <http://www.genengnews.com/gen-articles/using-isothermal-titration-calorimetry/1622/>.
97. themedicalbiochemistrypage. *Lineweaver-Burk plot*. [2012-04-11]; Available from: <http://themedicalbiochemistrypage.org/enzyme-kinetics.php>.
98. Wernisch, S. and W. Lindner, *Versatility of cinchona-based zwitterionic chiral stationary phases: Enantiomer and diastereomer separations of non-protected oligopeptides utilizing a multi-modal chiral recognition mechanism*. J. Chromatogr., A, 2012. **1269**: p. 297-307.
99. ICH, Q.R., *Validation of Analytical Procedures: Text and Methodology International conference on Harmonization*. Geneva, 2005. **1-13**.
100. Khlebtsov, B.N. and N.G. Khlebtsov, *On the measurement of gold nanoparticle sizes by the dynamic light scattering method*. Colloid J. **73**: p. 118-127.
101. Asgeirsson, B. and P. Cekan, *Microscopic rate-constants for substrate binding and acylation in cold-adaptation of trypsin I from Atlantic cod*. FEBS Lett., 2006. **580**: p. 4639-4644.
102. Treetharnmathurot, B., et al., *Effect of PEG molecular weight and linking chemistry on the biological activity and thermal stability of PEGylated trypsin*. Int. J. Pharm., 2008. **357**: p. 252-259.
103. Zelazko, M., J. Chrzanowska, and A. Polanowski, *Pancreatic proteolytic enzymes of ostrich purified on immobilized protein inhibitors. Characterization of a new form of chymotrypsin (Chtr1)*. Comp. Biochem. Physiol., Part B: Biochem. Mol. Biol., 2008. **151B**: p. 102-109.
104. Rovey, M. and P. Desnuelle, *Amino acids liberated during the hydrolysis of horse globin by crystalline pepsin, trypsin, and chymotrypsin*. Biochim. Biophys. Acta, 1951. **7**(Copyright (C) 2013 American Chemical Society (ACS). All Rights Reserved.): p. 600-1.

12 Curriculum Vitae

Marcella Patricia Eder

Kontakt Daten

Mobil: +43 (0) 69912904988 E-Mail: marcella.eder@gmx.at

Ausbildung:

WS 2006 – SS 2013	Studium der Chemie, Universität Wien
September 2002 – Juni 2006	Bundesoberstufenrealgymnasium, Wiener Neustadt
September 1998 – Juni 2002	Bundesgymnasium Zehnergasse, Wiener Neustadt
September 1994 - Juni 1998	Musikvolksschule, Wiener Neustadt